PhD Thesis

Self-similar evolution of fast magnetic reconnection in free space: a new model for astrophysical reconnection

新田 伸也

Shin-ya NITTA

Department of Astronomical Science,
The Graduate University for Advanced Studies (SOKENDAI)

A dissertation submitted for the degree of Doctor of Philosophy

(January, 2003)

謝辞

私に国立天文台での研究の機会を与えてくれた柴田一成教授（京都大）に感謝します。柴田さんは研究に関する議論に於いて強力にサポートしてくれただけでなく、絶えず私を励ましてくださり、アルバイトを紹介してくださり、私の授業料支払いの保証人にさえなってくださいました。柴田さんの援助なくして今日の私はあり得ません。同時に私の指導教官を引き受けてくださった、観山正見教授（国立天文台／総研大）と櫻井隆教授（国立天文台／総研大）に感謝します。扱いにくいであろう、きかん坊の私を暖かく迎えて下さり、あらゆる束縛無しに自由に研究させてくださった寛容さをとてもありがたく思います。セミナーなどに於けるコメントは的確で、考えを客観的に整理し説得力を増すために大いに役立ちました。

本博士論文の研究内容の共同研究者である、前澤洌教授（宇宙研）と田沼俊一博士（京都大）に感謝します。前澤さんは私の修士時代の指導教官でもあり、本学位論文での研究の全ての出発点は、修士時代の前澤さんとの議論にあります。田沼さんは、コンピュータの苦手な私に代わって、数値シミュレーションの計算実行の全てを引き受けてくださいました。

かつて柴田さんが国立天文台で活躍していた頃の柴田組の皆さん、及び、ＭＨＤ合宿に参加してくださった千葉大、京都大の皆さんに感謝します。特に工藤哲洋博士（西オンタリオ大）には公私に渡って様々に励ましていただきました。工藤さんとは１０年以上の付き合いがあります。かつて工藤さんは私から見て後輩でしたが、ここ５年くらいの工藤さんの勢いには凄まじいものがあり、最後の方では立場が逆転し、指導されることさえありました。夜型研究者の私は、徹夜で導いたばかりの結果を朝型の工藤さんに報告して、議論にのってもらうのがとても楽しみでした。工藤さんは、私の夢の中でまで議論に付き合ってくださり、しかも、しばしばブレークスルーにつながる大変に重要なコメントをして下さいました。夢の中の工藤さんにも感謝しなければなりません。このことも、工藤さんとの議論が、私自身のスキルの向上に深く役立ったことを示していると思います。横山央明博士（国立天文台）にも感謝します。横山さんは、現在の日本における磁気リコネクション研究の若手第１の人材であり、この人が私の研究の発展途上段階に於いて様々なコメントを下さったことは、研究を加速し、議論を深め、発展性を持たせるために大変に役立ちました。より若手の皆さんにとって、私はやっかいで少し怖い先輩であったかも知れません。私は急速に成長する皆さんに追い抜かれないよう、必死に努力せねばなりませんでした。このことがお互いの成長を少しでも加速できたことを願っています。

国立天文台理論天文学研究系の皆さんに感謝します。研究分野の点で、私は理論部の異端児であったにもかかわらず、セミナーに於いては私の研究に興味を示していただき、分野外であるが故の有益なコメントを下さいました。このことが、私自身の研究を客観的に見直すきっかけになったことは言うまでもありません。理論部内でのセミナーや行事に対して、アルバイトに追われていた私はサボってばかりでしたが、当時理論部助手であった犬塚修一郎博士（京都

大）には「新田さん自身の研究にとって一番良いようにやってください」という暖かい言葉を掛けていただき、居心地の悪い思いをせずに済みました。和田桂一博士、小久保英一郎博士、鈴木建博士は、公私に渡って私の良き相談相手になってくださいました。またいつか、満開の桜の下で語り明かしたいと思います。コンピュータ音痴の私は、計算機係の折戸学博士、長島雅裕博士、小山洋博士には助けられてばかりでした。彼らの助けがなかったら、私は本当に「紙とペンの世界」に閉じこもってしまったはずです。泉塩子氏は、事務能力のほとんど無い私を常にサポートしてくださいました。お腹を空かせたときに、サンドウィッチなどご馳走していただいたことも忘れません。寺澤真理子博士は、最後の１年間を非常に多忙に過ごしていた私にとっての安らぎを与えてくれました。彼女との会話がなければ、休日がほとんど取れなかったこの１年間は、味気なくとても荒んだものであったに違いありません。彼女のおかげで、忙しいなりに楽しく充実した研究生活を送れました。ありがとう！

国立天文台管理部の皆さんにも感謝します。特に、総研大担当の松浦孝氏と前任の塩谷誠氏（東京学芸大）にはお世話になりました。庶務課の皆さん（特に山下芳子氏、水谷由紀氏、電通大に転出された大西智之氏）には、様々に支援していただき、感謝しています。

私が研究活動を持続できたのは、沢山のアルバイトに恵まれたことに負うています。非常勤講師の窓口になって下さり、様々な援助を頂いた平山淳教授（明星大）、柳澤正久博士、伊東敏雄教授（電気通信大）、明星大学理工学部（物理学、機械工学、電気工学）のみなさん、北里大学基礎科学センター・物理学研究室のみなさんに感謝します。

関東圏の多くの大学に於いて、私の担当した数多くの学生達に感謝します。あなた方が支払ってくれた授業料によって、私は研究活動を継続できました。どんなに疲れていて、どんなに研究が停滞しているときでも、私の講義に期待して参加してくれているあなた方の前に立つと、頑張らざるを得ませんでした。あなた方に話すために私が準備した全ての話題は、雑談ネタも含めて、私自身にとっても糧となりました。あなた方が居てくれたおかげで、私は自堕落にならずに済んだと思っています。いつか、対等の立場で共に仕事のできる日が来ることを願っています。

「一本書こう会」会員の皆さんに感謝します。この会は、論文を発表し続けることが必要不可欠と考える研究者の集まりで、１９９５年当時苦境にあった私自身がつぶれないよう、公言実行の機会とするために、自作自演で結成したものです。メンバーも最初は少人数でほとんどが学生の身分でしたが、論文を書かねば奢らされる、とのプレッシャーからひたすら仕事に励み、次々と出世しました。私自身も、９６年には遅蒔きながらも一つ目の博士号を取得できました。現在は３０名を超える会員が各国に分布しており、私は、常に会員の皆さんの視線を意識してきたからこそ、今日までなんとか研究者として生き延びることができました。おかげで、劣等生の私も実力以上にがんばれたと思います。これからも頑張ってタダ酒を飲みましょう！

私がしばしば必要とするリフレッシュのために開催した宴会に参加してくださった全ての方々にも感謝します。旧・総研大プレハブ時代には、非常に大勢の方が私の企画した宴席に同

席してくださいました。皆さんの健在ぶりを目にすることで私も励まされました。「ぶらっくほーる」の皆さんは、私に大いに期待してくださり、いつも破格の待遇で迎えて下さいました。特に顧金蘭氏、張瑩氏に感謝します。みなさん、これからも一緒に飲んでください。

休日がほとんどなく殺伐としがちだったこの１年間で、私の唯一の楽しみはサイクリングでした。私に自転車の道を示し、アルバイトに疲れた私をいつも暖かく迎え、ただ酒を飲ませてくださった手塚明氏（手塚商店）に感謝します。また、手塚商店の常連客の皆さん、特に池田年広氏に感謝します。

私の旧い友人達にも感謝します。名古屋大学時代の友人達、特に大城宣実博士（津嘉山酒造）、阪本雄二博士（広島国際大）、フェリークラブのみなさん（浅井紀久夫博士[メディア教育開発センター]、小菅（佐藤）陽子氏、高橋英則博士[東京大]、度会英教博士[宇宙開発事業団]）らの励ましのおかげで、逆境の中にあっても、私は笑いながら研究者として在り続けることができ、東京への進出も可能となりました。中学生時代より絶えず私に期待し続けてくれた故郷・松山の友人達、特に冨永大輔＆裕子夫妻、松岡秀夫氏、渡部（小倉）恵理子氏、谷口（中田）豊美氏、永山篤氏に感謝します。遠い昔に、私がこれらの人たちに向かって放った大言は、９３年から５年あまり続いた苦境にあった時、私自身に向かって跳ね返ってきました。旧い友たちの暖かい眼差しは、壊れかけていた精神を確かに救ってくれました。ありがとう！

かつて私の周りに居て、私を見ていてくれた全ての皆さんに感謝します。特に、永年に渡って支えてもらいながら、何ら厚意に報いることのできなかった西森美貴に。私は、皆さんの見えざる視線を意識することによって、自分の活性を保つことができました。今後も努力を続け、皆さんの会話の中で私に関する話題が出たときに、皆さんが少しでも誇りを感じられるような人間でありたいと思います。

本学位論文の英文校正には、Yolande McLean氏が力を貸してくださいました。彼女とは以前から友人としての付き合いがありましたが、最後にお互いのプロとしての仕事を確かめ合うことができ、喜びを感じます。

最後になりましたが、私の家族に感謝します。両親は、私の放蕩ぶりをなんら咎めることなく、ここ２５年以上に渡って見逃してくれました。祖父母は、私に代わって私の両親を支えてくださり、また私自身のことも励ましてくれました。おかげで、日本人では珍しい２つの博士号を取ることができました。私の妹弟も、堅気とは言い難い私に対して寛容でした。特に妹・頼子は、私に代わって、身体障害を持つ両親の世話を全面的に看てくれました。そのために彼女が犠牲にしたものの大きさを私は理解しているつもりです。彼女の苦労と思いやりを無駄にしないためにも、今後もがんばり続けようと思います。

abstract

We present a new model for time evolution of the fast magnetic reconnection in free space, which is characterized by self-similarity. The possibility of this type of evolution is verified by numerical simulations. We also find an analytical solution which is consistent with the numerical result.

In many cases of astrophysical problems, e.g., solar flares or geomagnetospheric substorms, the spatial scale of the reconnection system significantly expands as time proceeds. The focus of this work is on this expanding phase. The resultant spatial scale of the reconnection system is much larger than the initial scale (its dynamic range is $\sim 10^5 - 10^7$ in order of magnitude). Thus, actual astrophysical reconnection must be treated as an evolutionary process in a free space which is free from any influence of external circumstances, at least in its expanding phase just after the onset. Eventually, the evolution will be strongly influenced by these external circumstances, and will settle into a final state. Even in this final state, we can expect the influence of the expanding phase will continue to affect the later evolution of the system.

In spite of this, most previous numerical works focused on the character of evolution strongly affected by artificial boundary conditions on the simulation boundary. On the other hand, most analytical works focused on a stationary state of the reconnection as a boundary problem. However, we do not know how we should impose a well-described boundary condition for these cases, because it is actually determined as a result of the evolutionary process of this expanding phase. Hence, the freely expanding phase is essential to our understanding of the properties of astrophysical magnetic reconnections.

Our new model for magnetic reconnection aims to clarify a realistic evolution and spontaneous structure formation in free space. We assume the reconnection arising in an asymptotically uniform current sheet system (the Harris current sheet). The only fixed spatial scale in this system is the initial current sheet thickness, which is finite. Such a system probably has a self-similar solution, because when the system sufficiently matures, there is no fixed proper spatial scale in the system other than the size of the expanding system itself. Thus, it is worthwhile to study the possibility of self-similar evolution of magnetic reconnection. We do this both numerically and analytically as outlined below.

First we study it numerically, wishing to obtain evidence of self-similar evolution of the system. The reconnection is supposed to be triggered by artificially enhanced resistivity in the middle of the current sheet, which is held as a constant, independent of the time. This is a simplified model for anomalous resistivity. We were able to carry the computer simulation for the period while the system expanded by almost three orders

of magnitude in the spatial scale and we succeeded in finding the expected self-similar expansion of the system. The characteristic structure around the diffusion region is quite similar to the Petschek model which is characterized by a pair of slow-mode shocks and the fast-mode rarefaction-dominated inflow. In the outer region, a vortex-like return flow takes place driven by fast-mode compression caused by the piston effect of the reconnection jet takes place. The entire reconnection system expands self-similarly.

However, owing to technical reasons in computer simulation, the dynamic range of the expansion in the spatial scale studied by our numerical simulation is not sufficient to constitute evidence that the obtained evolution is truly a self-similar one. In order to check this, we sought a self-similar solution of the inflow region by an analytical study and compared the solution with our numerical result. By assuming that deviation owing to the reconnection from the initial equilibrium state is very small, we can analyse it with a perturbative method. This approximation is relevant for the inflow region to the original current sheet. We adopt a traditional mathematical method called the Grad-Shafranov approach. After a long derivation, we obtain several equations for the inflow region. One of them is a second order partial differential equation of the elliptical type for the magnetic flux function. We call it the Grad-Shafranov [G-S] equation. Each of the other equations shows an algebraic relation between a physical quantity and the magnetic flux function. Thus, by solving the G-S equation under a relevant boundary condition, we can obtain the distribution of magnetic flux function which shows the magnetic structure of the system. Once we obtain the magnetic flux function, we can easily derive the distributions of other quantities from other equations. The obtained solution for the inflow region is fairly consistent with our numerical solution.

This analytical study confirms the existence of self-similar growth. On the other hand, numerical study by time-dependent computer simulation verifies the stability of the self-similar growth with respect to any MHD mode. Hence, these two approaches are complementary, and their results confirm the stable self-similar evolution of the fast magnetic reconnection system.

Contents

1. INTRODUCTION

It is widely accepted that magnetic reconnection takes place very commonly as a powerful energy converter in astrophysical plasma systems. However, there still remain many open questions, not only regarding the microscopic physics of the resistivity, but also the macroscopic magnetohydrodynamical (MHD) structure. In this work, our attention is focused on the macroscopic evolutionary properties of magnetic reconnection.

We consider reconnection in an anti-parallel magnetic configuration called a "current sheet system". In this system, two similarly uniform magnetized regions are set in contact, divided by a boundary. We assume that the directions of the magnetic field on both sides are anti-parallel. In this case, the boundary carries a strong electric current, hence we call it the current sheet. If resistivity is enhanced in this current sheet, it plays an important role in energy conversion from the magnetic form to others. In resistive plasmas, there are two fundamental processes of magnetic energy conversion. One is magnetic diffusion, and another is magnetic reconnection.

The best known process of energy conversion in resistive plasmas from magnetic to other forms is Ohmic dissipation (magnetic diffusion). We must note, however, that plasmas are highly conductive in most astrophysical problems. Since the resistivity is very small, energy conversion by magnetic diffusion takes a very long time (see section 2.3), and is not applicable to many astrophysical phenomena with very violent energy releases, e.g., solar flares. Even in such a case, the majority believes that magnetic reconnection can convert the magnetic energy very quickly (see section 2.5). This is why we must study magnetic reconnection.

Magnetic reconnection is a kind of macroscopic instability arising in current sheet systems. The magnetic energy stored in the current sheet system is released by the reconnection and converted to kinetic or thermal energy. This energy release is caused by a topological change in the magnetic field lines. Such a process commonly takes place in resistive plasmas. Previous studies presented several theoretical and numerical models of reconnection. These are reviewed in section 2.

Such energy conversion in the current sheet system is very important in many astrophysical plasma systems. The most famous example is the relation between solar activity and geomagnetospheric activity, called solar flares and geomagnetospheric substorms. In this case, at least three current sheet systems are included. The first one is in the solar corona (see figure 1). The second and third are on the day-side and the night-side of the geomagnetosphere, respectively (see figure 2). Recent observations and numerical simulations suggest that similar phenomena seemingly activated by magnetic reconnection are universal, e.g., flares in accretion disks of young stellar objects (YSOs, see Koyama et al. 1994, Hayashi et al. 1999), galactic ridge X-ray emissions (GRXE, see Koyama et al. 1986, Tanuma et al. 1999).

We must note that the actual magnetic reconnection in astrophysical systems usually grows over a huge dynamic range in its spatial dimension. For example, the initial scale of the reconnection system can be defined by the initial current sheet thickness, but this is too small to be observed in typical solar flares. We do not have any convincing estimate of the scale, but if we estimate it to be of the order of the ion Larmor radius, it is extremely small ($\sim 10^0$ [m] in the solar corona). Finally, the reconnection system develops to a scale of the order of the initial curvature radius of the magnetic field lines ($\sim 10^7$ [m] $\sim 1.5\%$ of the solar radius for typical solar flares). The dynamic range of the spatial scale is obviously huge ($\sim 10^7$ for solar flares). For geomagnetospheric substorms, their dynamic range of growth is also large ($\sim 10^4$ for substorms). Such a very wide dynamic range of growth suggests that the evolution of the magnetic reconnection should be treated as a development in "free space", and that the outer circumstance does not affect the evolutionary process of magnetic reconnection, at least at the expanding stage just after the onset of reconnection.

However, no reconnection model evolving in a free space has been studied. We should note that most previous theoretical and numerical works on reconnection treated it as a boundary problem strongly influenced by external circumstances. These previous results are reviewed in section 2.

In actual numerical studies, there is a serious and inevitable difficulty: For magnetic reconnection to be properly studied, the thickness of the current sheet must be sufficiently resolved by simulation mesh size. Usually, the thickness of the current sheet is much smaller than the entire system. Hence, in previous works, we have been

forced to cut a finite volume out of actual large-scale reconnection systems for numerical studies.

Of course, we wish to realize that the boundary conditions of this type of finite simulation box reproduce the evolution in unbounded space. However, we should note that, in actual simulations, the boundary of such a simulation box necessarily affects the evolution inside the box, even if we use so-called "free" boundary conditions. This has an adverse influence on the evolutionary process of the numerically simulated magnetic reconnection: When the reconnection proceeds and physical signals propagating from the inner region cross the boundaries of the simulation box, the subsequent evolution is necessarily affected by the boundary conditions. This is because the information propagated through the boundary is completely lost and such an artificially cut-out simulation box will never receive the proper response of the outer regions. Additionally, numerical and unphysical signals emitted from the boundary may disturb the evolution. Such artificially affected evolution is obviously unnatural, and the resultant stationary state should differ from actual reconnection occurring in a free space.

Even in previous numerical studies aimed at clarification of the time evolution of reconnection (for example, series of studies originated by Ugai & Tsuda 1977 or Sato & Hayashi 1979), the evolution could not be followed for a long time. This is mainly owing to restriction of the size of the simulation box, hence application of the results was limited to spatial scales typically, say, a hundred times the spatial scale of the diffusion region. We are interested in an evolutionary process in a free space without any influence external circumstances. In such a system, the evolution and resultant structure would be quite different from these previous numerical models.

The same problem also appears in previous theoretical works. We must realize that astrophysical magnetic reconnection is essentially a non-stationary process because it grows in a huge spatial dynamic range. Most of these works, however, for mathematical simplicity, treat a stationary state of the reconnection in a finite volume (for example, see Priest & Forbes 1986). These are obviously a boundary problem and solutions must be influenced by boundary conditions. The problem is that we do not know how we should set the boundary condition in order to simulate external influences. In general, it is impossible to set. Hence, the situations argued in previous works are rather artificial and unnatural. It is obviously pointless to argue the actual evolutionary process in a free space.

From the above discussion, we can see what we have to do: We must clarify the nature of magnetic reconnection evolving with no external influence. This is possible by numerical simulation if we take a very wide simulation box compared with the initial thickness of the current sheet, and simulate the evolutionary process, while no wave emitted from the inside reaches the simulation boundary. The result is presented in section 4. A brief summary of the obtained evolutionary process is below.

We suppose a two-dimensional equilibrium state with anti-parallel magnetic field distribution, as in the Harris solution. When magnetic diffusion takes place in the current sheet by some localized resistivity, magnetic reconnection will occur, and a pair of reconnection jets is ejected along the current sheet. This causes a decrease in total pressure near the reconnection point. Such information propagates outward as a rarefaction wave. In a low-β plasma ($\beta \ll 1$ in the region very distant from the current sheet [asymptotic region]; as typically encountered in astrophysical problems), the propagation speed of the fast-magnetosonic wave is isotropic, and is much larger than that of other wave modes. Thus, information about the decreasing total pressure propagates almost isotropically as a fast-mode rarefaction wave (hereafter FRW) with a speed almost equal to the Alfvén speed V_{A0} in the asymptotic region. Hence, the wave front of the FRW (hereafter FRWF) has a cylindrical shape except near the point where the FRWF intersects with the current sheet. When the FRWF sufficiently expands, the initial thickness of the current sheet becomes negligible compared with the system size $V_{A0}t$, where t is the time from the onset of reconnection. In such a case, there is only one characteristic scale, i.e., the radius of the FRWF ($V_{A0}t$), which increases linearly as time proceeds. This is just the condition for self-similar growth. A detailed scenario of this process is argued in section 3.

In order to clarify the evolutionary process of magnetic reconnection in a free space, a numerical study of this process has been performed by our group (see Nitta, Tanuma, Shibata and Maezawa 2001). This study is presented in the first half of this paper (see section 4). We have discovered

a self-similar evolutionary process of fast reconnection as we expected. In our work, a stable self-similar growth of the reconnection system was shown. However, the simulated dynamic range of self-similar growth was still not enough ($\sim 10^3$) owing to the restriction of computer memory and CPU time. In order to make our model convincing, our numerical result should be coupled with an analytic study to find a self-similar solution.

In the latter half of this paper, our attention is focused on the analytic study of the self-similar stage of magnetic reconnection in a free space (see section 5). Such an analytic approach has the following importance:

1) By finding the analytic solution for self-similar growth, we can verify the possibility of self-similar evolution more rigorously. We set the initial thickness of the current sheet D. The self-similar stage is realized in the limit of $V_{A0}t \gg D$. However, in the computer simulation, we can only perform calculations for a finite duration, owing to technical reasons. Hence, we will never reach the exact self-similar stage. But, if we can verify that the result of the numerical simulation resembles the analytic self-similar solution, we can accept that the result presented by our numerical simulation is truly a self-similar evolution.

2) Existence of the analytic solution ensures that the self-similar growth will continue indefinitely. This is important because, for technical reasons, in the computer simulation, we cannot continue the calculation longer than we did in Nitta et al. (2001). Of course, we should note that when the system sufficiently grows to a scale similar to the initially imposed system size (e.g., the scale of the flux tube in the case of solar flares), this self-similar evolution must be modified by its circumstance. We should also note that such analytic treatment cannot ensure the stability of the self-similar evolution, while it is ensured by our numerical simulation. Thus the analytic treatment and numerical simulation are complementary.

2. SUMMARY OF PREVIOUS STUDIES FOR MAGNETIC RECONNECTION

We briefly summarize here the history of previous studies of magnetic reconnection as an elementary process in resistive plasmas. Development of the study for fundamental models reviewed here was presented between the mid-60s and mid-80s, and there has not been any essential development since that era. However, as we have discussed in the previous section, we still have no relevant models for astrophysical reconnection.

The energy conversion processes due to resistivity are categorized into two types. In the first type, the resistivity directly converts the magnetic energy by the Joule heating process (in other words, Ohmic dissipation). In the other type, the resistivity plays an indirect but important role in energy conversion. The resistivity allows a change in the topology of field lines. A point-like merging of two anti-parallel magnetic field lines is called a magnetic reconnection. After the reconnection of the two field lines, the plasma on each line is accelerated by the Lorentz force (or the magnetic tension) and creates a strong bipolar flow along the original current sheet. In this case, we can clearly understand that resistivity is simply a trigger of energy conversion, and the main energy conversion is driven by the Lorentz force. Several models for energy conversion in the current sheet system have been presented over the past 40 years. We summarize four representative models of these in the following section.

2.1. *Diffusion region*

In order to achieve the merging of two magnetic field lines, the breaking of the frozen-in condition is necessary. This is equivalent to existence of the magnetic diffusion in the resistive plasmas. We call the region in which the reconnection occurs the "diffusion region." The diffusion region is defined as the region in which the magnetic diffusion speed is greater than the convection speed of the plasmas (in another word, $|\boldsymbol{v} \times \boldsymbol{B}| < \mu\eta|\boldsymbol{j}|$, where $\boldsymbol{v}$ is the convection speed, $\boldsymbol{B}$ is the magnetic field, μ is the magnetic permeability [we suppose its value is equal to the value for the vacuum, because we treat very thin plasma throughout this paper], η is the magnetic diffusivity and $\boldsymbol{j}$ is the current density). In many astrophysical problems, the current sheet system is filled with highly conducting plasmas. In such systems, the magnetic diffusion is efficient only inside a current sheet in which the spatial gradient of the magnetic field strength is large.

2.2. *Reconnection Rate*

When we argue the energy conversion through the reconnection, the key term is the reconnection rate which is a measure of the conversion speed of the system. The reconnection rate is usually

a self-similar evolutionary process of fast reconnection as we expected. In our work, a stable self-similar growth of the reconnection system was shown. However, the simulated dynamic range of self-similar growth was still not enough ($\sim 10^3$) owing to the restriction of computer memory and CPU time. In order to make our model convincing, our numerical result should be coupled with an analytic study to find a self-similar solution.

In the latter half of this paper, our attention is focused on the analytic study of the self-similar stage of magnetic reconnection in a free space (see section 5). Such an analytic approach has the following importance:

1) By finding the analytic solution for self-similar growth, we can verify the possibility of self-similar evolution more rigorously. We set the initial thickness of the current sheet D. The self-similar stage is realized in the limit of $V_{A0}t \gg D$. However, in the computer simulation, we can only perform calculations for a finite duration, owing to technical reasons. Hence, we will never reach the exact self-similar stage. But, if we can verify that the result of the numerical simulation resembles the analytic self-similar solution, we can accept that the result presented by our numerical simulation is truly a self-similar evolution.

2) Existence of the analytic solution ensures that the self-similar growth will continue indefinitely. This is important because, for technical reasons, in the computer simulation, we cannot continue the calculation longer than we did in Nitta et al. (2001). Of course, we should note that when the system sufficiently grows to a scale similar to the initially imposed system size (e.g., the scale of the flux tube in the case of solar flares), this self-similar evolution must be modified by its circumstance. We should also note that such analytic treatment cannot ensure the stability of the self-similar evolution, while it is ensured by our numerical simulation. Thus the analytic treatment and numerical simulation are complementary.

2. SUMMARY OF PREVIOUS STUDIES FOR MAGNETIC RECONNECTION

We briefly summarize here the history of previous studies of magnetic reconnection as an elementary process in resistive plasmas. Development of the study for fundamental models reviewed here was presented between the mid-60s and mid-80s, and there has not been any essential development since that era. However, as we have discussed in the previous section, we still have no relevant models for astrophysical reconnection.

The energy conversion processes due to resistivity are categorized into two types. In the first type, the resistivity directly converts the magnetic energy by the Joule heating process (in other words, Ohmic dissipation). In the other type, the resistivity plays an indirect but important role in energy conversion. The resistivity allows a change in the topology of field lines. A point-like merging of two anti-parallel magnetic field lines is called a magnetic reconnection. After the reconnection of the two field lines, the plasma on each line is accelerated by the Lorentz force (or the magnetic tension) and creates a strong bipolar flow along the original current sheet. In this case, we can clearly understand that resistivity is simply a trigger of energy conversion, and the main energy conversion is driven by the Lorentz force. Several models for energy conversion in the current sheet system have been presented over the past 40 years. We summarize four representative models of these in the following section.

2.1. *Diffusion region*

In order to achieve the merging of two magnetic field lines, the breaking of the frozen-in condition is necessary. This is equivalent to existence of the magnetic diffusion in the resistive plasmas. We call the region in which the reconnection occurs the "diffusion region." The diffusion region is defined as the region in which the magnetic diffusion speed is greater than the convection speed of the plasmas (in another word, $|\boldsymbol{v} \times \boldsymbol{B}| < \mu\eta|\boldsymbol{j}|$, where $\boldsymbol{v}$ is the convection speed, $\boldsymbol{B}$ is the magnetic field, μ is the magnetic permeability [we suppose its value is equal to the value for the vacuum, because we treat very thin plasma throughout this paper], η is the magnetic diffusivity and $\boldsymbol{j}$ is the current density). In many astrophysical problems, the current sheet system is filled with highly conducting plasmas. In such systems, the magnetic diffusion is efficient only inside a current sheet in which the spatial gradient of the magnetic field strength is large.

2.2. *Reconnection Rate*

When we argue the energy conversion through the reconnection, the key term is the reconnection rate which is a measure of the conversion speed of the system. The reconnection rate is usually

defined as the ratio of the Alfvén wave transit timescale across the system length to the energy conversion timescale. It is conventionally defined by the inflow Alfvén Mach number M_i. The energy source (fuel) of the process is the magnetic energy of the system. The "energy converter" (engine) is located in the current sheet. Hence, the energy conversion speed (power) is determined by how much magnetic energy is injected per unit time into the converter.

We should note that the magnetic flux is frozen into the highly conducting plasma, thus the conversion speed is in proportion to the inflow speed if other quantities are fixed. To make a non-dimensional parameter denoting the reconnection rate, we adopt the Alfvén speed outside the current sheet as the normalization quantity. Finally we can see that the inflow Alfvén Mach number M_i denotes the reconnection rate.

One of the most important questions about magnetic reconnection is what condition determines the reconnection rate, by which we can estimate the speed of energy conversion. Since reconnection can arise only in resistive plasmas, one may think that the reconnection rate mainly depends upon the magnetic Reynolds number R_m which represents the ratio of the diffusion timescale of the magnetic field to the Alfvén wave transit timescale. However, we should note that the magnetic diffusivity of astrophysical plasma systems is very small ($R_m \sim 10^{14}$ for the solar corona). This naturally leads us to the question of how the plasma system having such small resistivity can attain an effective energy conversion mechanism like in a solar flare. We review here the development of previous models of magnetic reconnection from the viewpoint of the reconnection rate.

2.3. *Simple Diffusion Model*

The most basic energy conversion in resistive plasmas is the Joule dissipation. We review here the model called the "simple diffusion model". The diffusion region spreads throughout the entire system in this model. This model does not include the process of magnetic reconnection, but it is important to understand the advantage of reconnection as an energy converter in comparison with the simple diffusion. This process can convert the magnetic energy of the current sheet system by diffusion and annihilation of anti-parallel field lines. So many researchers argue this process, the origin of this model is unclear. In lieu of the original research, we refer to a text by Tajima & Shibata (1997) as our reference.

Let us estimate the timescale for energy conversion by this process. We consider a box-shaped region involving a current sheet at the center (see figure 3). We set the scale of the box as L. The magnetic field strength is B and the mass density is ρ. These values are assumed to be uniform except in the current sheet. The magnetic diffusivity is η which is related to the conductivity σ as $\eta = 1/(\mu\sigma)$ where μ is the magnetic permeability. When the annihilation starts, the thickness of the current sheet increases due to the magnetic diffusion. At last, the thickness of the current sheet will grow to the system dimension L. We can clearly understand that the annihilation slows as the current sheet thickens. Therefore the timescale τ is determined by the slowest diffusion speed, and is estimated as $\tau_D = L^2/\eta$. On the other hand, this system has another timescale: the Alfvén transit time $\tau_A = L/V_A$ where $V_A \equiv B/\sqrt{\mu\rho}$ is the Alfvén speed. We can normalize the diffusion time as $R_m \equiv \tau_D/\tau_A = LV_A/\eta$, which is called the magnetic Reynolds number.

Let us evaluate for the case of the solar flare. The magnetic Reynolds number for the Spitzer resistivity is estimated as

$$R_m \sim 10^{14} \frac{(L/10^7[\mathrm{m}])(T/10^6[\mathrm{K}])^{3/2}(B/10^{-2}[\mathrm{T}])}{n/10^{15}[\mathrm{m}^{-3}]}, \tag{1}$$

where T is the temperature and n is the electron number density. In this case, the Alfvén transit time is estimated as $\tau_A \sim 10[\mathrm{s}]$ with $V_A \sim 10^6[\mathrm{m\ s}^{-1}]$. Thus we obtain the energy conversion timescale $\tau = \tau_D = R_m\tau_A \sim 10^{15}[\mathrm{s}] \sim 10^8[\mathrm{yr}]$ (the reconnection rate $M_i \sim 1/R_m \sim 10^{-14}$). However, the actual timescale of the solar flare is typically $10^2[\mathrm{s}]$. The energy conversion timescale of this model is obviously too long to explain the solar flare. Hence, we need a more efficient energy conversion model.

2.4. *Sweet-Parker Model*

The first model including the reconnection is presented by Sweet (1958) and Parker (1957, 1963). In order to increase the conversion speed, they induce the plasma inflow toward the current sheet (see figure 4). This inflow suppresses the increase in the current sheet thickness and

keeps it constant. Thus, annihilation speed does not decrease as time proceeds in contrast to the simple diffusion model. The magnetic field convected by the inflow can efficiently vanish in this way. However, the injected plasma cannot vanish like the magnetic field. This convected plasma is ejected along the original current sheet. In order to achieve this outflow, Sweet and Parker impose the reconnection of the convected magnetic field lines. The outflow is ejected by the tension of the reconnected field lines, and accelerated to almost Alfvén speed at the inflow region.

Here, we abbreviate a detailed discussion, but can obtain the resultant conversion timescale $\tau \sim \sqrt{R_m}\tau_A$. If we evaluate for the case of solar flares, we obtain $\tau \sim 10^8$[s] $\sim 10^1$[yr] (the reconnection rate $M_i \sim 1/\sqrt{R_m} \sim 10^{-7}$). The conversion speed is considerably improved compared with the simple diffusion model, but is still too slow for a relevant model of a solar flare.

2.5. *Petschek Model*

A completely different mechanism of energy conversion in the current sheet system is proposed by Petschek (1964). In the following, we argue the essence of this model and explain how it differs from the previous two models.

In the previous two models (the simple diffusion model and the Sweet-Parker model), the speed of energy conversion is mainly controlled by magnetic diffusion. Hence the conversion speed is very low for the case of an extremely large magnetic Reynolds number (this means very small resistivity) which is frequently encountered in astrophysical problems. The resultant timescale for energy conversion explicitly depends on the magnetic Reynolds number. We call such a process a "slow" process (another name is "magnetic combustion", because the timescale is determined by magnetic diffusion).

In the Petschek model, the main process of energy conversion is slow-mode wave propagation. An outline of the Petschek model is shown in figure 5. One must note the existence of a pair of slow-mode shocks (figure-X-shaped discontinuity along the current sheet). The inflow toward the current sheet collides with the original current sheet plasma. If the inflow speed is relevant, it creates a slow-mode shock. Outside and inside the figure-X-shaped slow shock are the up-stream and down-stream regions, respectively. From the nature of the slow shock, the magnetic field of the down-stream region is weakened. The released fraction of up-stream magnetic energy is converted mainly to kinetic energy of the bulk motion in the down-stream region. We must note that the slow shock is an accelerator, because it is a strong current layer, thus the Lorentz force (tension of the reconnected field line) makes a bipolar plasma jet along the original current sheet (the "sling-shot" mechanism). If the greater part of the magnetic energy is converted to the kinetic energy of the plasma jets, its speed is similar to the Alfvén speed in the inflow region.

We abbreviate again a detailed discussion of the energy conversion timescale of this model. The resultant timescale is $\tau \sim \log(R_m)\tau_A$. We should note that the timescale for energy conversion does not explicitly depend on the magnetic Reynolds number R_m (here "explicit" means dependence of a power function of R_m). We call this kind of highly efficient energy conversion a "fast process" (another name is "magnetic explosion", because the timescale is determined by wave propagation). The Petschek model is the first presented model of a fast process. This is easy to understand if we notice that the main conversion process of this model is not magnetic diffusion, but slow-mode wave propagation. The estimated timescale for typical solar flares is thus $\tau \sim 10^2$[s] (the reconnection rate is roughly estimated as $M_i \sim 1/\log R_m \sim 10^{-1}$: in detailed estimation by Vasyliunas [1975] results $M_i \sim 10^{-2}$) as a maximum value. This is good agreement with the actual flares.

However, its conversion speed is restricted by the nature of the inflow region as we see in the following discussion. We discuss here the theoretical optimization of energy conversion apart from its astrophysical interest. The inflow region of this model is altered from its original state by the fast-mode rarefaction wave emitted from the vicinity of the "X-point". Ejection of the bipolar reconnection jets results in a decrease in total pressure near the X-point, and hence the magnetic field near the X-point is weakened. This nature of fast-mode rarefaction suppresses the magnetic diffusion near the X-point. The greater the reconnection speed becomes, the more significant this rarefaction of the magnetic field becomes. This process naturally leads to a maximum reconnection speed. A detailed discussion appears in Vasyliunas (1975) and Priest & Forbes (1986), and the resultant maximum reconnection rate is

of the order of 10^{-2}. We should notice that the energy conversion itself is mainly carried by the slow shock, but this process is triggered and controlled by reconnection at the X-point. Hence, the fast-mode rarefaction nature limits the energy conversion speed.

2.6. *Sonnerup Model*

Sonnerup (1970) proposed a somewhat artificial model of the fast process which enables a higher energy conversion speed than does the Petschek model. The essence of the limitation of maximum conversion rate in the Petschek model is owing to the nature of the fast-mode rarefaction. In order to cancel the effect of fast-mode rarefaction, he considered adding the slow-mode rarefaction wave (the hybrid rarefaction, see figure 6) into the inflow region. In this hybrid rarefaction, a decrease in the magnetic field strength by fast-mode rarefaction is suppressed by the slow-mode rarefaction, compared with the Petschek model. The same situation is independently proposed by Yeh and Axford (1970) from their study of the spatial self-similar solution. Thus, the limitation of the maximum reconnection speed is canceled and we can attain a desirable conversion speed.

However, we should notice that the slow-mode rarefaction wave which is necessary to achieve this hybrid rarefaction cannot be emitted from the region near the X-point because the inflow region is up-stream from the slow shock. Hence this slow-mode rarefaction wave must be imposed by a boundary condition (an artificial edge is needed at the side boundary; see figure 6). In addition, that boundary condition must be tuned to achieve a situation in which the two wave fronts of this slow-mode rarefaction wave from both side boundaries cross precisely at the X-point. The majority thinks that such fine tuning is naturally impossible in astrophysical problems, and this model might be treated as simply a theoretical possibility.

2.7. *Driven Reconnection vs. Spontaneous Reconnection*

Hereafter we call reconnection with a fast process "fast reconnection." One of our main interests is to understand the essential control factor of fast reconnection. There are two historical roots with respect to this problem. One root is called "driven" reconnection. In models of driven reconnection, external circumstances control the system through boundary conditions. Another root is "spontaneous" reconnection. In models of spontaneous reconnection, the system controls itself spontaneously. We review here the essence of these roots and propose a new context: that of self-similar reconnection.

Numerical studies of magnetic reconnection as an elementary process were carried out by Japanese researchers in the late '70s. First, Ugai and Tsuda (1977) succeeded in obtaining a Petschek-like fast reconnection with their computer simulation. They supposed that localized resistivity is enhanced and kept constant in the middle of the current sheet. This is a model of anomalous resistivity. The entire simulation box is bounded by a so-called "free boundary" (normal derivatives of each quantity at the boundary are set to vanish). Hence, the system is controlled by resistivity and evolves spontaneously. After a period equal to the Alfvén transit time across the system scale, a pair of slow shocks is formed. The fast-mode rarefaction is dominant in the inflow region. These properties are anticipated by the Petschek model. Their numerical model is called "spontaneous reconnection".

Sato and Hayashi (1979) numerically studied fast reconnection, but their supposed situation was differed critically from that of Ugai and Tsuda (1977). There are two essential differences between Sato and Hayashi (1979) and Ugai and Tsuda (1977). Sato and Hayashi set the resistivity as an increasing function of the current density. They also set a boundary condition in which inhomogeneous plasma inflow is artificially injected toward the current sheet. As a result, resistivity is enhanced where strong inflow compresses the current sheet. The reconnection occurs and evolves to a Petschek-like structure (which is characterized by a pair of slow shocks). In this case, the inflow boundary condition crucially determines the resistivity, and hence the reconnection rate. Their numerical model is called an "(externally) driven reconnection".

Several theoretical models are reviewed by Priest and Forbes (1986) . They aimed to make a unified scheme of previous models from the viewpoint of the boundary problem. They considered stationary reconnection occurring in a rectangular shaped region, and obtained a family of solutions including the Petschek type and the Sonnerup type as particular cases. The conditions imposed on the inflow boundary determine which member

of the family occurs. These solutions vary continuously as a functional of the inflow boundary condition. We can see that their discussion is clearly focused on driven reconnection.

We clarify our standpoint here with respect to the controversy over differences between driven and spontaneous reconnection. Our discussion is focused on the evolution of time-dependent reconnection in a free space. In such a system, external circumstances corresponding to the boundary condition in previous works never influences, in principle. Hence, the reconnection system must grow spontaneously. The system will expand according to the wave propagation emitted from the central region. This expansion phase will continue, at least, while the fastest signal travels a proper length of the system. We try to find a solution for this expanding phase, and argue the property of this new type of spontaneous reconnection.

3. SCENARIO FOR EVOLUTIONARY PROCESS OF SELF-SIMILAR RECONNECTION

The scenario for the self-similar evolution of magnetic reconnection is summarized as follows. This paper extends in greater detail some of the themes already sketched in Nitta (1988).

We suppose a global MHD equilibrium for an anti-parallel magnetic field configuration with an embedded current sheet as the initial state. We apply Cartesian coordinates, whose x-axis is taken to be along the current sheet and y-axis is perpendicular to the current sheet. We assume uniformity in the z-direction and hence treat a two-dimensional MHD problem. Hereafter we study only the configuration on the $x-y$ plane.

The initial state is supposed to be the Harris solution (see figure 7),

$$B_x = B_0 \tanh(y/D) \,, \tag{2}$$

$$P = \frac{{B_0}^2}{2\mu}\left(\beta + \frac{1}{\cosh^2(y/D)}\right) \,, \tag{3}$$

where D is the initial thickness of the current sheet, B_0 the asymptotic strength of the magnetic field, P the gas pressure, and β the ratio of gas to magnetic pressure (so-called plasma β value) in the asymptotic region ($|y| \gg D$). We should remark again that our attention is focused on free evolution without any influence of the boundary conditions.

1) Onset of reconnection (resistive stage: $t \lesssim D/V_{A0}$)

When a microscopic disturbance takes place, a localized resistivity is enhanced in the current sheet (see figure 7). This resistivity induces magnetic diffusion, and anti-parallel magnetic field lines begin to reconnect. This stage will correspond to the Sweet-Parker type of reconnection or to the resistive tearing mode instability (Furth et al. 1963). Once the reconnection of field lines begins, the total pressure in the vicinity of the reconnection point should decrease owing to the ejection of a pair of bipolar plasma jets (reconnection jets) along the current sheet (see figure 8).

In a low-β plasma ($\beta \ll 1$ in the asymptotic region; this is the usual case in astrophysical problems), the propagation speed of the fast-magnetosonic wave is much higher than that of other wave modes. The information of decreasing total pressure near the reconnection point propagates almost isotropically as a fast-mode rarefaction wave (hereafter FRW) with a speed almost equal to the Alfvén speed V_{A0} in the asymptotic region ($|y| \gg D$). Hence the wave front of the FRW (hereafter FRWF) has a circular shape except near the point where the FRWF touches the current sheet.

2)Induction of the inflow ($t > D/V_{A0}$)

As the FRW propagates in the asymptotic region, the resultant total pressure gradient induces a plasma inflow toward the current sheet (see figure 9). Outside the FRWF, plasmas do not move because no signal reaches that region yet. Hence the expansion speed and the shape of the FRWF are kept constant throughout the evolution.

3)Self-similar evolution (self-similarly evolving fast reconnection stage: $t \gg D/V_{A0}$)

When the flow toward the current sheet develops sufficiently, a pair of slow-mode shocks forms along the current sheet. After formation of the slow shock, energy conversion is drastically enhanced. The greater part of the magnetic energy is converted at the slow shock. Hence this stage represents "fast reconnection". Once this system of fast reconnection is set up, the dimension of the

of the family occurs. These solutions vary continuously as a functional of the inflow boundary condition. We can see that their discussion is clearly focused on driven reconnection.

We clarify our standpoint here with respect to the controversy over differences between driven and spontaneous reconnection. Our discussion is focused on the evolution of time-dependent reconnection in a free space. In such a system, external circumstances corresponding to the boundary condition in previous works never influences, in principle. Hence, the reconnection system must grow spontaneously. The system will expand according to the wave propagation emitted from the central region. This expansion phase will continue, at least, while the fastest signal travels a proper length of the system. We try to find a solution for this expanding phase, and argue the property of this new type of spontaneous reconnection.

3. SCENARIO FOR EVOLUTIONARY PROCESS OF SELF-SIMILAR RECONNECTION

The scenario for the self-similar evolution of magnetic reconnection is summarized as follows. This paper extends in greater detail some of the themes already sketched in Nitta (1988).

We suppose a global MHD equilibrium for an anti-parallel magnetic field configuration with an embedded current sheet as the initial state. We apply Cartesian coordinates, whose x-axis is taken to be along the current sheet and y-axis is perpendicular to the current sheet. We assume uniformity in the z-direction and hence treat a two-dimensional MHD problem. Hereafter we study only the configuration on the $x-y$ plane.

The initial state is supposed to be the Harris solution (see figure 7),

$$B_x = B_0 \tanh(y/D) \ , \tag{2}$$

$$P = \frac{{B_0}^2}{2\mu}\left(\beta + \frac{1}{\cosh^2(y/D)}\right) \ , \tag{3}$$

where D is the initial thickness of the current sheet, B_0 the asymptotic strength of the magnetic field, P the gas pressure, and β the ratio of gas to magnetic pressure (so-called plasma β value) in the asymptotic region ($|y| \gg D$). We should remark again that our attention is focused on free evolution without any influence of the boundary conditions.

1) Onset of reconnection (resistive stage: $t \lesssim D/V_{A0}$)

When a microscopic disturbance takes place, a localized resistivity is enhanced in the current sheet (see figure 7). This resistivity induces magnetic diffusion, and anti-parallel magnetic field lines begin to reconnect. This stage will correspond to the Sweet-Parker type of reconnection or to the resistive tearing mode instability (Furth et al. 1963). Once the reconnection of field lines begins, the total pressure in the vicinity of the reconnection point should decrease owing to the ejection of a pair of bipolar plasma jets (reconnection jets) along the current sheet (see figure 8).

In a low-β plasma ($\beta \ll 1$ in the asymptotic region; this is the usual case in astrophysical problems), the propagation speed of the fast-magnetosonic wave is much higher than that of other wave modes. The information of decreasing total pressure near the reconnection point propagates almost isotropically as a fast-mode rarefaction wave (hereafter FRW) with a speed almost equal to the Alfvén speed V_{A0} in the asymptotic region ($|y| \gg D$). Hence the wave front of the FRW (hereafter FRWF) has a circular shape except near the point where the FRWF touches the current sheet.

2)Induction of the inflow ($t > D/V_{A0}$)

As the FRW propagates in the asymptotic region, the resultant total pressure gradient induces a plasma inflow toward the current sheet (see figure 9). Outside the FRWF, plasmas do not move because no signal reaches that region yet. Hence the expansion speed and the shape of the FRWF are kept constant throughout the evolution.

3)Self-similar evolution (self-similarly evolving fast reconnection stage: $t \gg D/V_{A0}$)

When the flow toward the current sheet develops sufficiently, a pair of slow-mode shocks forms along the current sheet. After formation of the slow shock, energy conversion is drastically enhanced. The greater part of the magnetic energy is converted at the slow shock. Hence this stage represents "fast reconnection". Once this system of fast reconnection is set up, the dimension of the

system indefinitely develops self-similarly (see figure 10).

This scenario for the evolution is confirmed by our numerical simulations. The outline and results of the simulations are shown in the next section.

4. NUMERICAL APPROACH

In order to demonstrate the feasibility of the self-similar evolution of magnetic reconnection, we try to study it by numerical simulation. We can see typical examples of self-similar evolution in free space in the following subsections.

4.1. *Outlines*

We simulate time evolution of the 2-D magnetic reconnection in free space (see figure 7). The initial equilibrium state is supposed to be expressed by the Harris solution (see section 3). We impose symmetry conditions on the lines $x = 0$ and $y = 0$ and find solutions for the quadrant $0 \leq x$ and $0 \leq y$. A locally enhanced resistivity is put at the center of the current sheet (i.e., in the region $0 \leq x \leq 2D$, $0 \leq y \leq 2D$ in figure 7). In this region, the value of resistivity is assumed to be uniform and is kept constant throughout the evolution.

Our attention is focused on such evolutionary processes as are free from the influence of outer boundary conditions. For this purpose, we place the outer boundaries as far from the reconnection region as possible and observe the evolution that takes place before any signal from the central region reaches the boundaries. To model such a wide simulation region, we adopt a non-uniform mesh as follows: In the vicinity of the diffusion region ($x, y \leq 20D$), the mesh size is $D/10$ in both the x and y directions to obtain a high spatial resolution. Outside this region, the mesh size increases exponentially in both x and y directions. The maximum mesh size is $30D$ in both directions (as a result, our mesh has a very long, slender shape at large distances along the $x-$ or $y-$ axis).

We use the 2-step Lax-Wendroff scheme with artificial viscosity to solve the following 2-D resistive MHD equations:

$$\frac{\partial \rho}{\partial t} + \boldsymbol{\nabla} \cdot (\rho \boldsymbol{v}) = 0, \tag{4}$$

$$\rho \frac{\partial \boldsymbol{v}}{\partial t} + \rho(\boldsymbol{v} \cdot \boldsymbol{\nabla})\boldsymbol{v} + \boldsymbol{\nabla} P = \boldsymbol{J} \times \boldsymbol{B}, \tag{5}$$

$$\frac{\partial \boldsymbol{B}}{\partial t} - \boldsymbol{\nabla} \times (\boldsymbol{v} \times \boldsymbol{B}) = -\boldsymbol{\nabla} \times (\mu\eta \boldsymbol{J}), \tag{6}$$

$$\frac{\partial e}{\partial t} + \boldsymbol{\nabla} \cdot [(e + P)\boldsymbol{v}] = \mu\eta |\boldsymbol{J}|^2 + \boldsymbol{v} \cdot \boldsymbol{\nabla} P \tag{7}$$

where ρ, $\boldsymbol{v}$, P, $\boldsymbol{B}$, η, e and $\boldsymbol{J}$ are the mass density, velocity, gas pressure, magnetic field, magnetic diffusivity, internal energy, and current density ($= \boldsymbol{\nabla} \times \boldsymbol{B}/\mu$), respectively. We use the equation of the state for ideal gas, i.e., $P = (\gamma - 1)e$ where γ is the specific heat ratio (=5/3).

4.2. *Parameters & Normalization*

The only parameters for this simulation are the plasma β value and the magnetic Reynolds number R_m. $\beta^{1/2}$ denotes the ratio of the Alfvén wave transit timescale to the sound transit timescale. Similarly, R_m denotes the ratio of the magnetic diffusion timescale to the Alfvén wave transit timescale. In most astrophysical problems, we can set β to be much smaller than unity (e.g., $\beta \sim 10^{-2}$ for solar corona). R_m is much larger than unity (e.g., $R_m \sim 10^{14}$ for solar flares if we estimate proper spatial scale by typical dimension of the magnetic flux tube; see equation 1).

However, the situation with $\beta \ll 1$ and/or $R_m \gg 1$ is very difficult to treat numerically, because we must solve the problem with a very wide dynamic range of timescales. Therefore, we choose moderate values as approximations for these parameters as follows (we call this a typical case or case A; see below).

$$\beta \equiv \frac{P_0}{{B_0}^2/8\pi} = 0.2 , \tag{8}$$

$$R_m \equiv \frac{V_{A0}}{\eta/D} = 24.5 , \tag{9}$$

where P_0, B_0 and V_{A0} are the gas pressure, magnetic field strength and Alfvén speed in the asymptotic region far from the current sheet (uniform in this region), respectively, and η is the magnetic diffusivity in the diffusion region ($x, y \leq 2D$, see figure 7).

One might think that the above adopted value for magnetic Reynolds number (24.5) is considerably apart from a realistic value ($\sim 10^{14}$; see equation [1]). We must note the difference of

system indefinitely develops self-similarly (see figure 10).

This scenario for the evolution is confirmed by our numerical simulations. The outline and results of the simulations are shown in the next section.

4. NUMERICAL APPROACH

In order to demonstrate the feasibility of the self-similar evolution of magnetic reconnection, we try to study it by numerical simulation. We can see typical examples of self-similar evolution in free space in the following subsections.

4.1. *Outlines*

We simulate time evolution of the 2-D magnetic reconnection in free space (see figure 7). The initial equilibrium state is supposed to be expressed by the Harris solution (see section 3). We impose symmetry conditions on the lines $x = 0$ and $y = 0$ and find solutions for the quadrant $0 \leq x$ and $0 \leq y$. A locally enhanced resistivity is put at the center of the current sheet (i.e., in the region $0 \leq x \leq 2D$, $0 \leq y \leq 2D$ in figure 7). In this region, the value of resistivity is assumed to be uniform and is kept constant throughout the evolution.

Our attention is focused on such evolutionary processes as are free from the influence of outer boundary conditions. For this purpose, we place the outer boundaries as far from the reconnection region as possible and observe the evolution that takes place before any signal from the central region reaches the boundaries. To model such a wide simulation region, we adopt a non-uniform mesh as follows: In the vicinity of the diffusion region ($x, y \leq 20D$), the mesh size is $D/10$ in both the x and y directions to obtain a high spatial resolution. Outside this region, the mesh size increases exponentially in both x and y directions. The maximum mesh size is $30D$ in both directions (as a result, our mesh has a very long, slender shape at large distances along the $x-$ or $y-$ axis).

We use the 2-step Lax-Wendroff scheme with artificial viscosity to solve the following 2-D resistive MHD equations:

$$\frac{\partial \rho}{\partial t} + \nabla \cdot (\rho \boldsymbol{v}) = 0, \tag{4}$$

$$\rho \frac{\partial \boldsymbol{v}}{\partial t} + \rho(\boldsymbol{v} \cdot \nabla)\boldsymbol{v} + \nabla P = \boldsymbol{J} \times \boldsymbol{B}, \tag{5}$$

$$\frac{\partial \boldsymbol{B}}{\partial t} - \nabla \times (\boldsymbol{v} \times \boldsymbol{B}) = -\nabla \times (\mu\eta \boldsymbol{J}), \tag{6}$$

$$\frac{\partial e}{\partial t} + \nabla \cdot [(e + P)\boldsymbol{v}] = \mu\eta |\boldsymbol{J}|^2 + \boldsymbol{v} \cdot \nabla P \tag{7}$$

where ρ, $\boldsymbol{v}$, P, $\boldsymbol{B}$, η, e and $\boldsymbol{J}$ are the mass density, velocity, gas pressure, magnetic field, magnetic diffusivity, internal energy, and current density ($= \nabla \times \boldsymbol{B}/\mu$), respectively. We use the equation of the state for ideal gas, i.e., $P = (\gamma - 1)e$ where γ is the specific heat ratio (=5/3).

4.2. *Parameters & Normalization*

The only parameters for this simulation are the plasma β value and the magnetic Reynolds number R_m. $\beta^{1/2}$ denotes the ratio of the Alfvén wave transit timescale to the sound transit timescale. Similarly, R_m denotes the ratio of the magnetic diffusion timescale to the Alfvén wave transit timescale. In most astrophysical problems, we can set β to be much smaller than unity (e.g., $\beta \sim 10^{-2}$ for solar corona). R_m is much larger than unity (e.g., $R_m \sim 10^{14}$ for solar flares if we estimate proper spatial scale by typical dimension of the magnetic flux tube; see equation 1).

However, the situation with $\beta \ll 1$ and/or $R_m \gg 1$ is very difficult to treat numerically, because we must solve the problem with a very wide dynamic range of timescales. Therefore, we choose moderate values as approximations for these parameters as follows (we call this a typical case or case A; see below).

$$\beta \equiv \frac{P_0}{{B_0}^2/8\pi} = 0.2\ , \tag{8}$$

$$R_m \equiv \frac{V_{A0}}{\eta/D} = 24.5\ , \tag{9}$$

where P_0, B_0 and V_{A0} are the gas pressure, magnetic field strength and Alfvén speed in the asymptotic region far from the current sheet (uniform in this region), respectively, and η is the magnetic diffusivity in the diffusion region ($x, y \leq 2D$, see figure 7).

One might think that the above adopted value for magnetic Reynolds number (24.5) is considerably apart from a realistic value ($\sim 10^{14}$; see equation [1]). We must note the difference of

the adopted spatial scales to estimate the magnetic Reynolds number between them. When we estimate the proper spatial scale by the entire system size ($\sim 10^7$[m] for solar flares), we obtain $R_m \sim 10^{14}$ for the Spitzer resistivity. However, we adopt here the current sheet thickness ($D \sim 10^0$[m] for solar flares) for the proper spatial scale. In addition, we suppose that an anomalous resistivity which is much larger, say, in 5 orders of magnitude than the Spitzer resistivity in the following simulations. Thus, the realistic value of magnetic Reynolds number is $\sim 10^2$ for solar flares, and we can understand that the above adopted value (24.5) is a good approximation.

We normalize physical quantities as follows: the constants V_{A0}, D and ρ_0 are used to normalize the dimensions [L T^{-1}], [L] and [M L^{-3}], respectively, where V_{A0} is the Alfvén speed and ρ_0 is the mass density in the asymptotic region. In the normalized units, the values of other physical quantities are expressed as $P_0 = 0.6$, $B_0 = 8.7$, $c_{s0} = 0.4$ and $\eta = 0.1$, where c_{s0} is the sound speed at the initial state (uniform in the simulation box).

We have performed numerical simulations for the following models. The main results discussed in the following sections are based on case A. Other cases are performed for comparison to the typical case A.

Case A: Typical case (figures 11, 13, 14, 15, 16, 17, 18, 19, 20, 32 and 33). Details are explained in the previous section.

Case A': Larger simulation box (figure 12). Mesh size is coarser than in the typical case in order to study the evolution subsequent to case A. The maximum mesh size is 100 in both directions. Other parameters are identical to those of the typical case. The initial condition is equal to case A.

Case B: Circular resistive region (Nitta 1988). The resistivity is distributed in a circular region ($r \leq 1$ where r is distance from the origin) as an exponentially decaying function of r with maximum value at the center.

Case C: Larger resistivity (figure 31). The diffusivity ($\eta = 0.5$) is larger than the typical case ($\eta = 0.1$). Other parameters are identical to those in the typical case.

Case D: Unmagnetized upper half region (figure 33 [dashed line]). As the initial condition, the lower half region ($y \leq 3000$) is filled with uniformly magnetized plasma, while the upper half ($y > 3000$) is unmagnetized. The magnetic field falls off as a tangent-hyperbolic function of y with the characteristic decaying scale of 1000. Other parameters are identical to those in the typical case.

4.3. *Simulation Results*

The most significant feature of our results is the self-similar expansion of the entire reconnection system, which means that a solution at a particular moment is the same as that in the past or in future if we change the spatial scaling in proportion to time from the onset. A sequence of six snapshots shown in figure 11 shows the time evolution of the reconnection system. The subsequent evolution (case A') is shown in figure 12 (to follow the evolution for a longer time, we adopted larger meshes than figure 11). Each figure represents a snapshot of the evolution at the denoted time. Note that the scale of both axes expands in proportion to time. We call this "zoom-out coordinates". The color contours of the magnetic pressure and the configuration of the magnetic field lines are shown in figures 11 and 12. The blue arc denotes the FRWF. The sequence in figures 11 and 12 clearly shows that the distribution of physical quantities (e.g., the magnetic pressure and the magnetic field lines) approaches a stationary solution in the zoom-out coordinates. As we will see, other quantities have the same property.

In order to remove the ambiguity of the term "self-similar evolution", let us consider the following situation: Let distribution of a physical quantity, say Q, be time-varying in the fixed coordinates (i.e., $Q = f[\boldsymbol{r}, t]$). When we measure the distribution of Q in the zoom-out coordinates, if $Q = g(\boldsymbol{r}')$ (where $\boldsymbol{r}' \equiv \boldsymbol{r}/[V_{A0}t]$ is the position vector from the origin [the center of the diffusion region] in the zoom-out coordinates, with $\boldsymbol{r}$ being the position vector in the original fixed coordinates) and is independent of the time, we can say that the distribution of Q is self-similarly expanding at speed V_{A0}. We have verified that our case is exactly the case of self-similar evolution. In our case, Q denotes any of the variables ρ, P, $\boldsymbol{v}$, $\boldsymbol{B}$, and any combination of these quantities (e.g., magnetic pressure, total pressure, etc.) Hence we can conclude that our result shows self-similar evolution.

Figure 13 shows the evolution of the velocity field. We can see the self-similar evolutionary character of this field. The upper panel shows the velocity field (red arrows) and the magnetic pres-

sure distribution (color contours) at $t = 2449.$, and the lower panel shows the distribution of the same quantities at $t = 8818.1$. These two panels look almost the same, except that the spatial scale is different.

Just after the onset of reconnection, the solution changes its form as time proceeds even if it is expressed in the zoom-out coordinates (i.e., $t \lesssim 1200$). The evolution during this stage depends significantly on the resistivity model. During the period much later than the onset (say, $t \gtrsim 1200$), the evolution gradually settles into the self-similar stage (stationary solution in the zoom-out coordinates). All of the physical quantities shown in figures 14 (density), 15 (gas pressure), 16 (B_x; the x-component of magnetic field), 17 (V_x; x-component of velocity) and 18 (V_y; the y-component of velocity) clearly show this relaxation to the self-similar stage. These figures represent the distribution of physical quantities in the zoom-out coordinates. Note that the scale of the horizontal axis varies in proportion to time. Also note that the location of x of the cross section placed parallel to the y-axis is also shifted in proportion to time ($x = 0.3V_{A0}t$; the yellow vertical line in figure 5). This procedure ensures that we take a cross section at the same place in the zoom-out coordinates. We can clearly see that the solution in the zoom-out coordinates is quasi-stationary. This is equivalent to saying that the evolution is self-similar. The reconnection system indefinitely grows self-similarly once the solution approaches the stationary solution in the zoom-out coordinates.

One may think that the estimated duration of time required for reaching the self-similar stage ($t \sim 1200$) is so much longer than in the Alfvén transit timescale, which is unity in our normalization. We should note that the formation of the slow shock is not caused by the FRW propagation itself but by the induced inflow. The speed of this inflow is found to be of the order of $10^{-2}V_{A0}$. Hence, the inflow transit timescale is of the order of 10^2 in the normalized time unit. The relaxation timescale of this flow may be estimated to be several times the inflow transit timescale. Thus, the period $t \sim 1200$ is comparable to the inflow relaxation timescale.

The detailed structure of the self-similar solution at $t = 8818$ is shown in figures 19 and 20. The color contours show the distributions of the total pressure (figure 19) and magnetic pressure (figure 20). The white lines are magnetic field lines. The red arrows show velocity vectors of plasmas. The blue arc denotes the FRWF. The velocity field inside the reconnection outflow is intentionally omitted to clarify the velocity structure of the inflow region.

In figure 20, we see the reconnection jet confined by the slow-mode shock along the current sheet ($y \sim 0$, $0 \leq x \lesssim 2000$). We can also see the plasmoid enclosed by the slow shock ($y \sim 0$, $2000 \lesssim x \lesssim 7000$). The magnetic energy is mainly converted at the slow shock. Hence, this is a "fast reconnection" similar to that in the Petschek model. The contours of the total pressure (see figure 19) represent the effect of the fast-mode wave propagation. The FRW is produced by the ejection of the reconnection jet. As the FRW propagates from the reconnection point ($x = y = 0$), the total pressure decreases in its vicinity (the blue region in figure 19). The resultant total pressure gradient induces inflow toward the reconnection point. This inflow slightly converges as it approaches the current sheet. Such convergence is a property of the fast-mode rarefaction-dominated inflow as pointed out by Vasyliunas (1975). These properties (slow shock formation and converging inflow) suggest that the central region of this reconnection system is indeed very similar to that of the Petschek model. However, we should note the following differences from the original Petschek model:

The ejected reconnection jet and the plasmoid propagate along the initial current sheet. This strong, dense flow of plasma produces a high total pressure region (red region in figure 19) near the spearhead of the plasmoid due to a "piston" effect (fast-mode compression). A vortex-like return-flow gushes out of this high total pressure region. This return-flow is the property of the evolution process that has not been pointed out in previous works. A fast-mode shock is formed in front of the plasmoid. A contact discontinuity is formed at the interface between the outflow driven by the reconnection and the plasmas in the initial current sheet. But we cannot identify these discontinuities in figures 19 and 20 since the scale of the discontinuities is very small compared to the total system length (see Abe & Hoshino 2001). To go into details about the structure of the reconnection jet and the plasmoid is beyond the scope of this paper.

4.4. *Summary of numerical study*

We have presented a new model for describing the evolutionary process of magnetic reconnection: the self-similar evolution model.

The possibility of this type of evolution has been demonstrated by numerical simulations. An outline of the evolutionary process has been given in section 3.

We should note that, in this new model, propagation of the fast-mode rarefaction wave (FRW) plays an important role in the self-similar expansion of the reconnection system. The FRW propagates almost isotropically at a constant speed of V_{A0} (the Alfvén speed in the asymptotic region) in the case of low β plasmas ($\beta \ll 1$). The only characteristic scale of the system at a later stage (the self-similar evolution stage, see figure 10) is the radius of the circular wave front of the FRW (FRWF) because the initial current sheet thickness D, which is a fixed characteristic scale, is negligible in comparison with the scale of the FRWF in this stage. This fact suggests the possibility of a self-similar solution. In fact, the results of our numerical simulation (see figures 11, 12) clearly show that the evolution settles into a stationary state if these results are expressed in the zoom-out coordinates (see section 4.3). This is equivalent to saying that such evolution is self-similar. Again, note that the self-similar evolution is achieved only in the last stage of evolution ($t \gg D/V_{A0}$), in which the fixed characteristic scale (D or the size of the resistive region) is negligible as compared to the system size (the radius $V_{A0}t$ of the FRWF). Of course, at that stage, the shape and size of the resistive region, which are artificially given in the model, no longer influence the evolution.

This new type of reconnection system represents "fast" reconnection. As the FRW propagates to the uniform region (the asymptotic region $y \gg D$), an inflow is induced by the decrease in total pressure near the reconnection point. Figure 20 clearly shows that a pair of slow shocks is formed by this induced flow toward the current sheet. These slow shocks efficiently convert magnetic energy to kinetic or thermal energy of plasma. Of course, the speed of this energy conversion is determined by the slow-mode wave speed, and is independent of the magnetic diffusion speed ($\propto {R_m}^0$). Hence, this energy release is a fast one, and we can call it fast reconnection.

5. ANALYTICAL APPROACH

The spatial dynamic range of the self-similar evolution verified by our simulation is restricted ($\sim 10^2$) for technical reasons. In order to ensure that the evolution we have discovered is truly a self-similar one, let us study this problem using an analytical method.

5.1. *Basic assumptions*

We focus our attention on the inflow region of the reconnection system that is spontaneously evolving without any influence from outer boundary conditions. Macroscopic aspects of this evolution are well described by fluid approximation; hence, we can use MHD equations for this research. In the fast reconnection models, resistivity plays an important role only in the diffusion region that is in the current sheet; thus, we can neglect the resistive effects in the inflow region. In the usual astrophysical plasma systems, the plasma-β value is very small (typically $\beta \sim 10^{-2}$ for the solar corona). Hence, we can assume that the system is filled with non-resistive and pressure-free (cold) plasmas (except, of course, inside the current sheet).

We study reconnection starting from an equilibrium state of a two-dimensional current sheet system with anti-parallel magnetic distribution, as in the Harris solution. As discussed in the previous section, the self-similar stage arises in a very late period ($V_{A0}t \gg D$). This means that the initial current sheet thickness D becomes negligible in comparison with the system size $V_{A0}t$. We can estimate only one system size using the fast-mode wave transit scale $V_{A0}t$. This is equivalent to assuming an infinitesimally thin current sheet.

In the case of Petschek-type reconnection, the resultant reconnection rate is of the order of 10^{-2}, which is consistent with our numerical simulation for self-similar fast reconnection (see section 4). We can expect a rather small reconnection rate in many cases. This means that the variation of physical quantities from initial equilibrium due to reconnection is very small, and we can treat such variation using a perturbation method.

5.2. *Zoom-out coordinates*

A "self-similar solution" can be regarded as a stationary solution in the "zoom-out coordinates system" that is defined as

$$\boldsymbol{r}' \equiv \boldsymbol{r}/(V_{A0}t) \ , \tag{10}$$

4.4. *Summary of numerical study*

We have presented a new model for describing the evolutionary process of magnetic reconnection: the self-similar evolution model.

The possibility of this type of evolution has been demonstrated by numerical simulations. An outline of the evolutionary process has been given in section 3.

We should note that, in this new model, propagation of the fast-mode rarefaction wave (FRW) plays an important role in the self-similar expansion of the reconnection system. The FRW propagates almost isotropically at a constant speed of V_{A0} (the Alfvén speed in the asymptotic region) in the case of low β plasmas ($\beta \ll 1$). The only characteristic scale of the system at a later stage (the self-similar evolution stage, see figure 10) is the radius of the circular wave front of the FRW (FRWF) because the initial current sheet thickness D, which is a fixed characteristic scale, is negligible in comparison with the scale of the FRWF in this stage. This fact suggests the possibility of a self-similar solution. In fact, the results of our numerical simulation (see figures 11, 12) clearly show that the evolution settles into a stationary state if these results are expressed in the zoom-out coordinates (see section 4.3). This is equivalent to saying that such evolution is self-similar. Again, note that the self-similar evolution is achieved only in the last stage of evolution ($t \gg D/V_{A0}$), in which the fixed characteristic scale (D or the size of the resistive region) is negligible as compared to the system size (the radius $V_{A0}t$ of the FRWF). Of course, at that stage, the shape and size of the resistive region, which are artificially given in the model, no longer influence the evolution.

This new type of reconnection system represents "fast" reconnection. As the FRW propagates to the uniform region (the asymptotic region $y \gg D$), an inflow is induced by the decrease in total pressure near the reconnection point. Figure 20 clearly shows that a pair of slow shocks is formed by this induced flow toward the current sheet. These slow shocks efficiently convert magnetic energy to kinetic or thermal energy of plasma. Of course, the speed of this energy conversion is determined by the slow-mode wave speed, and is independent of the magnetic diffusion speed ($\propto {R_m}^0$). Hence, this energy release is a fast one, and we can call it fast reconnection.

5. ANALYTICAL APPROACH

The spatial dynamic range of the self-similar evolution verified by our simulation is restricted ($\sim 10^2$) for technical reasons. In order to ensure that the evolution we have discovered is truly a self-similar one, let us study this problem using an analytical method.

5.1. *Basic assumptions*

We focus our attention on the inflow region of the reconnection system that is spontaneously evolving without any influence from outer boundary conditions. Macroscopic aspects of this evolution are well described by fluid approximation; hence, we can use MHD equations for this research. In the fast reconnection models, resistivity plays an important role only in the diffusion region that is in the current sheet; thus, we can neglect the resistive effects in the inflow region. In the usual astrophysical plasma systems, the plasma-β value is very small (typically $\beta \sim 10^{-2}$ for the solar corona). Hence, we can assume that the system is filled with non-resistive and pressure-free (cold) plasmas (except, of course, inside the current sheet).

We study reconnection starting from an equilibrium state of a two-dimensional current sheet system with anti-parallel magnetic distribution, as in the Harris solution. As discussed in the previous section, the self-similar stage arises in a very late period ($V_{A0}t \gg D$). This means that the initial current sheet thickness D becomes negligible in comparison with the system size $V_{A0}t$. We can estimate only one system size using the fast-mode wave transit scale $V_{A0}t$. This is equivalent to assuming an infinitesimally thin current sheet.

In the case of Petschek-type reconnection, the resultant reconnection rate is of the order of 10^{-2}, which is consistent with our numerical simulation for self-similar fast reconnection (see section 4). We can expect a rather small reconnection rate in many cases. This means that the variation of physical quantities from initial equilibrium due to reconnection is very small, and we can treat such variation using a perturbation method.

5.2. *Zoom-out coordinates*

A "self-similar solution" can be regarded as a stationary solution in the "zoom-out coordinates system" that is defined as

$$\boldsymbol{r}' \equiv \boldsymbol{r}/(V_{A0}t) \ , \tag{10}$$

where $\boldsymbol{r}$ is the position vector from the reconnection point in the conventional coordinate system (hereafter we call this the "fixed coordinates system") and $\boldsymbol{r}'$ is the position vector in the zoom-out coordinates system. One must note that V_{A0} in equation (10) represents the Alfvén speed in the asymptotic region far from the current sheet and is constant throughout the evolution. The term $\boldsymbol{r}'$ can be expressed as $\boldsymbol{r}' = x\boldsymbol{i}+y\boldsymbol{j}+z\boldsymbol{k}$, where the x-axis is parallel to both the current sheet and the initial anti-parallel magnetic field, the y-axis is perpendicular to the current sheet, and the z-axis is parallel to the current sheet but is perpendicular to the initial magnetic field (hence, ∂_z=0 in this two-dimensional problem). The origin of this coordinates system is at the reconnection point, which is chosen to be the center of the current sheet.

Let us express the MHD variables in a non-dimensional form. Note that we give a general formalism here, and hence gas pressure remains in the following equations (when we solve these equations actually, we will take the cold limit and neglect the pressure terms). We adopt the following normalization in this paper:

$$\boldsymbol{v} = V_{A0}(\boldsymbol{v}' + \boldsymbol{r}') \quad (11)$$

$$\rho = \rho_0 \cdot \rho'(\boldsymbol{r}') \quad (12)$$

$$\boldsymbol{B} = V_{A0}\sqrt{\mu_0\rho_0} \cdot \boldsymbol{B}'(\boldsymbol{r}') \quad (13)$$

$$P = \beta/2 \cdot \rho_0 {V_{A0}}^2 \cdot P'(\boldsymbol{r}') \quad (14)$$

where μ_0 is the magnetic permeability in a vacuum, and $\beta \equiv (C_{s0}/V_{A0})^2$ with C_{s0} being the sound speed in the asymptotic region. Note that we use SI units throughout this section.

5.3. *Non-dimensional MHD equations in zoom-out coordinates*

By using the above normalizations, the MHD equations in zoom-out coordinates can be put into the following non-dimensional form:

$$\boldsymbol{\nabla}' \cdot (\rho'\boldsymbol{v}') = -2\rho' \quad (15)$$

$$\boldsymbol{\nabla}' \cdot [\rho'\boldsymbol{v}'\boldsymbol{v}' - \boldsymbol{B}'\boldsymbol{B}' + \boldsymbol{I}(\beta P' + B'^2)/2] = -3\rho'\boldsymbol{v}' \quad (16)$$

$$\boldsymbol{\nabla}' \cdot (\boldsymbol{v}'\boldsymbol{B}' - \boldsymbol{B}'\boldsymbol{v}') = -\boldsymbol{B}' \quad (17)$$

$$P'\rho'^{-\gamma} = 1 \quad (18)$$

where $\boldsymbol{I}$ is the unit tensor and γ is the specific heat ratio.

The left-hand side of each equation is very similar to its counterpart in ordinary MHD equations (see equations [A7]-[A10]), but strange source terms appear on the right-hand side. These source terms appear as apparent effects in the zoom-out coordinates. We should note that our main focus is on the structure of the inflow region, which is located outside the diffusion region and upstream from the slow shock as in the Petschek model. Resistivity does not play any important role in the inflow region. Thus, we can use ideal (non-resistive) MHD equations. For simplicity, we adopt the polytropic relation instead of the full energy equation. The flow does not experience a violent entropy production in the inflow region (upstream of the slow shock). Thus, the polytropic variation is a good approximation in the inflow region.

5.4. *Perturbative expansion*

We treat here a slow energy conversion induced by magnetic reconnection. The word "slow" used here means a very small reconnection rate and should not be confused with what it denotes in the term "slow reconnection", which usually means an explicit dependence of the reconnection rate on the magnetic Reynolds number. As we found numerically, the self-similar reconnection that we wish to study is "fast" reconnection in the sense that the reconnection rate does not depend on the magnetic Reynolds number (at most, it depends logarithmically).

In such a case, deviation owing to reconnection from the initial state is very small in the inflow region. Hence, we can adopt the perturbative expansion method. We treat the quantities of the initial equilibrium state to be of the zeroth order, and any variation from it should be treated as a first order quantity. In this paper, our attention is focused on fundamental properties of self-similar reconnection; thus, we treat up to the first order variation. We can recognize that the small expansion parameter in this work is the reconnection rate.

We assume an anti-parallel two-dimensional magnetic distribution with an infinitesimally thin current sheet. Note that the self-similar stage is established in the case where there is no fixed proper length in the system. However, the system does have a fixed scale: the initial thickness D of the current sheet is finite. Thus, such a self-similar stage is reached only if $V_{A0}t \gg D$ (see

section 4.4).

This initial equilibrium state (uniform distribution) is expressed as

$$\boldsymbol{B}'_0 = \boldsymbol{i}\ , \tag{19}$$
$$\boldsymbol{v}'_0 = -\boldsymbol{r}'\ , \tag{20}$$
$$P'_0 = 1\ , \tag{21}$$
$$\rho'_0 = 1\ , \tag{22}$$

in the upper half-plane $y > 0$. The quantities having subscript 0 are the zeroth order quantities.

The first order quantities represent the deviation from the initial equilibrium. By substituting the expansion form of each quantity

$$\boldsymbol{B}' = \boldsymbol{B}'_0 + \boldsymbol{B}'_1\ , \tag{23}$$
$$\boldsymbol{v}' = \boldsymbol{v}'_0 + \boldsymbol{v}'_1\ , \tag{24}$$
$$P' = P'_0 + P'_1\ , \tag{25}$$
$$\rho' = \rho'_0 + \rho'_1\ , \tag{26}$$

together with equations (19) - (22) into the MHD equations (15)-(18) in the zoom-out coordinates, we obtain the equations for each order of magnitude. The zeroth order equations are satisfied automatically since the zeroth order quantities show the uniform equilibrium state (see Appendix B).

In order to solve the reconnection in a low-β plasma, let us take here the cold limit $\beta \to 0$.

We obtain the first order equations (see Appendix B),

$$\boldsymbol{\nabla}' \cdot \boldsymbol{v}'_1 - \boldsymbol{r}' \cdot \boldsymbol{\nabla}' \rho'_1 = 0\ , \tag{27}$$
$$-\boldsymbol{r}' \cdot \boldsymbol{\nabla}' \boldsymbol{v}'_1 - \boldsymbol{i} \cdot \boldsymbol{\nabla}' \boldsymbol{B}'_1 + \boldsymbol{\nabla}'(\boldsymbol{i} \cdot \boldsymbol{B}'_1) = 0\ , \tag{28}$$
$$\boldsymbol{r}' \cdot \boldsymbol{\nabla}' \boldsymbol{B}'_1 + \boldsymbol{i} \cdot \boldsymbol{\nabla}' \boldsymbol{v}'_1 - \boldsymbol{r}' \cdot (\boldsymbol{\nabla}' \rho'_1)\boldsymbol{i} = 0\ , \tag{29}$$
$$P'_1 = \gamma \rho'_1\ . \tag{30}$$

Note that even in the cold limit, the dimensionless gas pressure P' has a finite value (see equation [14]). When we obtain the value of dimensionless density ρ', we can easily obtain P' by equations (25) and (30). By solving these first order equations, we can obtain the self-similar solution.

5.5. *Linearized Grad-Shafranov equation*

We adopt the method of the Grad-Shafranov (G-S) equation. The above basic equations (27)-(30) show that every physical quantity can be expressed as a function of the z-component A'_1 of magnetic vector potential. Basic physical quantities are related to A'_1 in the following way (see Appendix C).

$$\boldsymbol{B}'_1 = \boldsymbol{\nabla}' \times A'_1 \boldsymbol{k} \tag{31}$$
$$v'_{1x} = 0 \tag{32}$$
$$v'_{1y} = x\frac{\partial A'_1}{\partial x} + y\frac{\partial A'_1}{\partial y} - A'_1 \tag{33}$$
$$\rho'_1 = \frac{\partial A'_1}{\partial y} \tag{34}$$
$$P'_1 = \gamma\frac{\partial A'_1}{\partial y} \tag{35}$$

where the subscript x and y denote the x- and y-components of the vector quantities.

By substituting these functional forms into the above linearized MHD equations (27)-(30), we can obtain the G-S equation for this linearized situation (see Appendix C):

$$(1-x^2)\frac{\partial^2 A'_1}{\partial x^2} - 2xy\frac{\partial^2 A'_1}{\partial x \partial y} + (1-y^2)\frac{\partial^2 A'_1}{\partial y^2} = 0\ . \tag{36}$$

In our zoom-out coordinates, the Alfvén wavefront (or the fast-mode wave front in the cold plasma limit $\beta \to 0$; [the FRWF]) emitted from the reconnection point is a unit circle. Hence, we solve the G-S equation inside the FRWF.

We should note that equation (36) is a Tricomi-type second-order partial differential equation. We refer to region $|\boldsymbol{r}'| < 1$ of the upper half-plane ($y > 0$) as the region R and $|\boldsymbol{r}'| > 1$ as $\bar{R}$. The equation is elliptic in R and hyperbolic in $\bar{R}$. Region R is affected by the FRW emitted from the diffusion region. In $\bar{R}$, there is no difference from the initial equilibrium state (uniform distribution), because no signal propagates here yet. We do not need to solve for region $\bar{R}$. Hence, in the following, we solve the elliptic equation (36) for R under boundary conditions at the FRWF and at the bottom boundary ($y = 0$, which is the junction surface to the reconnection jet).

It is convenient to rewrite the G-S equation (36) and the other relations (32)-(35) in polar coordinates (r, θ), because the boundary of the FRWF has a circular shape. We denote by $r \equiv \sqrt{x^2+y^2}$ the distance from the reconnection point $x = y = 0$ and by θ the angle in the $x-y$ plane from the x-axis (i.e., $\tan\theta = y/x$). The G-S equation and the other relations are rewritten as

$$r^2(1-r^2)\frac{\partial^2 A_1'}{\partial r^2}+\frac{\partial^2 A_1'}{\partial \theta^2}+r\frac{\partial A_1'}{\partial r}=0\ , \qquad (37)$$

and

$$v_{1x}' = 0 \qquad (38)$$

$$v_{1y}' = r\frac{\partial A_1'}{\partial r}-A_1' \qquad (39)$$

$$\rho_1' = \sin\theta\frac{\partial A_1'}{\partial r}+\frac{\cos\theta}{r}\frac{\partial A_1'}{\partial \theta} \qquad (40)$$

$$P_1' = \gamma\rho_1'\ . \qquad (41)$$

We solve the G-S equation (37) numerically in the region $r<1$, $0<\theta<\pi$ with boundary conditions at $r=1$ and $\theta=0,\ \pi$ (see next subsection).

5.6. *Boundary conditions*

At the FRWF ($r=1$), the deviation of any quantity from the initial equilibrium state must vanish (see equations [31]-[35] and [38]-[41]). Thus, $A_1'=const.$ and should be a C^1-class continuous function at $r=1$. Without any loss of generality, we can set $A_1'=0$ and $\partial_r A_1'=0$ on $r=1$.

Note that if we impose a Dirichlet type boundary condition $A_1'=0$ at $r=1$, another condition $\partial_r A_1'=0$ (this means $\boldsymbol{B}_1'=0$ at $r=1$) is automatically satisfied. This is easily understood from equation (37). The first two terms on the left-hand side vanish at $r=1$, then $\partial_r A_1'$ must vanish if these quantities are continuous at this point.

The boundary condition at $y=0$ is not trivial as at $r=1$. This boundary corresponds to the slow shock and is the interface between the inflow region and the shocked region (reconnection jet). We need a precise physical discussion to determine the junction condition for this boundary. Instead of solving this difficult problem, we set the boundary condition at this interface by adopting the result of our numerical simulation (see section 4).

Our previous simulation gives information for every quantity just outside the slow shock. We adopt the following simple functional form of A_1' approximating the boundary values of A_1' from our previous simulation,

$$A_1'(|x|, y=0)$$

$$= (-\frac{|x|}{x_c}+1)A_0 \qquad (42)$$

(for $|x|\le x_m$)

$$= \frac{x_m/x_c-1}{1-x_m}(|x|-1)A_0 \qquad (43)$$

(for $x_m<|x|<1$) .

where A_0 ($\ll 1$) is the value of A_1' at the reconnection point $x=y=0$ (this shows the reconnection rate v_{1y}' at $x=y=0$; see equation [33]), x_c is the location of the contact discontinuity (the interface between the original current sheet plasma and the reconnected inflow plasma), and x_m is the location of the minimum of A_1'. Thus, we have set a complete Dirichlet-type boundary problem for the linearized G-S equation (37). We set A_0, x_c and x_m to be consistent with our numerical simulation. For example, the figures shown in the next section are for the case $A_0=0.055$, $x_c=0.64$, $x_m=0.84$.

We compare the model boundary value defined above and the simulation result (case A in section 4.2) of A_1' along the slow shock in figure 21. The solid and dotted lines show the approximated model adopted here and the simulation result, respectively. The actual slow shock has a small tilt angle from the x-axis, so that, when plotting the simulation result (dotted line), we have projected the A_1' values obtained at the slow shock onto the x-axis. The two straight line segments constituting the model boundary condition have been determined in such a way that they pass the simulated values at the X-point ($x=0$, $A_1'=0.055$; this value represents the reconnection rate), at the contact point ($x=0.64$, $A_1'=0$; the vanishing A_1' corresponds to the contact point between the initial current sheet plasma and the inflow plasma), and at the minimum A_1' ($x=0.84$). We can see that the solid line approximates the dotted line reasonably well.

5.7. *Self-similar solution*

By using the SOR routine, we numerically solve the linearized G-S equation (37) under the Dirichlet type boundary condition as discussed in the previous section. A typical result ($A_0=0.055$, $x_c=0.64$, $x_m=0.84$; see the last section) is obtained in the figures 22 (A_1'), 24 (v_{1y}'), and 26 (ρ_1').

Let us compare the results of this semianalytic study with the results of our simulation in section 4. Figures 22, 24 and 26 are the semianalytic results showing the first order quantities solved here: the magnetic vector potential (z-component), velocity (y-component), and mass density, respectively. Figures 23, 25 and 27 show the numerical results in section 4: the variation from the initial equilibrium of the magnetic vector potential (z-component), velocity (y-component), and mass density, respectively. Each quantity is renormalized in the way explained in section 5.2 (see equations [10]-[14]). Small numbers affixed to some of the contours denote the level values at these points. We easily find that the results of the semianalytic study are consistent with the result of our numerical simulation, not only in the topological sense of contours, but also quantitatively.

In order to reinforce the above discussion, we compare profiles of magnetic vector potential (z-component), velocity (y-component) and mass density for the numerical solution and the semianalytic solution. Figures 28, 29 and 30 show profiles of the flux function (1st order), velocity field (y-component) and mass density (1st order) distribution at $x = 0.5$, respectively. The dashed line and the solid line in each figure show the numerical and semi-analytic solutions, respectively. We clearly can find that both solutions are fairly consistent near the FRWF ($y \sim 1$). As we discussed in section 5.4, we cannot adopt a perturbative method inside the reconnection jet ($y < 0.05$), because the deviation from the initial equilibrium is very large in that region.

Though outside the slow shock, the analytical solution gradually separates from the numerical solution as the inflow approaches the slow shock. This is owing to the following two reasons:

The first is concerned with a finite thickness of the reconnection jet. As we note in section 5.6, though the slow shock has a finite opening angle from the original current sheet, we have set a boundary condition which imitates the junction condition between the inflow and the reconnection jet at $y = 0$ to obtain the analytic solution. This necessarily results in a slight discrepancy between the numerical result and the analytic result near the slow shock. The locus of the slow shock at $x = 0.5$ is $y \sim 0.05$. Thus if we shift the curves for the analytic solution (solid line) toward the right with 0.05 of the graduation of the abscissa in figures 28 and 29, the discrepancy near the slow shock will almost vanish.

The second reason is an effect of the converging/diverging inflow induced by the fast-mode rarefaction/compression. We can see the converging inflow near the reconnection point in our numerical result (about $x < 4000$ of figure 19, which corresponds to $x < 0.4$ in the zoom-out coordinates). The diverging inflow also arises near the plasmoid (about $5000 < x < 7000$ of figure 19, which corresponds to $0.5 < x < 0.8$ in the zoom-out coordinates). As shown in equation (32), however, the $x-$component of the velocity is zero in the linear approximation, hence any effect of the converging or diverging inflow is neglected. This naturally leads to a discrepancy typically in the density distribution between the analytic result and the numerical result as follows: In the region near $x = 0.5$, the inflow diverges into a Petschek-like converging flow and a vortex-like return flow. Thus, the density indicated by the numerical result should be smaller than that in the analytic result which does not include any converging or diverging flow. If we take account of higher order terms in the analytic work, both results will coincide.

Here, we have succeeded in verifying that (1) the results of our numerical simulation (see section 4) truly represent a self-similar growth and (2) this self-similar growth is stable over a long duration. The spatial dynamic range of the numerical study is limited (at most $\sim 10^3$) by technical restrictions (e.g., restriction of memory and CPU time), but the fact that the results of the numerical simulation are consistent with the semianalytic solution suggests that the self-similar growth will continue indefinitely. On the other hand, the stability of the semianalytic solution with respect to any MHD mode is certified by the numerical simulation. We can say that our semianalytic study and numerical simulation complement each other.

5.8. *Summary of Semi-analytical study*

Together with our time-dependent numerical simulation (see section 4), the linearized perturbation solution discussed in this paper has ensured the existence of the self-similar growth of fast magnetic reconnection.

Thus, we propose here a new model describing the "self-similar evolution of fast reconnection." The time-dependent simulation directly solving the MHD equations numerically is effec-

tive for checking the stability of the evolving system. However, the duration of the simulation is restricted because of the restrictions of computer memory and run time or the stability of the simulation code itself. Hence, even if we find behavior resembling self-similarity in the simulation results, we cannot be convinced that this behavior is a true one that may continue indefinitely.

On the other hand, an analytical study has the following properties: If we solve the MHD equations in the zoom-out coordinates under the stationary assumption and obtain a (semi-) analytic solution that is identical to the solution of the numerical simulation, we can be convinced that the numerically obtained solution, which seems to be self-similar, is truly a self-similar one. On the other hand, an analytical study of the stationary equation does not give information on the stability of the solution.

From these arguments, we can reach the following conclusion: our time-dependent numerical study and analytical study complement each other in establishing a model of "self-similar evolution of fast reconnection."

6. DISCUSSION

6.1. *Conditions for self-similar reconnection*

The self-similar evolution of magnetic reconnection will be realized in systems in which (1) the initial spatial scale of the disturbance (e.g., scale of microscopic instabilities that will lead to anomalous transport phenomena, $\sim 10^0$ m if we estimate it by the ion Larmor radius in the typical case of solar flares) is much smaller than the entire spatial scale of the system (e.g., the curvature radius of the loop of a magnetic flux tube, $\sim 10^7 - 10^8$ m in the typical case of solar flares) and (2) there is no proper spatial scale except the one that linearly expands with time (e.g., the radius of the FRWF in our case). In such a system, the magnetic reconnection triggered by the initial disturbance can evolve as the FRW propagates (see section 3). The spatial scale of the FRW propagation is the unique proper scale of the system if it is much larger than the initial current sheet thickness. The spatial dynamic range of the evolution is determined by the ratio of the entire system scale to the initial disturbance scale. In the above-mentioned case of typical solar flares, it will be of the order of 10^7. In such a system, the external boundary does not affect the evolution for a certain amount of time after the onset of reconnection. This means that the system can freely evolve, independent of the outer boundary condition. Such a very wide dynamic range and only one evolving spatial scale strongly suggest the possibility of a self-similar solution. In fact, we have obtained a self-similar solution both numerically and analytically.

We can expect that the size and shape of the resistive region no longer influence the evolution, because the dimension of the resistive region is negligible as compared to that of the entire system. In fact, we can numerically confirm that evolution at the later stage is insensitive to the resistivity model (see figure 31 and section 6.2).

It is important to check whether such self-similar solutions are stable or not. We have verified by our numerical simulations that our self-similarly evolving solution is stable with respect to any MHD mode over $\sim 10^2$ of the spatial dynamic range of evolution.

Biernat, Heyn and Semenov (1987) and Semenov et al. (1992) analytically studied the evolutionary process of magnetic reconnection in a situation similar to that described in this paper. They treat the reconnection rate as a free parameter that can be varied arbitrarily as a function of time. From this perspective, the case they treated is also categorized as spontaneous reconnection. Their analysis gives a general formalism of spontaneous time-varying reconnection. However, in their works, plasma of the inflow region is assumed to be incompressible for analytical convenience. This means that the sound speed is infinitely high even when the Alfvén speed is finite. This is equivalent to assuming that the inflow region is filled with extremely high-β plasmas (note that $\beta \sim$ [sound speed]^2/ [Alfvén speed]^2). Needless to say, this assumption is unsuitable for most astrophysical problems. Contrary to our case, a fast-mode wave emitted from the central region instantly propagates to infinity. Although the proper spatial scale determined by the fast-mode wave propagation does not exist in the case of Biernat et al. (1987), there is a possibility that the structure formed by slow-mode waves can be self-similar, because the propagation speed of their slow-mode wave is finite. Our work is understood as an extension of their work on realistic low-β astrophysical plasma systems.

6.2. *Adequacy of resistivity model*

tive for checking the stability of the evolving system. However, the duration of the simulation is restricted because of the restrictions of computer memory and run time or the stability of the simulation code itself. Hence, even if we find behavior resembling self-similarity in the simulation results, we cannot be convinced that this behavior is a true one that may continue indefinitely.

On the other hand, an analytical study has the following properties: If we solve the MHD equations in the zoom-out coordinates under the stationary assumption and obtain a (semi-) analytic solution that is identical to the solution of the numerical simulation, we can be convinced that the numerically obtained solution, which seems to be self-similar, is truly a self-similar one. On the other hand, an analytical study of the stationary equation does not give information on the stability of the solution.

From these arguments, we can reach the following conclusion: our time-dependent numerical study and analytical study complement each other in establishing a model of "self-similar evolution of fast reconnection."

6. DISCUSSION

6.1. *Conditions for self-similar reconnection*

The self-similar evolution of magnetic reconnection will be realized in systems in which (1) the initial spatial scale of the disturbance (e.g., scale of microscopic instabilities that will lead to anomalous transport phenomena, $\sim 10^0$ m if we estimate it by the ion Larmor radius in the typical case of solar flares) is much smaller than the entire spatial scale of the system (e.g., the curvature radius of the loop of a magnetic flux tube, $\sim 10^7 - 10^8$ m in the typical case of solar flares) and (2) there is no proper spatial scale except the one that linearly expands with time (e.g., the radius of the FRWF in our case). In such a system, the magnetic reconnection triggered by the initial disturbance can evolve as the FRW propagates (see section 3). The spatial scale of the FRW propagation is the unique proper scale of the system if it is much larger than the initial current sheet thickness. The spatial dynamic range of the evolution is determined by the ratio of the entire system scale to the initial disturbance scale. In the above-mentioned case of typical solar flares, it will be of the order of 10^7. In such a system, the external boundary does not affect the evolution for a certain amount of time after the onset of reconnection. This means that the system can freely evolve, independent of the outer boundary condition. Such a very wide dynamic range and only one evolving spatial scale strongly suggest the possibility of a self-similar solution. In fact, we have obtained a self-similar solution both numerically and analytically.

We can expect that the size and shape of the resistive region no longer influence the evolution, because the dimension of the resistive region is negligible as compared to that of the entire system. In fact, we can numerically confirm that evolution at the later stage is insensitive to the resistivity model (see figure 31 and section 6.2).

It is important to check whether such self-similar solutions are stable or not. We have verified by our numerical simulations that our self-similarly evolving solution is stable with respect to any MHD mode over $\sim 10^2$ of the spatial dynamic range of evolution.

Biernat, Heyn and Semenov (1987) and Semenov et al. (1992) analytically studied the evolutionary process of magnetic reconnection in a situation similar to that described in this paper. They treat the reconnection rate as a free parameter that can be varied arbitrarily as a function of time. From this perspective, the case they treated is also categorized as spontaneous reconnection. Their analysis gives a general formalism of spontaneous time-varying reconnection. However, in their works, plasma of the inflow region is assumed to be incompressible for analytical convenience. This means that the sound speed is infinitely high even when the Alfvén speed is finite. This is equivalent to assuming that the inflow region is filled with extremely high-β plasmas (note that $\beta \sim$ [sound speed]^2/ [Alfvén speed]^2). Needless to say, this assumption is unsuitable for most astrophysical problems. Contrary to our case, a fast-mode wave emitted from the central region instantly propagates to infinity. Although the proper spatial scale determined by the fast-mode wave propagation does not exist in the case of Biernat et al. (1987), there is a possibility that the structure formed by slow-mode waves can be self-similar, because the propagation speed of their slow-mode wave is finite. Our work is understood as an extension of their work on realistic low-β astrophysical plasma systems.

6.2. *Adequacy of resistivity model*

In our simulation, localization and stationarity of resistivity are essential assumptions. Since resistivity cannot be derived from MHD equations, we must adopt for it a certain model. In the problem of magnetic reconnection in astrophysical plasmas, so-called anomalous resistivity plays a part in the magnetic diffusion. In order to make a realistic model, the physical process causing the anomalous resistivity is very important, but remains as an open question.

In addition, as discussed in section 2.7, there is room for discussion concerning two different points of view about influences of the resistivity on the evolution of magnetic reconnection. Even in a case in which resistivity does not play crucial roles ("driven" reconnection), there is a prediction that fast reconnection will never be attained in a system with uniformly distributed resistivity (Biskamp 1986, Scholer 1989, Yokoyama & Shibata 1994). On the other hand, in a case in which resistivity plays crucial roles ("spontaneous" reconnection), the reason resistivity can be localized is still unclear. We know neither the origin of resistivity nor its influence on the reconnection system.

Our opinion of the resistivity model is that localization and stationarity of the resistivity are essential for self-similar evolution, but the evolution does not depend upon the value of the resistivity, the size or shape of the resistive region or the physical process causing the resistivity.

In order to justify our opinion, we must compare our simulation results with other resistivity models. As an example of a different resistivity model (case B), we have performed the following exercise (Nitta 1988): We assume a circular resistive region $r \leq D$ in the current sheet, where r is the distance from the origin and D is the initial thickness of the current sheet. In this resistive region, the resistivity is distributed as an exponentially decaying function of r. Simulation with this resistivity model also results in self-similar evolution of magnetic reconnection.

Another example (case C) we have tested has a resistive region of the same shape as that of the previous case (resistivity uniformly enhanced in the central square region), but the value of the resistivity is five times larger ($\eta = 0.5$ thus $R_m = 4.9$) than in the previous case ($\eta = 0.1$ thus $R_m = 24.5$). The result (see figure 31) is very similar to that of the original case (see figure 11). The evolution does not depend crucially on the value of resistivity.

In conclusion, we cannot identify any essential difference among these three cases. Hence, we believe that any model with a localized resistivity and an infinitely large system size will result in self-similar evolution.

Magnetic reconnection requires some processes to maintain an electric field (reconnection electric field) along the reconnection line in order to break up the frozen-in condition. In the diffusion region of the plasma system with an extremely large magnetic Reynolds number like in astrophysical problems, macroscopic MHD approximation is no longer valid, and the reconnection electric field should be caused by microscopic processes. The three resistivity models we have examined above are all based on the Ohmic term $\mu\eta J$, where μ is the magnetic permeability, η is the magnetic diffusivity and J is the current density in the diffusion region. In these models, the localized resistivity $\mu\eta$ is supposed to represent anomalous resistivity induced by anomalous collision between particles and waves as a result of micro-instabilities (e.g., the lower hybrid drift [LHD] instability [Huba et al. 1977; Shinohara et al.1998; Shinohara et al. 1999]).

However, in actual plasma systems, the reconnection electric field might arise from other terms of generalized Ohm's law (Biskamp 1997). Several collisionless processes to maintain the reconnection electric field have been proposed (e.g., the Hall current effect [Ma & Bhattacharjee 1996], the electron inertia effect [Tanaka 1995], or the whistler turbulence effect [Shay & Drake 1998]). Unfortunately, we do not have a definite strategy for including a reconnection electric field such as that produced by the above-mentioned microscopic processes in the macroscopic MHD regime. Thus, we adopted a simplified resistivity form in our Ohm's law.

Of course, the actual resistivity in astrophysical plasma systems cannot be described by the simple Ohm's law adopted in our simulation, but our self-similar evolution requires only a contrivance to keep a finite electric field along the reconnection line. We should emphasize again that self-similar evolution occurs in the last stage when the system scale becomes much larger than the initial current sheet thickness and the size of the diffusion region. Hence, such evolution can be described by macroscopic MHD and does not depend upon whether the central resistivity is caused by collisional or

collisionless processes.

6.3. *Control factor of diffusion speed*

There is no doubt that magnetic reconnection is induced by the magnetic resistivity in the current sheet. The efficiency of the energy conversion in the reconnection system is controlled by the inflow speed (i.e., the reconnection rate, see 2.2) which is balanced with the magnetic diffusion speed. Thus, one may think that to reveal the microscopic physics of resistivity is essential to understanding the reconnection, or that the value of resistivity is responsible for determining the diffusion speed. We must realize, however, that the diffusion speed v_d is not described only by the magnetic diffusivity η but also by the current sheet thickness D as like $v_d = \eta/D$. The current sheet thickness is obviously a value determined by a certain macroscopic process. Let us focus our interest on the macroscopic aspect of magnetic diffusion.

The author believes the following conjecture, which is supported by a number of experiences of numerical simulations (see section 6.2): The current sheet thickness seems to be self-regulated by the reconnection system itself to keep the diffusion speed constant. If the resistivity is small, the current sheet thins and *vice versa*. Hence, the diffusion speed as a result of dynamical evolution is insensitive to the value of resistivity.

In the MHD (fluid) approximation, the thickness of the current sheet can be infinitesimally small. Hence, the diffusion speed can remain finite if the resistivity is very small as in most astrophysical problems. Of course, in actual plasma systems, the possible minimum value of the current sheet thickness is bound by a scale of the order of the ion Larmor radius ($\sim$ 1m for the solar corona). Hence, this self-adjusting mechanism might break down if the resistivity is extremely small.

The core of all the problems is what process determines the diffusion speed (which is equivalent to the inflow speed). This is still an open question, but the author believes that the key process is not microscopic, but macroscopic. Once the reconnection has started, the FRW emitted from the reconnection point induces the inflow. Hence, the inflow speed should depend upon the magnitude of the FRW that should be determined by macroscopic fluid physics. However, this question remains an important matter of future investigation.

6.4. *Comparison with previous stationary models*

There are several theoretical models for steady state magnetic reconnection. We compare our self-similar evolution model with these previous models. Our discussion is focused only on fast reconnection, because the very quick energy conversion frequently observed in astrophysical phenomena suggests that fast reconnection should be considered the responsible mechanism.

The Petschek model (Petschek 1964) is characterized by a pair of slow shocks and fast-mode rarefaction in the inflow region. This fast-mode rarefaction wave is produced in the central reconnection region. As a result of fast-mode rarefaction, the gradient of the magnetic field strength near the neutral point decreases because of the bending of the magnetic field lines (Vasyliunas 1975). This process limits the diffusion speed and hence the reconnection rate (see section 2.5).

The Sonnerup model (Sonnerup 1970) was developed from the Petschek model. This model is characterized by a pair of slow shocks and a hybrid of fast-mode and slow-mode rarefaction. The fast-mode rarefaction wave is produced in the central region as in the Petschek model, but the slow-mode rarefaction wave is injected from the boundary. Because of the hybrid nature of rarefaction, the gradient of the magnetic field strength near the neutral point does not decrease as the inflow approaches the slow shock as in the Petschek model. Therefore, the Sonnerup model can attain the maximum reconnection rate possible for magnetic energy converters (Priest & Forbes 1986).

Our self-similar evolution is never influenced by the boundary conditions, so Sonnerup-type hybrid rarefaction does not take place at all in our case. Fast-mode rarefaction dominates in the vicinity of the diffusion region. As discussed in section 4.3, the central region of this self-similarly evolving system is of the Petschek-type. Therefore, the reconnection rate will be limited in a way similar to the original Petschek model. This point will be clarified in our future work.

Far from the central region, there is a region in which fast-mode compression takes place by the piston effect of the reconnection jet and the plasmoid. This fast-mode compression causes a vortex-like return flow (see figure 19). We can consider that this self-similar evolution includes the Petschek model as the inner solution. A

combined feature of the original Petschek model and the vortex-like flow properly characterizes the evolutionary process, and the entire system indefinitely expands self-similarly.

6.5. *Consistency between semianalytic and numerical studies*

In section 5.7, we compared our semianalytic result with our numerical result and notice significant similarity between them.

If we compare them quantitatively in detail, we notice that these two results are consistent in the region in which $v'_{1y} < 0$ (inflow region). However, in the region in which $v'_{1y} > 0$ (return flow region), the value of the semianalytic result is somewhat different from the numerical result. In this region, strong fast-mode compression (the "piston effect" of the reconnection jet) takes place, and, strictly speaking, our linearized treatment might not be suitable for application to the return flow region.

Thus, we can conclude that the inflow region is well described by our linearized theory. This is obviously due to the very small reconnection rate ($\sim 10^{-2}$; see Nitta et al. 2001). However, the mechanism leading to such a small reconnection rate is still unclear. In this self-similar reconnection model, the reconnection rate should be self-consistently determined by the dynamical evolution process. This point will be discussed in our future work.

6.6. *Near the FRWF*

The region near the FRWF ($r \sim 1$) actually has a complicated nature. The region near the spearhead of the reconnection jet (roughly, $r \sim 1$, $0 < \theta < \pi/8$) is influenced not only by the fast-mode rarefaction wave but also by the fast-mode compression wave induced by the "piston effect" of the jet. Hence, one might think that the term "FRWF" (fast-mode *rarefaction* wave front) is somewhat misleading.

However, we should notice that, in our linearized treatment, any nonlinear interaction between waves is completely neglected. Thus, the fast-mode rarefaction wave emitted from the vicinity of the reconnection point maintains a circular shape that is truly located at $r = 1$ in the zoom-out coordinates even if the compressional mode is superimposed. For this reason, we can continue to call it "FRWF".

6.7. *Boundary with reconnection jet*

In our analytic work, the boundary condition at $y = 0$, which corresponds to the junction condition to the reconnection jet, is artificially imposed, approximating the result of our numerical simulation. Needless to say, this boundary condition is more important than other boundary conditions (e.g., conditions at $r = 1$ or $\theta = \pi/2$), because it represents physical information about the reconnection jet and it crucially influences the solution of the inflow region. The process which determines this boundary condition will be treated in our future work.

One might think that the similarity of the boundary condition at $y = 0$ is not trivial and that the above boundary condition is imposed *ad hoc*. However, we must note that everything evolves self-similarly in this situation. In the self-similar stage $V_{A0}t \gg D$, the entire reconnection system including the reconnection jet has no proper length other than the scale of the FRWF $V_{A0}t$. Thus, it naturally follows that the reconnection jet itself will grow self-similarly, and hence the similarity growth of the reconnection jet is accomplished.

6.8. *Relation to driven model and spontaneous model*

We consider our self-similar reconnection model in comparison with the "driven" and "spontaneous" reconnection models. System size of the self-similar reconnection is determined by the size of the FRWF. In principle, the self-similar phase will continue until a signal from outside the FRWF reaches the system. Such a signal may occur in the following way: If the FRWF propagates into a non-homogeneous region, e.g., the boundary of the flux tube, the system will be influenced. If some waves from external circumstances come into the system, it will influence the evolution. Our discussion is focused on a case such that the evolution in a homogeneous region which is free from any influence of external circumstances. Hence, if we consider the entire system of our self-similar reconnection, the property of that evolutionary process must be spontaneously determined. From this point of view, our model is clearly a spontaneous reconnection model.

However if we focus our scope on an inner region having a fixed spatial scale in the vicinity of the diffusion region, we will see another aspect of

the self-similar model. For example, we consider a rectangular region with a fixed finite dimension around the X-point. The physical state of this inner region settles to a final state as the scale of the FRWF exceeds the scale of this region, even while the entire system continues to evolve. Such a situation of the inner region can be treated as a stationary solution for magnetic reconnection. Let us compare the property of this inner region with previously presented stationary reconnection models:

As we mentioned in section 4.3, the property of the inner region is quite similar to the original Petschek model which is characterized by the presence of the figure-X-shaped slow shock and the fast-mode rarefaction-dominated inflow. The entire system is spontaneously determined by the system itself, but the inner solution coincides with a particular solution (the Petschek-type) of the driven model.

We should note that the inflow toward the inner region is spontaneously determined by a self-consistent process of the self-similar evolution. One might think that the inflow toward the inner region may act as inflow injected by the boundary condition as in the driven reconnection model. If we tune the inflow boundary condition to a condition exactly equivalent to the flow expected from our self-similar model, the resultant solution of the inner region should be the same. This trivial fact shows that our self-similar solution of the inner region is particular to the driven model while the entire region is rather different from previous models.

6.9. *Applications to solar flares*

We discuss here the possibility of observation. The propagation speed of the FRW is estimated to be $\sim 10^6$ [m s^{-1}] for solar corona. Hence, the duration of the self-similar evolution is $10^1 - 10^2$[s]. Evolution having such a timescale will resolvable by the *Solar-B* project (required cadence of the *Solar-B* X-ray telescope [XRT] is 2 sec., which is sufficient to resolve the expected time evolution of the self-similar reconnection, see Golub 2000.).

This study has been motivated by the fact that actual reconnection has a very wide spatial dynamic range of evolution; in the case of geomagnetospheric substorms or solar flares; the dynamic range is $10^4 - 10^7$. Therefore, the early stage of evolution of magnetic reconnection can be approximated as evolution into free space without any influence of boundary conditions. This approximation is justified as long as the spatial scale of the reconnection system is much smaller than that of the entire system (e.g., the radius of curvature of the initial magnetic field lines). In the case of large solar flares, the typical radius of curvature is $\sim 10^{7-8}$ m and the typical Alfvén speed is $\sim 10^6$ m s^{-1}. Hence, we can predict from our self-similar model that during the interval $\sim 10^{7-8}/10^6 \sim 10^{1-2}$ s from the onset of magnetic reconnection, the evolution can be approximated by our self-similar evolution model, and the total power, integrated over the entire system, of the energy conversion increases in proportion to time. The author expects that coming observations by *Solar-B* will detect such phenomena.

Another property of our self-similar model is the characteristic structure of the inflow region. A vortex-like flow around the head of the plasmoid characterizes the evolutionary process (see figure 19). We may be able to verify our evolutionary model by detecting this kind of vortex flow.

It has recently been found that solar flares (and similar arcade formation events) are often associated with depletion of ambient plasma density, called "dimming", during their main energy release phase (Tsuneta 1996; Sterling and Hudson 1997). Tsuneta (1996) attributed this to the result of reconnection inflow (see also Yokoyama and Shibata 1997), while Sterling and Hudson (1997) interpreted it as being due to plasma ejection from the system. In the case of a large cusp-shaped flare (Tsuneta 1996), the timescale of the dimming is 10-20 minutes just at the onset of the flare, which is about 7-14 t_A (where t_A is the Alfvén transit time), and the ratio of depleted density to the initial density is ~ 0.2 during this period. Let us examine the possibility that the fast rarefaction wave associated with the reconnection inflow can account for the observed dimming at the onset of flares. In figure 32, a predicted X-ray image (in relative measure) of the reconnection system is shown. This figure is drawn from the result of case A. The temperature range is assumed to be $10^7 - 10^8$ K, which is plausible for solar flares. We can clearly find that a round dark region around the reconnection point expands as the FRW propagates isotropically. Our simulation results shown in figure 32 show that the ratio of depleted density to the ini-

tial density in the rarefaction wave is of the order of 0.1-0.2, consistent with observations (see figure 14).

In actual reconnection systems, the spatial scale (say L) of the region in which magnetic flux is piled up should be finite. This region is an energy reservoir of magnetic reconnection. Although the timescale of strict self-similar evolution in the bounded system ($L = finite$) is the Alfvén time ($t_A \equiv L/V_{A0}$), our self-similar evolution (especially near the reconnection point) may hold longer than the Alfvén time (up to a few to 10 t_A; see figure 33) even if the system is not in an exactly free space. The solid line in figure 33 shows the time variation of the electric field ($\mu\eta|\boldsymbol{J}|$) at the reconnection point ($x = y = 0$) for the typical case (case A). The intensity of the electric field is a measure of the reconnection rate of the system. The dashed line (case D) shows the reconnection rate for a case in which the lower half region ($y \leq 3000$) is filled with uniformly magnetized plasma, while the upper half region ($y > 3000$) is unmagnetized. In case D, the fast mode wave is reflected at the boundary at $y = 3000$ ($t = 3000$), and returns to the resistive region at $t = 6000$. Hence, the physical difference between these cases (case A and D) will appear after $t = 6000$. Figure 33 shows that the difference is only a few percent, and moreover, we cannot detect any significant difference between these two cases even after the reflected wave returns to the current sheet ($t \geq 6000$).

Consequently, basic characteristics (density and timescale) of a fast-mode rarefaction wave in a self-similar evolution of fast reconnection seem to account for observations of dimming associated with solar flares.

6.10. *Future outlook*

1) development to 3-D self-similar reconnection model

Our present discussion is restricted, for the sake of simplicity, to 2-D reconnection, in this as well as in the previous paper (Nitta et al. 2001). This model is plausible for a case in which resistivity enhancement is infinitely elongated in the z direction, perpendicular to the figures in this paper. However, actual current sheet systems have finite depth in the z direction (for example, radius of the flux tube or length of the arcade structure of a bunch of flux tubes). In such cases, reconnection might be triggered by a "point" -like resistivity enhancement. We must treat the evolution of such a system as a three-dimensional problem.

We can expect that self-similar growth also takes place in a 3-D system. As discussed in section 4.4, a sufficiently evolved system has only one proper spatial scale, i.e., the scale of the FRWF $V_{A0}t$, which is increasing in proportion to time (note that the propagation speed of the fast-mode is almost isotropic in a 3-D current sheet system filled with a low β plasma, hence the shape of the FRWF will be spherical). This is exactly the sort of situation that leads to self-similar expansion. Of course, detailed structure of the 3-D reconnection system will be different from that of our 2-D model, but essential properties will be common to both of them. Differences of 3-D evolution from the 2-D self-similar evolution model will be treated as a future problem.

We believe, however, our knowledge of 2-D self-similar reconnection obtained here is valuable even in 3-D situations, and the essence of self-similar growth has already been understood by our 2-D approximation. When we discuss the phenomenology of evolutionary reconnection by virtue of a self-similar reconnection model in the near future, we will need a more precise 3-D model.

2) elongated diffusion region

We discussed here a situation in which the diffusion region has finite and fixed spatial dimensions in the fixed coordinate. In such a case, we can treat the diffusion region as a point-like singularity in the self-similar stage. Thus, we obtained a self-similar solution having Petschek-like central structure. However, we must realize that geometrical shape and spatial dimension of the diffusion region will strongly depend upon a resistivity model which has not been derived from any discussion based on MHD. We do not yet have any reliable model of anomalous resistivity.

In the field of magnetic reconnection, the majority believes that anomalous resistivity plays important roles in the diffusion region. In many studies of MHD reconnection, anomalous resistivity is supposed to be an increasing function of the current density. We can expect that if the resistivity increases as a Hevyside function of current density with a large threshold value, the resultant diffusion region would have a pointed shape and

be located at the site of maximum inflow speed. On the other hand, if the resistivity moderately increases as a function of current density, the resultant diffusion region will elongate along the current sheet. Thus we can expect the resistivity model will strongly affect the resultant self-similar solution.

We note that current density is roughly proportional to current sheet thickness, and this thickness is controlled by the inflow speed toward the current sheet. Thus we can expect that if the inflow speed exceeds a threshold value, the resistivity is switched on at that point and behaves as a diffusion region. In the self-similar reconnection model, the distribution of this inflow speed is stationary in the zoom-out coordinates. Thus, it is possible to realize that the size of the diffusion region is fixed in the zoom-out coordinates. This means the length of the diffusion region linearly increases as the time proceeds. As discussed in Priest & Forbes (1986), the relative length of the diffusion region compared with the entire system size is very important in categorizing the solutions. If the size of the diffusion region is very small compared to the entire system size, it should be similar to the Petschek-like solution discussed in this thesis. On the other hand, if the size of the diffusion region is comparable to that of the entire system, the solution may be similar to the Sweet-Parker solution. This notion of an elongated diffusion region suggests that actual reconnection can be understood by continuous solutions ranging between the Petschek and Sweet-Parker solutions. This should provide a new unified scheme of spontaneous MHD reconnection.

We must note that such an elongated diffusion region might be unstable for some kinds of macroscopic instabilities (e.g., tearing-mode instability). This is an open question. We need a precise numerical simulation in order to check this kind of non-linear time evolution.

The author supposes the elementary process to enhance anomalous resistivity might not be unique, and each process might, case by case, enhance proper resistivity which has a proper dependence upon the current density. According to the difference of the enhanced resistivity, the resultant solution can vary to make various reconnection models.

Needless to say, the connection between the macroscopic physics of MHD reconnection and the microscopic physics of the origin of resistivity is very important. Indeed, we need a mesoscopic picture in order to understand the physics of the diffusion region. However, this is still unclear and such a mesoscopic study is very difficult at present. Such difficulty stimulates our theoretical effort to understand the complete physics of magnetic reconnection. I have a dream that one day I will establish a complete theory of astrophysical magnetic reconnection. My challenge has only just begun!

APPENDIX

APPENDIX A: DERIVATION OF MHD EQUATIONS IN ZOOM-OUT COORDINATES

We show the derivation of equations (15)-(18) briefly in this appendix. The zoom-out coordinates are defined by equation (10). The velocity in these new coordinates has been given in equation (11). This equation is deformed to

$$V_{A0}\boldsymbol{v}' = \boldsymbol{v} - V_{A0}\boldsymbol{r}' \ . \tag{A1}$$

The second term on the right-hand side is the apparent converging flow properly appearing in zoom-out coordinates. Physical quantities are put into nondimensional forms as in equations (11)-(14). With these preparations, we can derive the modified MHD equations in zoom-out coordinates.

Any scalar field, e.g., $f(\boldsymbol{r}, t)$ is transformed into zoom-out coordinates as $f(\boldsymbol{r}'[\boldsymbol{r}, t], t)$. Thus, the time derivative of any scalar field can be transformed as

$$\left.\frac{\partial f}{\partial t}\right|_{\boldsymbol{r}} = \left.\frac{\partial f}{\partial t}\right|_{\boldsymbol{r}'} + \frac{\partial \boldsymbol{r}'}{\partial t}\cdot\boldsymbol{\nabla}' f \tag{A2}$$

$$= \left.\frac{\partial f}{\partial t}\right|_{\boldsymbol{r}'} - \frac{1}{t}\boldsymbol{r}'\cdot\boldsymbol{\nabla}' f \tag{A3}$$

be located at the site of maximum inflow speed. On the other hand, if the resistivity moderately increases as a function of current density, the resultant diffusion region will elongate along the current sheet. Thus we can expect the resistivity model will strongly affect the resultant self-similar solution.

We note that current density is roughly proportional to current sheet thickness, and this thickness is controlled by the inflow speed toward the current sheet. Thus we can expect that if the inflow speed exceeds a threshold value, the resistivity is switched on at that point and behaves as a diffusion region. In the self-similar reconnection model, the distribution of this inflow speed is stationary in the zoom-out coordinates. Thus, it is possible to realize that the size of the diffusion region is fixed in the zoom-out coordinates. This means the length of the diffusion region linearly increases as the time proceeds. As discussed in Priest & Forbes (1986), the relative length of the diffusion region compared with the entire system size is very important in categorizing the solutions. If the size of the diffusion region is very small compared to the entire system size, it should be similar to the Petschek-like solution discussed in this thesis. On the other hand, if the size of the diffusion region is comparable to that of the entire system, the solution may be similar to the Sweet-Parker solution. This notion of an elongated diffusion region suggests that actual reconnection can be understood by continuous solutions ranging between the Petschek and Sweet-Parker solutions. This should provide a new unified scheme of spontaneous MHD reconnection.

We must note that such an elongated diffusion region might be unstable for some kinds of macroscopic instabilities (e.g., tearing-mode instability). This is an open question. We need a precise numerical simulation in order to check this kind of non-linear time evolution.

The author supposes the elementary process to enhance anomalous resistivity might not be unique, and each process might, case by case, enhance proper resistivity which has a proper dependence upon the current density. According to the difference of the enhanced resistivity, the resultant solution can vary to make various reconnection models.

Needless to say, the connection between the macroscopic physics of MHD reconnection and the microscopic physics of the origin of resistivity is very important. Indeed, we need a mesoscopic picture in order to understand the physics of the diffusion region. However, this is still unclear and such a mesoscopic study is very difficult at present. Such difficulty stimulates our theoretical effort to understand the complete physics of magnetic reconnection. I have a dream that one day I will establish a complete theory of astrophysical magnetic reconnection. My challenge has only just begun!

APPENDIX

APPENDIX A: DERIVATION OF MHD EQUATIONS IN ZOOM-OUT COORDINATES

We show the derivation of equations (15)-(18) briefly in this appendix. The zoom-out coordinates are defined by equation (10). The velocity in these new coordinates has been given in equation (11). This equation is deformed to

$$V_{A0}\boldsymbol{v}' = \boldsymbol{v} - V_{A0}\boldsymbol{r}' \ . \tag{A1}$$

The second term on the right-hand side is the apparent converging flow properly appearing in zoom-out coordinates. Physical quantities are put into nondimensional forms as in equations (11)-(14). With these preparations, we can derive the modified MHD equations in zoom-out coordinates.

Any scalar field, e.g., $f(\boldsymbol{r}, t)$ is transformed into zoom-out coordinates as $f(\boldsymbol{r}'[\boldsymbol{r}, t], t)$. Thus, the time derivative of any scalar field can be transformed as

$$\left.\frac{\partial f}{\partial t}\right|_{\boldsymbol{r}} = \left.\frac{\partial f}{\partial t}\right|_{\boldsymbol{r}'} + \frac{\partial \boldsymbol{r}'}{\partial t}\cdot\boldsymbol{\nabla}' f \tag{A2}$$

$$= \left.\frac{\partial f}{\partial t}\right|_{\boldsymbol{r}'} - \frac{1}{t}\boldsymbol{r}'\cdot\boldsymbol{\nabla}' f \tag{A3}$$

where the subscripts $\boldsymbol{r}$ and $\boldsymbol{r}'$ show the time derivative in fixed and zoom-out coordinates, respectively, and $\boldsymbol{\nabla}'$ denotes the spatial derivative with respect to $\boldsymbol{r}'$. Here we have used (10) to derive the second equality. The transform of the time derivative for any vector field is similar to this.

The gradient of any scalar field is transformed as

$$\nabla f|_{\boldsymbol{r}} = \frac{1}{V_{A0}t}\boldsymbol{\nabla}' f \ . \tag{A4}$$

The divergence and rotation of any vector field, e.g., $\boldsymbol{A}$ are transformed as

$$\nabla \cdot \boldsymbol{A} = \frac{1}{V_{A0}t}\boldsymbol{\nabla}' \cdot \boldsymbol{A} \tag{A5}$$

$$\nabla \times \boldsymbol{A} = \frac{1}{V_{A0}t}\boldsymbol{\nabla}' \times \boldsymbol{A} \ , \tag{A6}$$

respectively. By using these transformed notations, we can rewrite the MHD equations as follows:

$$\frac{\partial \rho}{\partial t} + \nabla \cdot (\rho \boldsymbol{v}) = 0 \ \ \text{(continuity eq.)} \tag{A7}$$

$$\frac{\partial (\rho \boldsymbol{v})}{\partial t} + \nabla \cdot \left(\rho \boldsymbol{v}\boldsymbol{v} - \frac{1}{\mu_0}\boldsymbol{B}\boldsymbol{B} \right) + \nabla \left(P + \frac{\boldsymbol{B}^2}{2\mu_0} \right) = 0 \ \ \text{(momentum eq.)} \tag{A8}$$

$$\frac{\partial \boldsymbol{B}}{\partial t} + \nabla \cdot (\boldsymbol{v}\boldsymbol{B} - \boldsymbol{B}\boldsymbol{v}) = 0 \ \ \text{(induction eq.)} \tag{A9}$$

$$P\rho^{-\gamma} = const. \ \ \text{(polytrope relation)} \tag{A10}$$

As a representative case, we will demonstrate the derivation of the modified continuity equation. The derivations for the other modified MHD equations are quite similar to this.

The original continuity equation

$$\left.\frac{\partial \rho}{\partial t}\right|_{\boldsymbol{r}} + \nabla \cdot (\rho \boldsymbol{v}) = 0 \tag{A11}$$

is transformed to

$$\left.\frac{\partial \rho}{\partial t}\right|_{\boldsymbol{r}'} - \frac{\boldsymbol{r}'}{t} \cdot \boldsymbol{\nabla}' \rho + \frac{1}{V_{A0}t}\boldsymbol{\nabla}' \cdot (\rho \boldsymbol{v}) = 0 \ . \tag{A12}$$

Here we suppose stationariness in the zoom-out coordinates (self-similar expansion). This makes the first term vanish. By substituting the normalization relations (11)-(14) into this transformed equation, we easily obtain the following equation:

$$\boldsymbol{r}' \cdot \boldsymbol{\nabla}' \rho' - \boldsymbol{\nabla}' \cdot [\rho' (\boldsymbol{v}' + \boldsymbol{r}')] = 0 \ . \tag{A13}$$

This equation is expanded to the form

$$-\boldsymbol{\nabla}' \rho' \cdot \boldsymbol{v}' - \rho' \boldsymbol{\nabla}' \cdot \boldsymbol{v}' - \rho' \nabla' \cdot \boldsymbol{r}' = 0 \ . \tag{A14}$$

We combine the first two terms to obtain $-\boldsymbol{\nabla}' \cdot (\rho' \boldsymbol{v}')$. We should note that in the two-dimensional problem, $\boldsymbol{\nabla}' \cdot \boldsymbol{r}' = 2$. Thus, we finally obtain the transformed continuity equation (15).

Similarly, we can easily obtain the other modified equations (16)-(18). Each derivation is not difficult, but is very tedious; hence, we omit detailed derivation here.

APPENDIX B: PERTURBATIVE RELATIONS

By assuming that the deviation by reconnection from the initial equilibrium state is very small, we derive the linearized relations. We expand each quantity approximately as in equations (23)-(26) with (19)-(22) and substitute them into the modified MHD equations (15)-(18). We obtain the linearized MHD equations as demonstrated below.

For example, we will demonstrate the derivation of the linearized continuity equation (27). The derivation of other linearized MHD equations is quite similar. We substitute the expansion forms (26) and (24) into the modified continuity equation (15). By expanding equation (15) up to the first order of magnitude, we obtain two equations: a zeroth order equation

$$\boldsymbol{\nabla}' \cdot (\rho_0' \boldsymbol{v_0}') = -2\rho_0' \tag{B1}$$

and a first order equation

$$\boldsymbol{\nabla}' \cdot (\rho_0' \boldsymbol{v_1}' + \rho_1' \boldsymbol{v_0}') = -2\rho_1' \ . \tag{B2}$$

The left hand side of the zeroth order equation is reduced to

$$\begin{aligned} \boldsymbol{\nabla}' \cdot (\rho_0' \boldsymbol{v_0}') &= \boldsymbol{\nabla}' \cdot (-\boldsymbol{r}') && \text{(B3)} \\ &= -2 \ . && \text{(B4)} \end{aligned}$$

The right hand side of this equation is -2. Thus, we can see that the zeroth order equation is trivial and contains no information. The left hand side of the first order equation is reduced to

$$\begin{aligned} \boldsymbol{\nabla}' \cdot (\rho_0' \boldsymbol{v_1}' + \rho_1' \boldsymbol{v_0}') &= \boldsymbol{\nabla}' \cdot \boldsymbol{v_1}' + \boldsymbol{\nabla}' \cdot (-\rho_1' \boldsymbol{r}') && \text{(B5)} \\ &= \boldsymbol{\nabla}' \cdot \boldsymbol{v_1}' - \boldsymbol{r}' \cdot \boldsymbol{\nabla}' \rho_1' - \rho_1' \boldsymbol{\nabla}' \cdot \boldsymbol{r}' \ . && \text{(B6)} \end{aligned}$$

By noting that the last term is $-2\rho_1'$ and together with the right-hand side, we obtain the linearized continuity equation (27). By similar reduction, we obtain the other linearized equations (28)-(30).

APPENDIX C: DERIVATION OF THE GRAD-SHAFRANOV EQUATION AND OTHER RELATIONS

We show here the reduction of equations (32)-(35). Let us start with the deformation of the linearized momentum equation (28). Each term of that equation is reduced as follows:

$$-\boldsymbol{i} \cdot \boldsymbol{\nabla}' \boldsymbol{B}_1' = -\frac{\partial^2 A_1'}{\partial x \partial y} \boldsymbol{i} + \frac{\partial^2 A_1'}{\partial x^2} \boldsymbol{j} \tag{C1}$$

$$\boldsymbol{\nabla}' (\boldsymbol{i} \cdot \boldsymbol{B}_1') = \frac{\partial^2 A_1'}{\partial x \partial y} \boldsymbol{i} + \frac{\partial^2 A_1'}{\partial y^2} \boldsymbol{j} \tag{C2}$$

$$-\boldsymbol{r}' \cdot \boldsymbol{\nabla}' \boldsymbol{v}_1' = -\left(x \frac{\partial v_{1x}'}{\partial x} + y \frac{\partial v_{1x}'}{\partial y} \right) \boldsymbol{i} - \left(x \frac{\partial v_{1y}'}{\partial x} + y \frac{\partial v_{1y}'}{\partial y} \right) \boldsymbol{j} \ . \tag{C3}$$

Then we obtain the reduced form of each component of equation (28) as

$$x \frac{\partial v_{1x}'}{\partial x} + y \frac{\partial v_{1x}'}{\partial y} = 0 \ , \tag{C4}$$

$$-\left(x \frac{\partial v_{1y}'}{\partial x} + y \frac{\partial v_{1y}'}{\partial y} \right) + \left(\frac{\partial^2}{\partial x^2} + \frac{\partial^2}{\partial y^2} \right) A_1' = 0 \ . \tag{C5}$$

Similarly, from the linearized induction equation (29), we obtain the following two equations:

$$x \frac{\partial^2 A_1'}{\partial x \partial y} + y \frac{\partial^2 A_1'}{\partial y^2} - \frac{\partial v_{1y}'}{\partial y} = 0 \ , \tag{C6}$$

$$x\frac{\partial^2 A'_1}{\partial x^2} + y\frac{\partial^2 A'_1}{\partial y \partial x} - \frac{\partial v'_{1y}}{\partial x} = 0 \ . \tag{C7}$$

We should note that these two equations from the induction equation have in common the information in

$$x\frac{\partial A'_1}{\partial x} + y\frac{\partial A'_1}{\partial y} - A'_1 - v'_{1y} = (\text{const. independent of } x,\ y) \ . \tag{C8}$$

The vector potential A'_1 has the freedom of an indeterminate constant; thus, the constant on the right-hand side can be absorbed into the potential, and we obtain equation (33).

We substitute the two components (C6) and (C7) of the induction equation into (C5) and obtain a single partial differential equation (36) for A'_1 after simple calculations. This is the G-S equation.

Another component of the momentum equation (C4) is transformed into a simple form:

$$\boldsymbol{r}' \cdot \boldsymbol{\nabla}' v'_{1x} = 0 \ . \tag{C9}$$

This equation clearly shows that v'_{1x} depends only on the angle θ from the x-axis. We should remember that $v'_{1x} = 0$ at $r' = 1$ (the FRWF). Thus, this equation implies $v'_{1x} = 0$ everywhere in our linearized analysis. This is equation (32).

The linearized continuity equation (27) is deformed using the above results. The first term is reduced with the help of equation (C6) as

$$\boldsymbol{\nabla}' \cdot \boldsymbol{v}'_1 = \frac{\partial v'_{1y}}{\partial y} \tag{C10}$$

$$= x\frac{\partial^2 A'_1}{\partial x \partial y} + y\frac{\partial^2 A'_1}{\partial y^2} \tag{C11}$$

$$= \boldsymbol{r}' \cdot \boldsymbol{\nabla}' \frac{\partial A'_1}{\partial y} \ . \tag{C12}$$

Together with the second term of equation (27), we can see that the continuity equation implies

$$\boldsymbol{r}' \cdot \boldsymbol{\nabla}' \left(\frac{\partial A'_1}{\partial y} - \rho'_1\right) = 0 \ . \tag{C13}$$

Similarly to the discussion of the previous paragraph, we obtain result (34) because we have set the boundary condition $\partial A'_1/\partial y = 0$ and $\rho'_1 = 0$ at the FRWF. Relation (35) is easily obtained from equation (30).

APPENDIX

REFERENCES

Abe, S.A., Hoshino, M., 2001, Earth Planets Space, 53, 663

Biernat, H.K., Heyn, M. & Semenov, V.S., 1987, JGR, 92, A4, 3392

Biskamp, D. 1986, Phys. Fluids, 29, 1520

Biskamp, D., 1997, Phys. Plasmas, 4 (5), 1964

Furth,H.P., Killeen,J., Rosenbluth,M.N., 1963, Phys.Fluids, 6, 459

Golub,L., 2000, "XRT Science Objectives in The 2nd Solar-B Science Meeting", P.47

Hayashi,M.R., Shibata,K., Matsumoto,R., 1999, proc of "Star formation 1999", P.288

Huba, J. D., Gladd, N. T. & Papadopoulos, K., 1977, GRL, 4, 125

Koyama,K., Maeda,Y., Ozaki,M., Ueno,S., Kamata,Y., Tawara,K., Skinner, S. & Yamauchi,S., 1994, PASJ, 46, L125

Koyama,K., Makishima,K., Tanaka,Y., & Tsunemi,H., 1986, PASJ, 38, 121

Ma, Z. W. & Bhattacharjee, A., 1996, GRL, 23, 1673

Nitta, S. 1988, Master thesis, Nagoya University (in Japanese)

Nitta, S., Tanuma, S., Shibata, K., Maezawa, K., 2001, ApJ, 550, 1119

Nitta, S., Tanuma, S., Maezawa, K., 2001, ApJ, 580, 538
Parker, E. N. 1963, ApJ Suppl. Ser., 8,177
Petschek,H.E. 1964, NASA Spec. Publ., 50, AAS-NASA Symposium on Physics of Solar Flares, 425
Priest,E.R. & Forbes,T.G. 1986, J.Geophys.Res, 91, 5579
Sato,T. & Hayashi,T. 1979, Phys.Fluids, 22, 1189
Scholer, M. 1989, JGR, 94, 8805
Semenov, V. S., Kubyshkin, I. V., Lebedeva, V. V., Rijnbeek, R. P., Heyn, M. & Biernat, H. K., 1992, Planet. Space Sci., 40, 63
Shay, M. A. & Drake, J. F., 1998, GRL, 25, 3759
Shinohara, I., Nagai, T., Fujimoto, M., Terasawa, T., Mukai, T., Tsuruda, K. & Yamamoto, T., 1998, JGR, 103, 20365
Shinohara, I. & Hoshino, M., 1999, Adv. in Space Res., 24, 43
Sonnerup, B. U. Ö, J. Plasma Phys. 1970, 4, 161
Sterling, A. C. & Hudson, H. S. 1997, ApJ 491 L55
Sweet, P. A. 1958, The neutral point theory of solar flares, in Electro-magnetic Phenomena in Cosmical Physics, ed. B.Lehnert (Cambridge University Press, London), 123
Tajima, T. & Shibata, K. 1997, Plasma Astrophysics (Reading, Massachusetts: Addison-Wesley), 223
Tanaka, M., 1995, Phys. Plasmas, 2, 2920
Tanuma,S., Yokoyama,T., Kudoh,T., Matsumoto,R., Shibata,K.& Makishima,K., 1999, PASJ, 51, 161
Tsuda,T. & Ugai,M. 1977, J. Plasma Phys., 18, 451
Tsuneta, S. 1996, ApJ, 456, 840 [erratum see ApJ, 464, 1055]
Ugai,M. & Tsuda,T. 1977, J. Plasma Phys., 17, 337
Ugai,M. & Tsuda,T. 1979, J. Plasma Phys., 22, 1
Ugai,M. 1999, Phys. Plasmas, 6, 1522
Vasyliunas,V.M. 1975, Rev.Geophys., 13, 303
Yokoyama,T. 1995, PhD thesis
Yokoyama, T. & Shibata, K. 1994, ApJ, 436, L197
Yokoyama, T. & Shibata, K. 1997, Fifth SOHO Workshop: The Corona and Solar Wind Near Minimum Activity. held at Institute of Theoretical Astrophysics. University of Oslo, Norway, 17-20 June, 1997. Edited by A. Wilson, European Space Agency, p.745

FIG. 1.— Reconnection in solar flares. Typical cases of reconnection in solar flares are shown. The solid lines show the magnetic field line. We find a current sheet system around the X-points in each panel. This figure is from Yokoyama (1995), courtesy of Dr. Yokoyama.

FIG. 2.— Geomagnetospheric reconnections. Thin solid lines with small arrows show the magnetic field lines. Thick arrows show the plasma flow. When the solar wind convects the southward magnetic field, the current sheet will be formed on the day-side of the geomagnetosphere (gray circle). At this point, a field line originating from the Earth reconnects with a field line of the solar wind, and changes its topology to open field lines. The reconnected field lines are convected to the night-side of the Earth, and accumulate to make a current sheet system (gray circle on night-side). The stored magnetic energy in the night-side region will be released by magnetic reconnection. This night-side reconnection induces a substorm. During this time, we can expect auroral activity around the magnetic poles of the Earth.

FIG. 3.— The simple diffusion model. Magnetic field lines (solid lines) are shown. In the lower panel, we can see the effect of magnetic diffusion (the thickening of the current sheet). By this process, magnetic energy in the system is converted to thermal energy due to Ohmic heating.

FIG. 4.— The Sweet-Parker model. Magnetic field lines (solid lines) and plasma flows (thick arrows) in the Sweet-Parker model are shown. The hatched region shows the diffusion region. The presence of the inflow suppresses the extension of the current sheet. Reconnected field lines eject the plasmas on the field line by Lorentz force.

FIG. 5.— The Petschek model. Magnetic field lines (solid lines) and plasma flows (thick arrows) in the Petschek model are shown. The hatched small region near the X-point is the diffusion region. The slow shocks are shown by dotted lines.

FIG. 6.— The Sonnerup model. Magnetic field lines (solid lines), plasma flows (thick arrows) and discontinuities (dotted lines) in the Sonnerup model are shown. The hatched small region near the X-point is the diffusion region. The Sonnerup model requires the corners to set the boundary condition producing slow-mode rarefaction waves. We can see that magnetic field strength near the X-point does not weaken in contrast to the Petschek model.

FIG. 7.— The simulation box and the initial state. We set the x axis of our Cartesian coordinates along the current sheet and the y axis perpendicular to the current sheet. We treat a 2-D MHD problem and assume uniformity in the z-direction. An artificially imposed resistive region is placed near the origin, and the resistivity is held constant (the diffusivity $\eta = 0.1$ in our dimensionless unit in the region $0 \leq x \leq 2D$, $0 \leq y \leq 2D$, and $\eta = 0$ outside). The initial state is the Harris solution, so physical quantities in the asymptotic region far outside the current sheet are uniform.

FIG. 8.— Schematic scenario of the evolutionary process.
1): Resistive stage ($t < D/V_{A0}$). When resistivity is locally enhanced in the current sheet, the magnetic field lines begin to reconnect, and a flow field is induced as in the Sweet-Parker model or in resistive tearing instability. Ejection of bipolar plasma flow (reconnection jets) causes a decrease in the total pressure around the reconnection point, and a fast-mode rarefaction wave (FRW) is emitted from the diffusion region.

FIG. 9.— 2): Induction of inflow ($t \gtrsim D/V_{A0}$). When the fast-mode rarefaction wave front (FRWF) propagates into the asymptotic region (the uniform region at $y \gg D$), the difference in the total pressure between the diffusion region and the FRWF induces the inflow. This inflow is slightly converging. This feature is characteristic of the fast-mode rarefaction dominated inflow.

FIG. 10.— 3): Self-similar evolution stage ($t \gg D/V_{A0}$). When the inflow sufficiently evolves, the inflow speed exceeds the slow mode propagation speed, and a pair of slow-mode shocks is formed along the current sheet. Once this show shock is formed, energy conversion by reconnection proceeds drastically (the fast reconnection). We should remark that this fast reconnection system continues to expand self-similarly and indefinitely as the FRWF propagates.

FIG. 11.— A sequence of six snapshots representing the evolutionary process of magnetic reconnection. The color contours denote the magnetic pressure distribution. The blue arc denotes the fast-mode rarefaction wave front (FRWF). The system self-similarly evolves after $t \sim 1224.7$ (case A).

FIG. 12.— Evolution subsequent to the sequence in figure 11. The mesh size for this figure is rougher than that of figure 11. We can clearly see that the self-similar evolution continues over a large spatial dynamic range (case A').

FIG. 13.— Velocity distribution in the inflow region at different times ($t = 2449$ and $t = 8818.1$). The velocity vectors are shown by red arrows on the background color contours of the magnetic pressure. We cannot see any essential difference between these two panels except for the spatial scaling. This indicates self-similarity of evolution of the velocity field. The velocity field inside the reconnection outflow is intentionally omitted to clarify the velocity in the inflow region, because it is much larger than the inflow velocity (case A).

FIG. 14.— Density profile along the y axis in the zoom-out coordinates (x coordinate expands in proportion to time). The profile gradually settles to a stationary state. We can roughly estimate the relaxation time scale as $t \sim 1200$. The depleted density in the rarefaction wave is of the order of 0.1-0.2 times the initial density (case A).

FIG. 15.— Gas-pressure profile along the y axis in the zoom-out coordinates. Obvious step-like feature near $x \sim 0.009$ is the Petschek-type slow shock (case A).

FIG. 16.— Magnetic field (x-component) profile along the y axis in the zoom-out coordinates. Obvious step-like feature near $x \sim 0.009$ is the Petschek-type slow shock (case A).

FIG. 17.— Velocity field (x-component) profile along the y axis in the zoom-out coordinates. Obvious step-like feature near $x \sim 0.009$ is the Petschek-type slow shock (case A).

FIG. 18.— Velocity field (y-component) profile along the y axis in the zoom-out coordinates. Obvious step-like feature near $x \sim 0.009$ is the Petschek-type slow shock. These profiles of physical quantities (figures 14, 15, 16, 17 and 18) clearly show that the solution is quasi-stationary in the zoom-out coordinates. This is equivalent to the presence of self-similar evolution (case A).

FIG. 19.— Detailed structure of the self-similar solution. The total pressure distribution is shown by color contours. The effects of the fast-mode wave are apparent in this figure. The effect of the fast-mode rarefaction wave (FRW) is clearly seen near the reconnection point. The piston effect (the fast-mode compression) takes place near the spearhead of the plasmoid. The inner structure near the reconnection point is quite similar to the Petschek model (case A).

FIG. 20.— Detailed structure of the self-similar solution. The magnetic pressure distribution is shown as color contours. The effects of the slow-mode wave are apparent in comparison with figure 19. A pair of slow-mode shocks, the reconnection jet, and the plasmoid are clearly shown (case A).

FIG. 21.— Boundary condition of A_1' along the slow shock ($y = 0$). The dotted line shows the result of our simulation in section 4 (Case A). The solid line is the approximated boundary condition adopted in this work. We can see the approximated model is very simple and gives good agreement with the simulation result.

FIG. 22.— Contours of the perturbed flux function (z-component of magnetic vector potential) A_1'. The contours show field lines for the first order magnetic field. The solid (dashed) contours correspond to the positive (negative) value of A_1' (The same applies to figures 24, 26, 23, 25 and 27). The contact discontinuity is located at $x = x_c \sim 0.64$, $y = 0$. The location of maximum value is at the reconnection point ($x = y = 0$), and that of minimum value is near the spearhead of the reconnection jet ($x = x_m \sim 0.84$, $y = 0$). Hence, the first order magnetic field is turned counter-clockwise along the left-half arcs, and clockwise in the right-half arcs. The direction of the zeroth order magnetic field is to the right in the upper-half plane. Thus the strength of the magnetic field is reduced by the first order variation in the vicinity of the reconnection point. This region is filled with the fast-mode rarefaction dominated inflow. This property is common to characteristic of the original Petschek model. On the other hand, the strength of the magnetic field is enhanced by the first order variation near the spearhead of the reconnection jet. This is caused by the fast-mode compression (piston effect) produced by the reconnection jet. This compressed region is characteristic of our dynamically evolving system, and quite different from previous stationary models.

FIG. 23.— The variation of flux function from the initial state (result of our simulation in section 4). We can see essentially the same feature in figures 25 and 27 except that the configuration near the x-axis ($y < 0.05$) is rather different. This is due to the existence of reconnection jets which are neglected in our present analytical study.

FIG. 24.— Contours of the y-component v'_{1y} of the velocity perturbation. The x-component of velocity perturbation is zero in the linear analysis. We should note that the value of v'_{1y} is equivalent to the strength of the electric field in the z direction (so-called reconnection electric field) in the normalized unit. The value near the reconnection point is negative. This means that the inflow is sucked into the reconnection jet. Positive values exist near the right-half outer boundary. This is outflow gushing out of the region near the spearhead of the reconnection jet. Hence, this outflow is a secondary flow properly characteristic of the evolutionary process. This outflow enhances the vortex-like flow. The value at the reconnection point ($x = y = 0$) represents the reconnection rate of the system, and the value is 0.055 from our simulation (see section 4).

FIG. 25.— The inflow velocity (y-component) (result of our simulation in section 4).

FIG. 26.— Contours of the perturbed density ρ'_1. If we divide this value by adiabatic constant γ, these contours show the perturbation in gas pressure P'_1 in the normalized unit. The density (hence pressure) is reduced near the reconnection point, and enhanced near the spearhead of the reconnection jet. These features are also caused by the fast-mode rarefaction and compression as discussed in the caption for figure 22.

FIG. 27.— The variation of density distribution from the initial state (result of our simulation in section 4).

FIG. 28.— The profile of the magnetic flux function (1st order) at $x = 0.5$. The dotted and solid lines show the numerical solution and the semi-analytic solution, respectively.

FIG. 29.— The profile of the velocity field (y-component) at $x = 0.5$. The dotted and solid lines show the numerical solution and the semi-analytic solution, respectively.

FIG. 30.— The profile of mass density distribution (1st order) at $x = 0.5$. The dotted and solid lines show the numerical solution and the semi-analytic solution, respectively.

FIG. 31.— The same as in figure 11, but for the case of larger resistivity (five times larger than that in the case of figure 11; $\eta = 0.5$, $R_m = 4.9$). We find no essential difference from the previous case. This result suggests that the self-similar evolution does not sensitively depend upon details of the resistivity model (case C).

FIG. 32.— X-ray flux distribution predicted by our model in relative measure. This figure shows the evolution of a virtual X-ray image in the fixed coordinates. The contours indicate the distribution of the emission measure $f \propto n^2 T^{1/2}$ which shows X-ray flux distribution in the assumed temperature range of $10^7 - 10^8$ K , where n is the particle number density and T the temperature. Our self-similar model may be applied to the observation of dimming (case A).

FIG. 33.— Evolution of the reconnection rate. The solid line shows the time variation of the electric field ($\mu\eta|\boldsymbol{J}|$) at the reconnection point ($x = y = 0$) in the case shown in figures 11 and 12. This quantity may be taken as the reconnection rate of the system (case A). In the same way, the dashed line shows the rate for the case in which the lower half region ($y \leq 3000$) is filled with uniformly magnetized plasma, while the upper half region ($y > 3000$) is unmagnetized. We cannot find any significant difference between these two cases even after the reflected wave from the interface between magnetized and unmagnetized regions returns to the current sheet ($t \geq 6000$) (case D).

Reconnection in Solar Flares

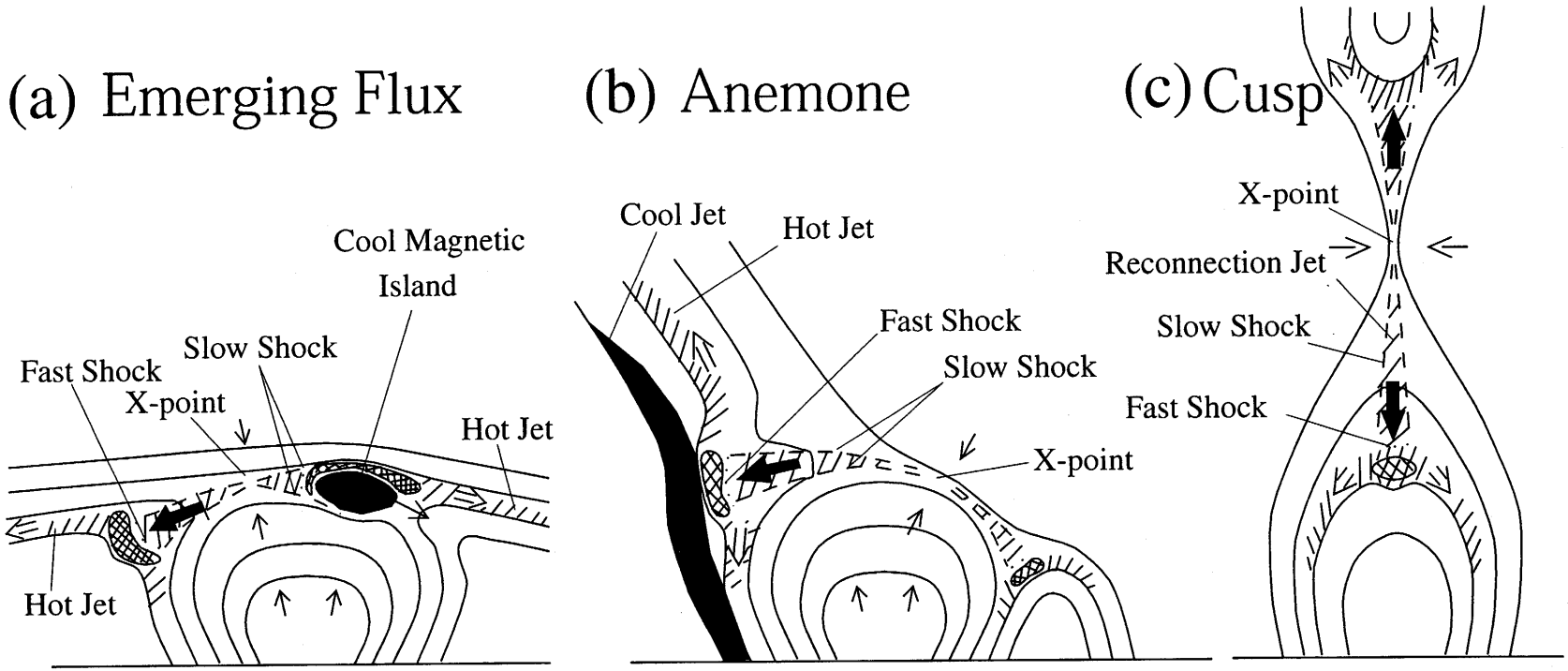

Fig. 1

Fig. 2

Substorm of the Earth

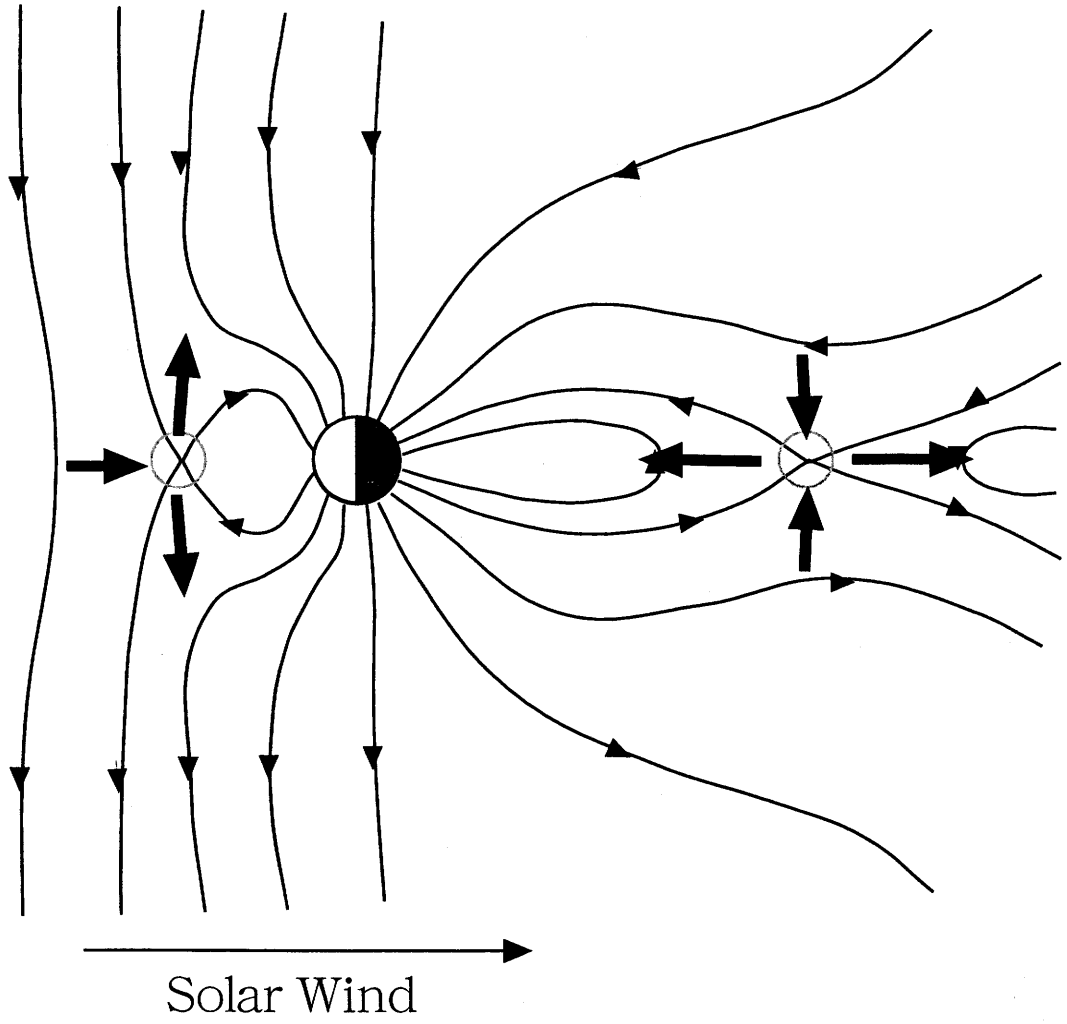

Fig. 3

Current sheet system & Simple diffusion model

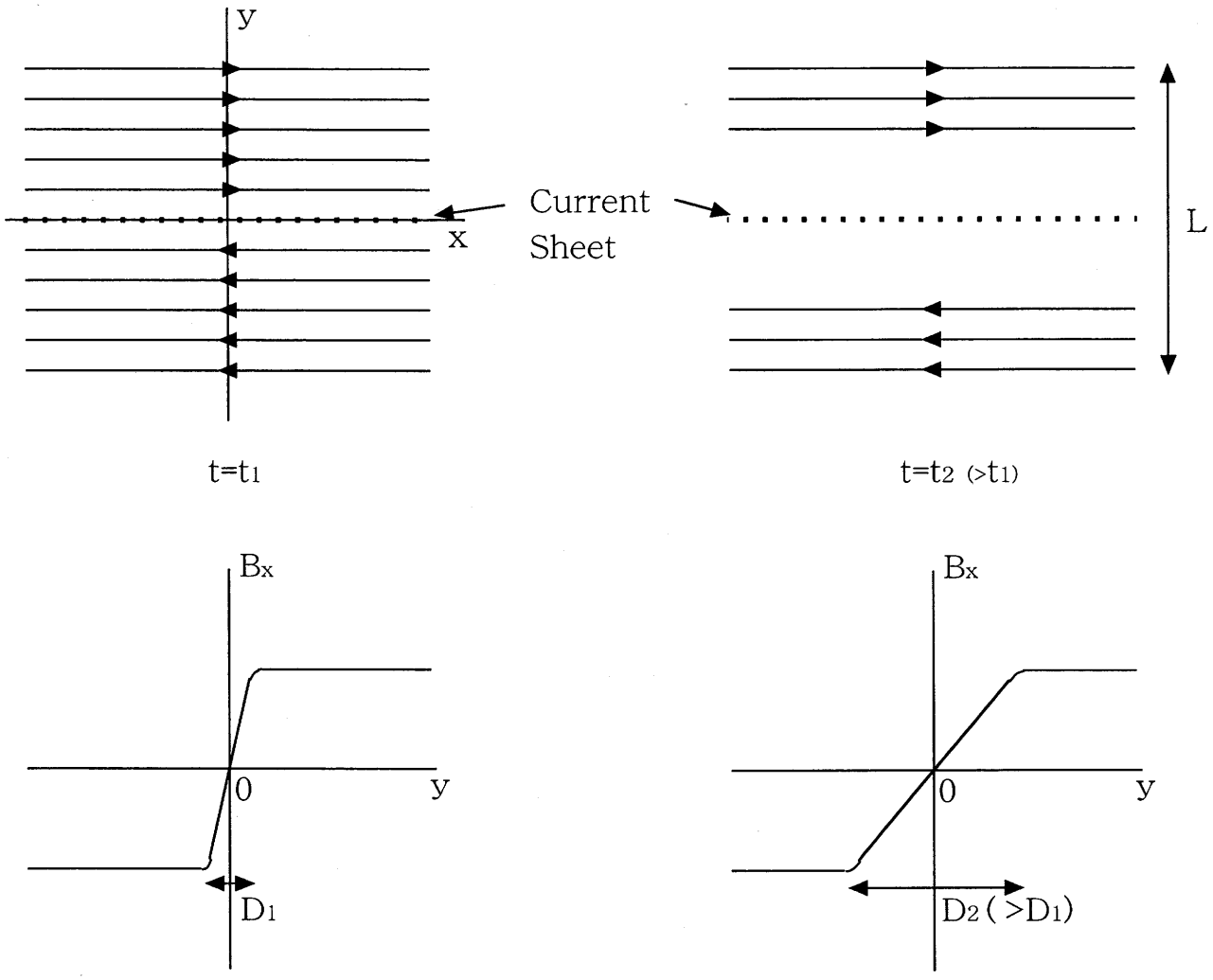

Fig. 4

Sweet-Parker Model

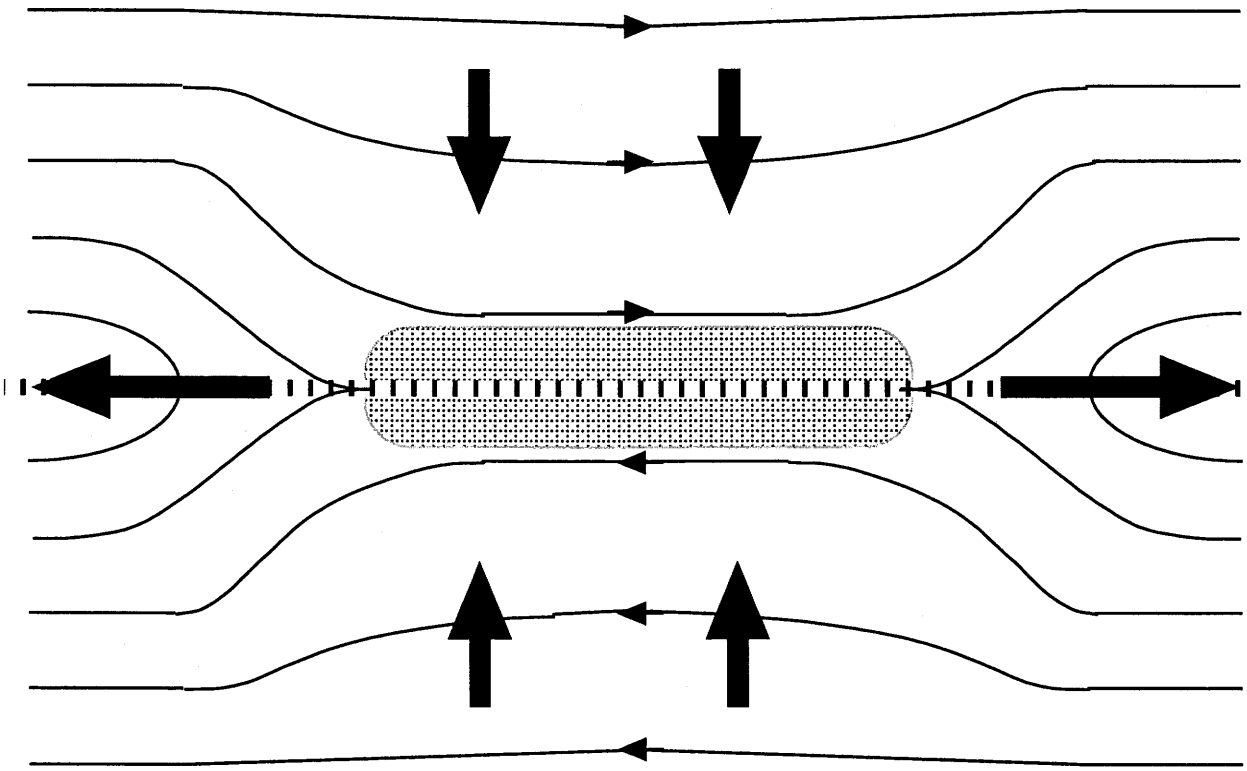

Fig. 5

Petschek Model

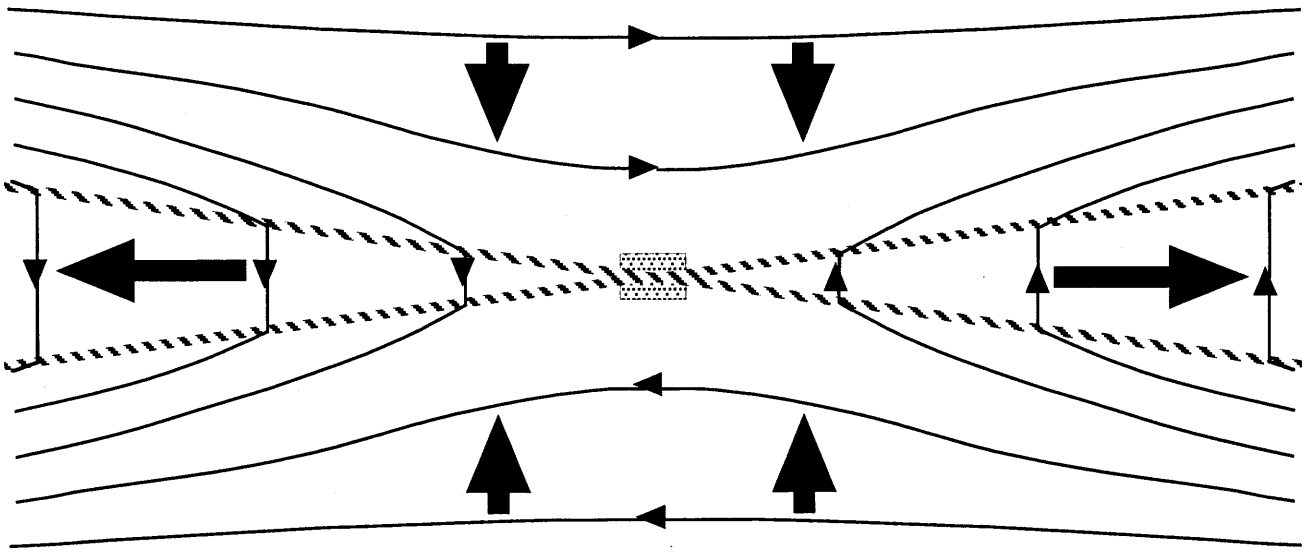

Fig. 6

Sonnerup Model

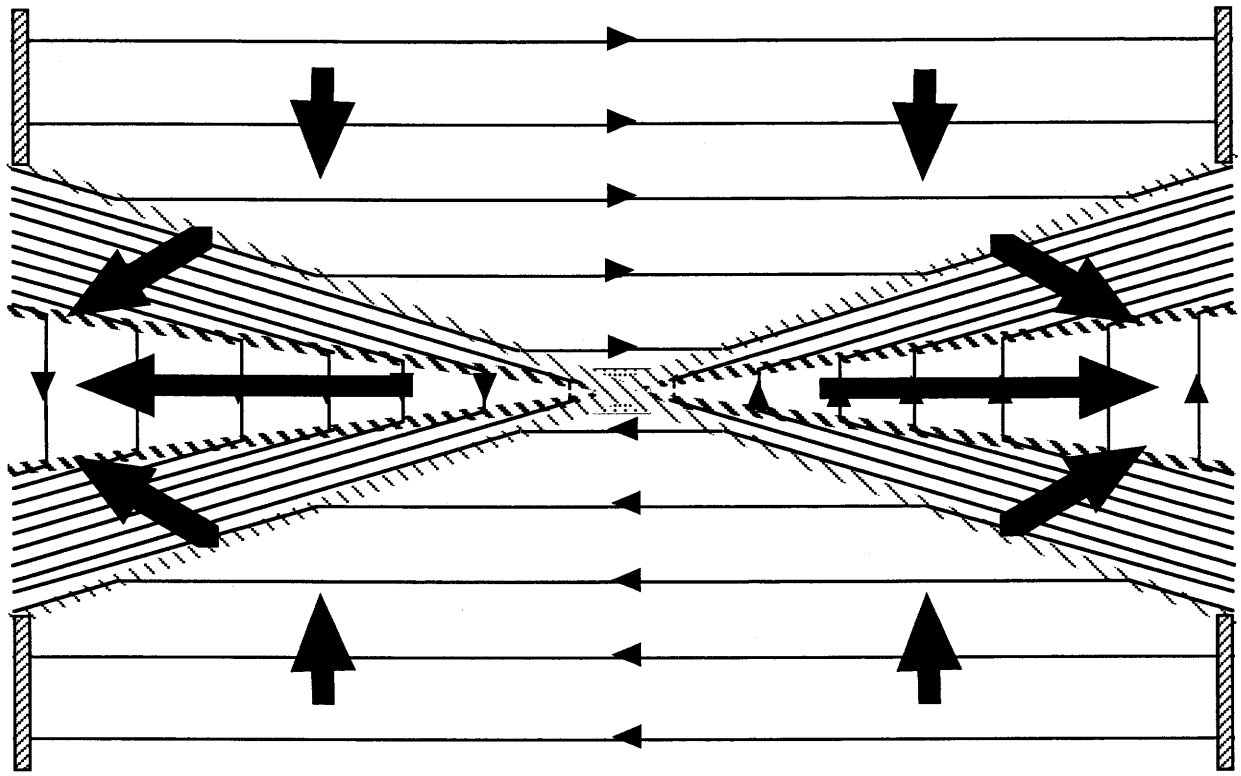

Fig. 7

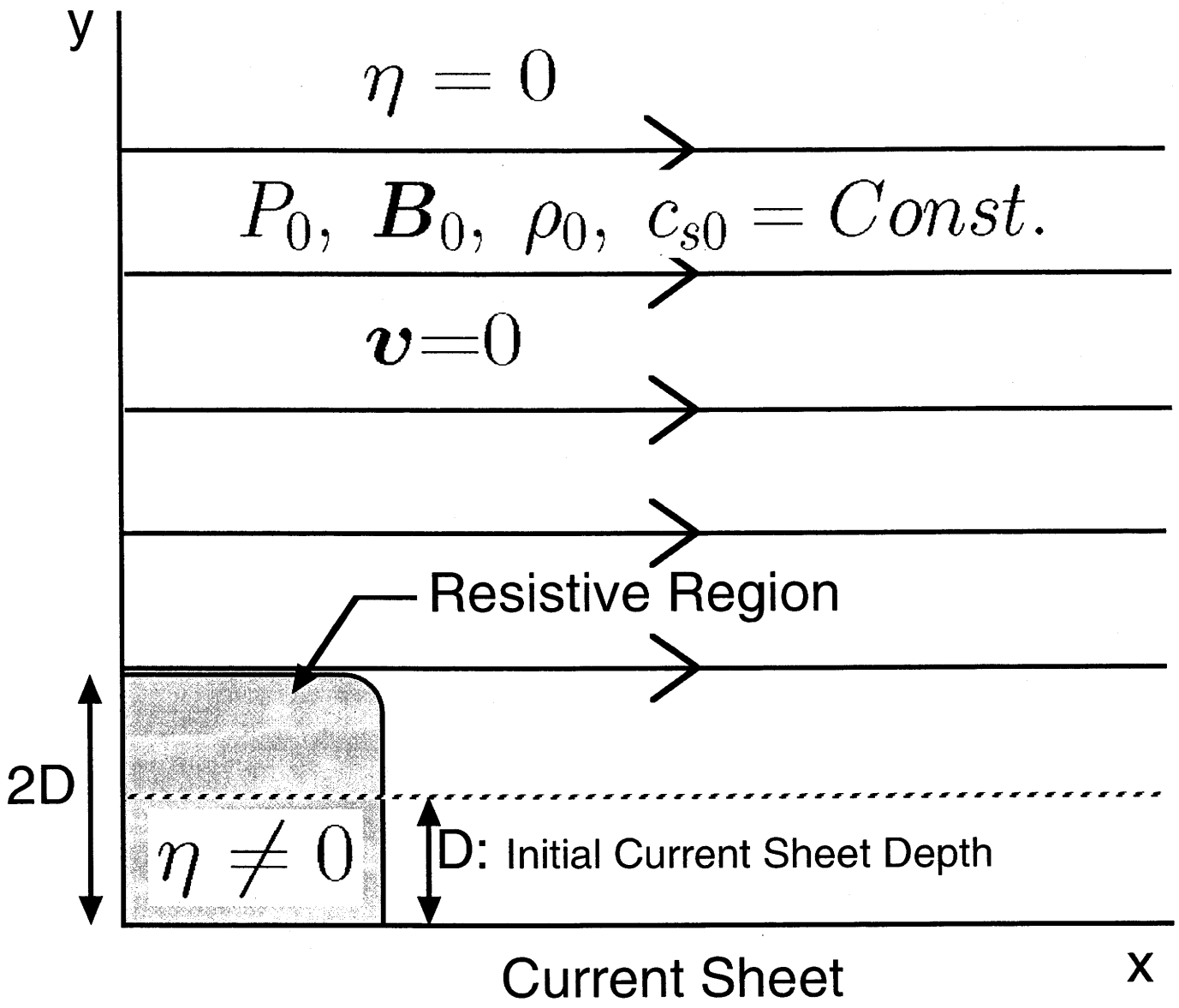
y
$\eta = 0$
$P_0,\ \boldsymbol{B}_0,\ \rho_0,\ c_{s0} = Const.$
$\boldsymbol{v}=0$
Resistive Region
2D
$\eta \neq 0$
D: Initial Current Sheet Depth
Current Sheet
x

Fig. 8

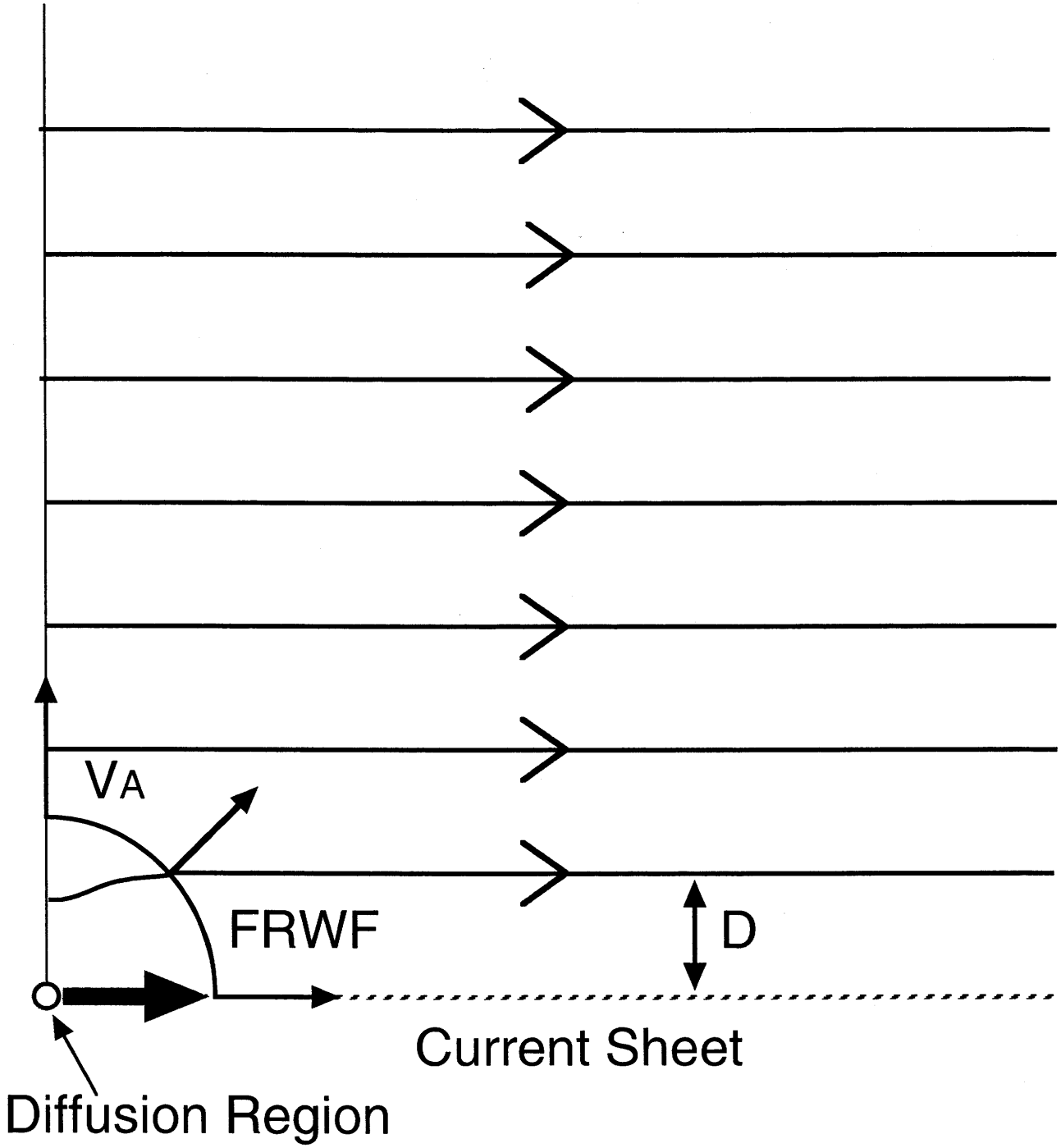

Fig. 9

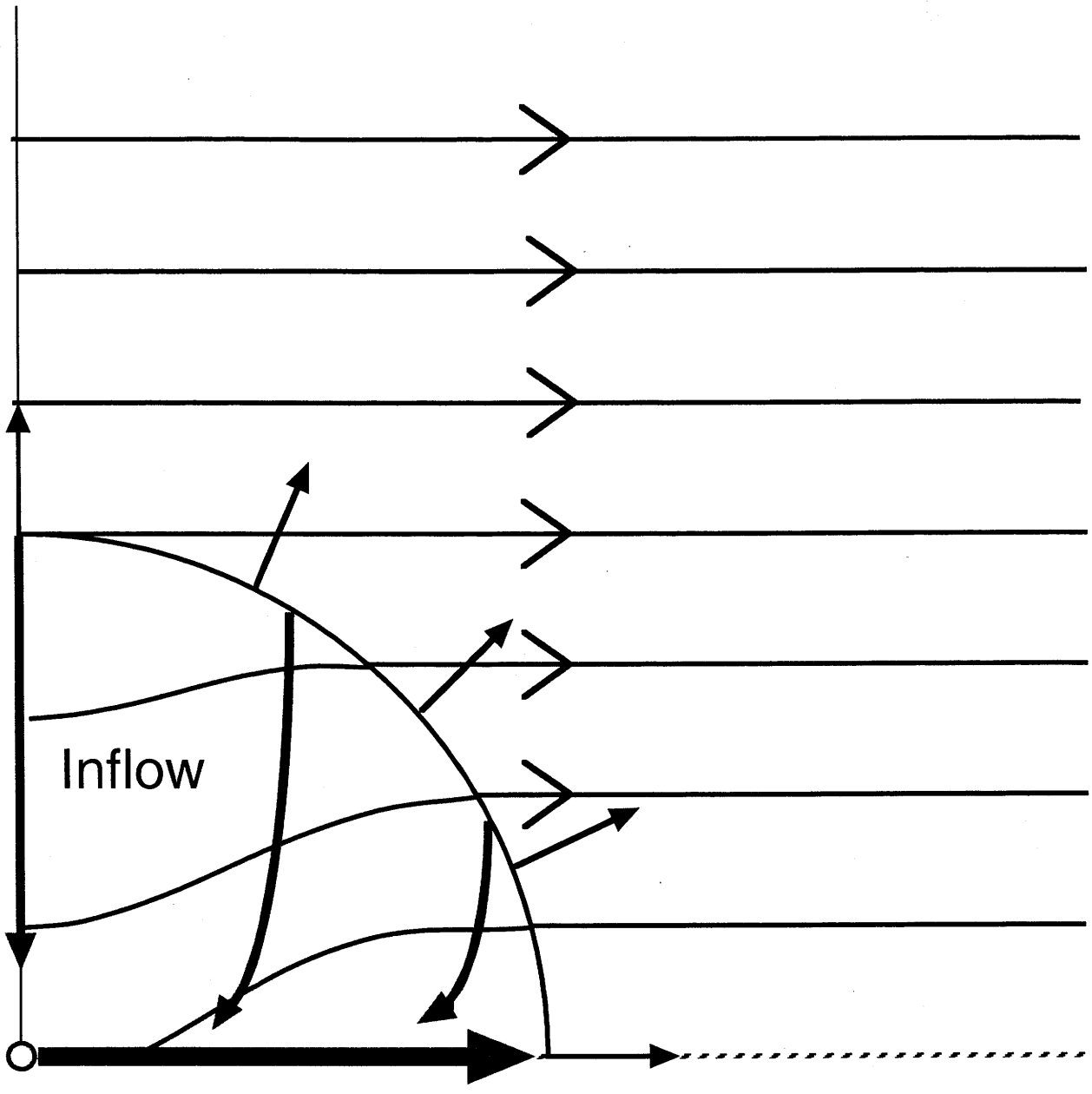

Fig. 10

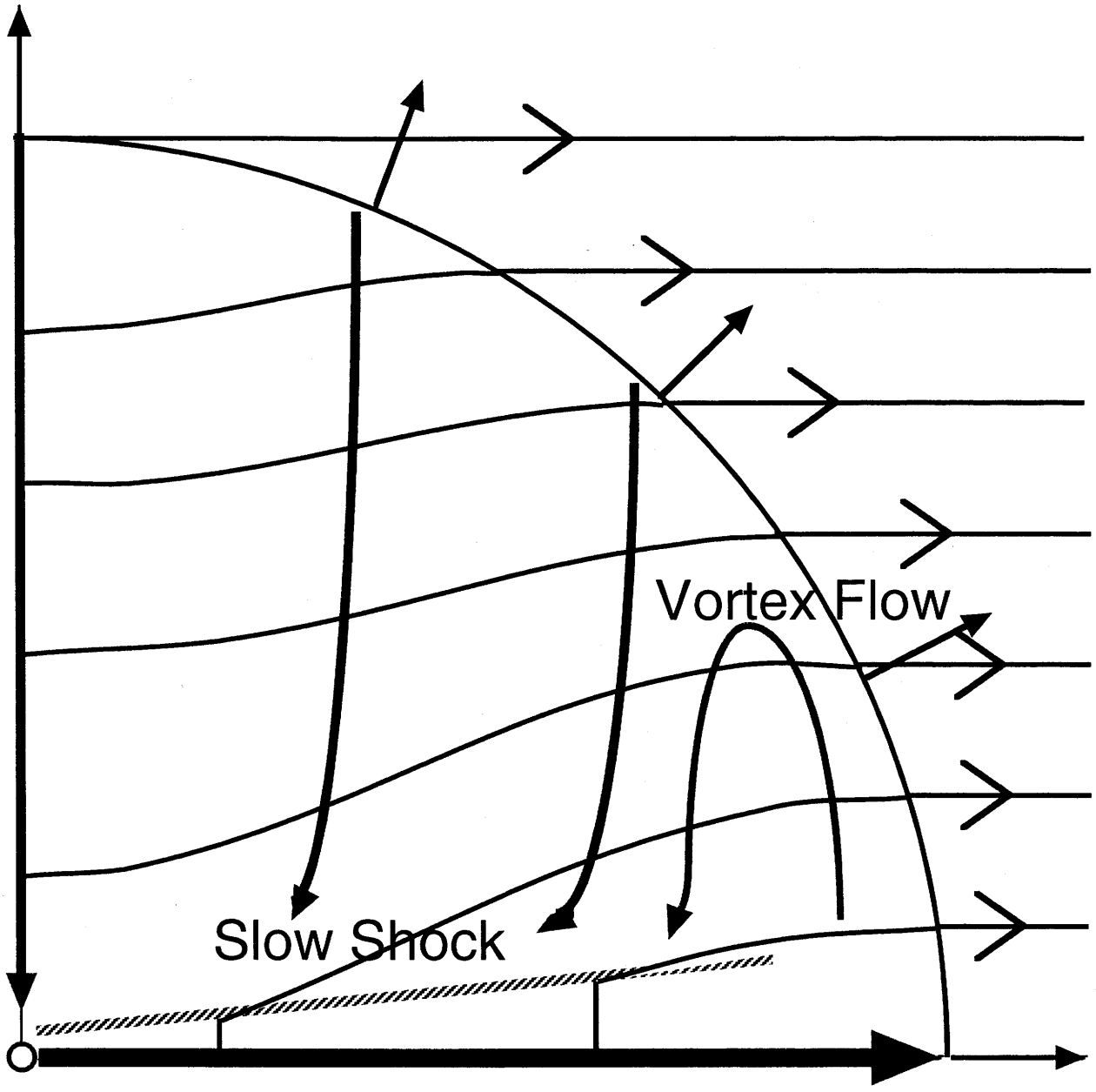

Self-Similar Evolution (Magnetic Pressure)

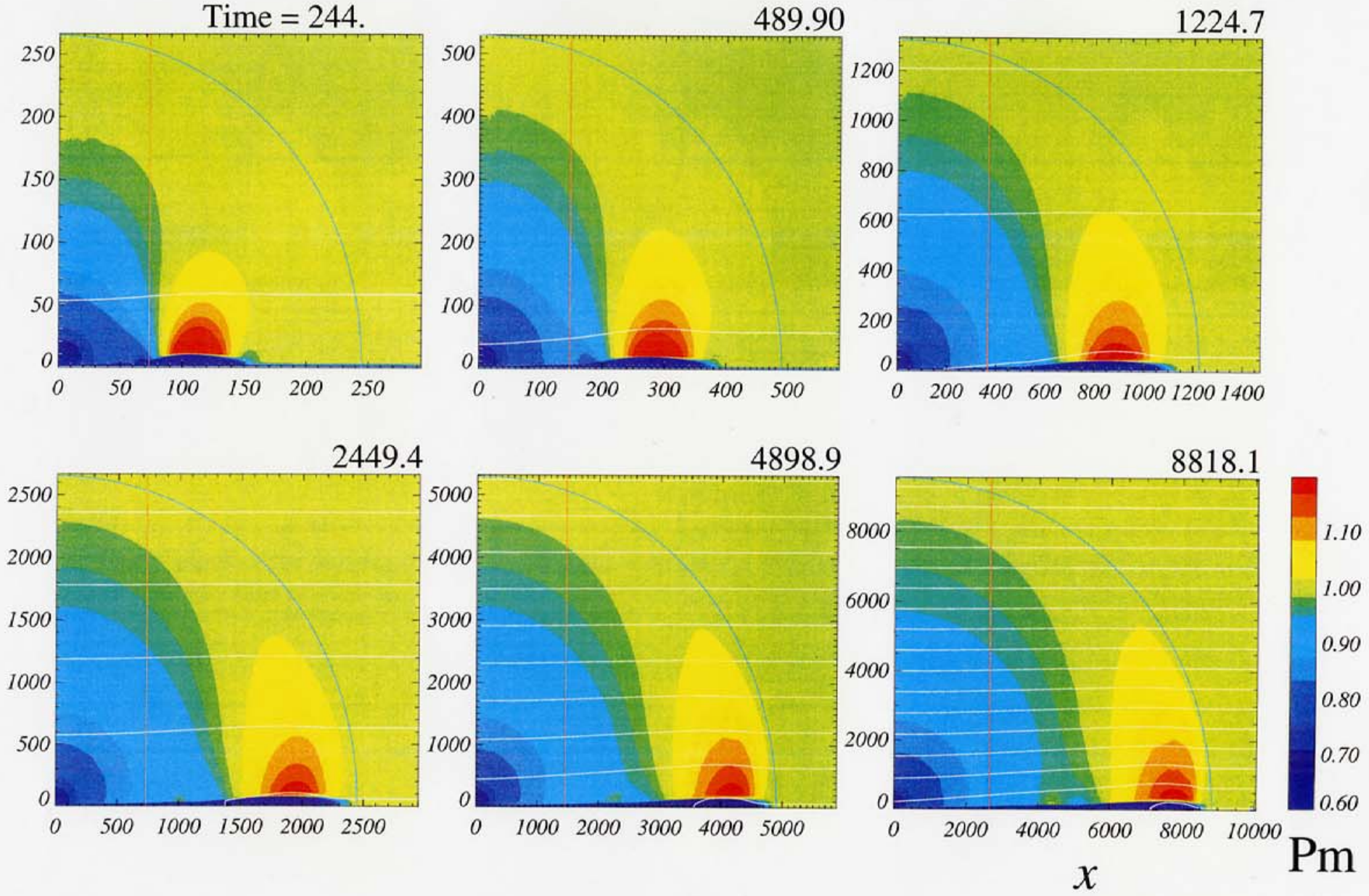

Fig. 11

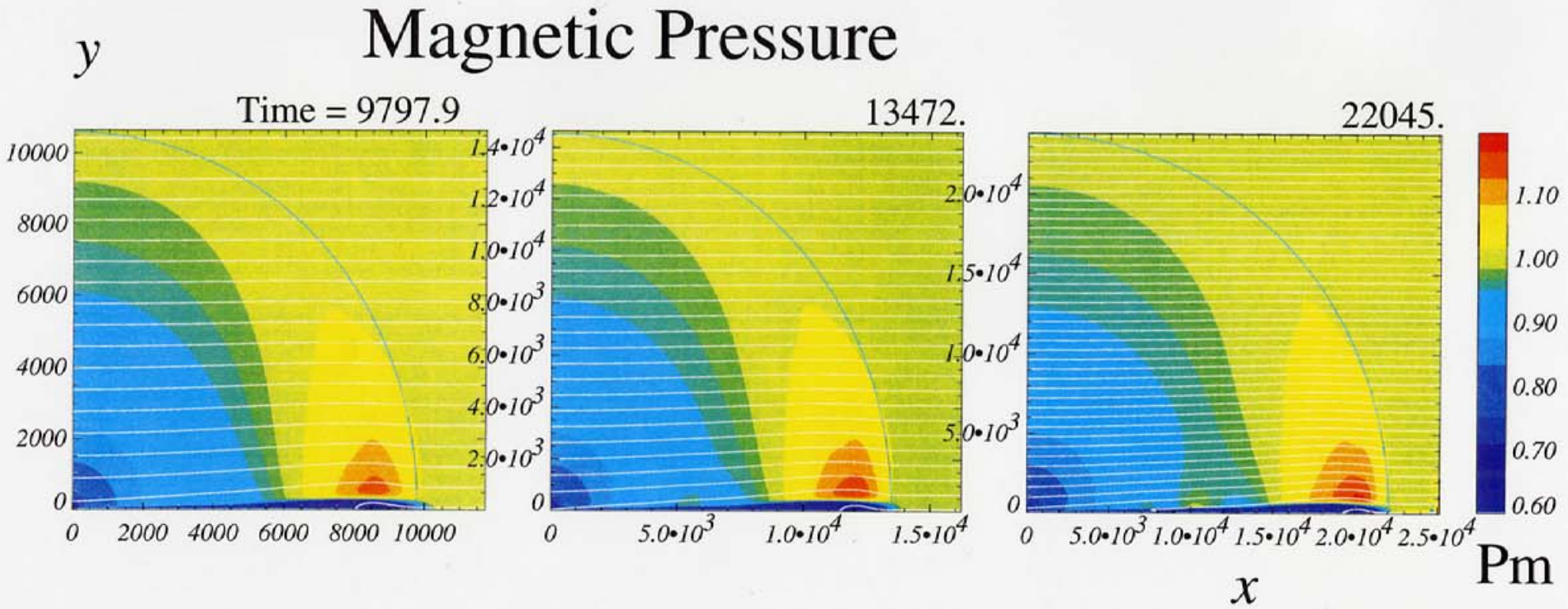
Magnetic Pressure
y
Time = 9797.9
13472.
22045.
10000
8000
6000
4000
2000
0
1.4•10^4
1.2•10^4
1.0•10^4
8.0•10^3
6.0•10^3
4.0•10^3
2.0•10^3
0 2000 4000 6000 8000 10000
2.0•10^4
1.5•10^4
1.0•10^4
5.0•10^3
0 5.0•10^3 1.0•10^4 1.5•10^4
0 5.0•10^3 1.0•10^4 1.5•10^4 2.0•10^4 2.5•10^4
x
1.10
1.00
0.90
0.80
0.70
0.60
Pm

Fig. 12

Fig. 13

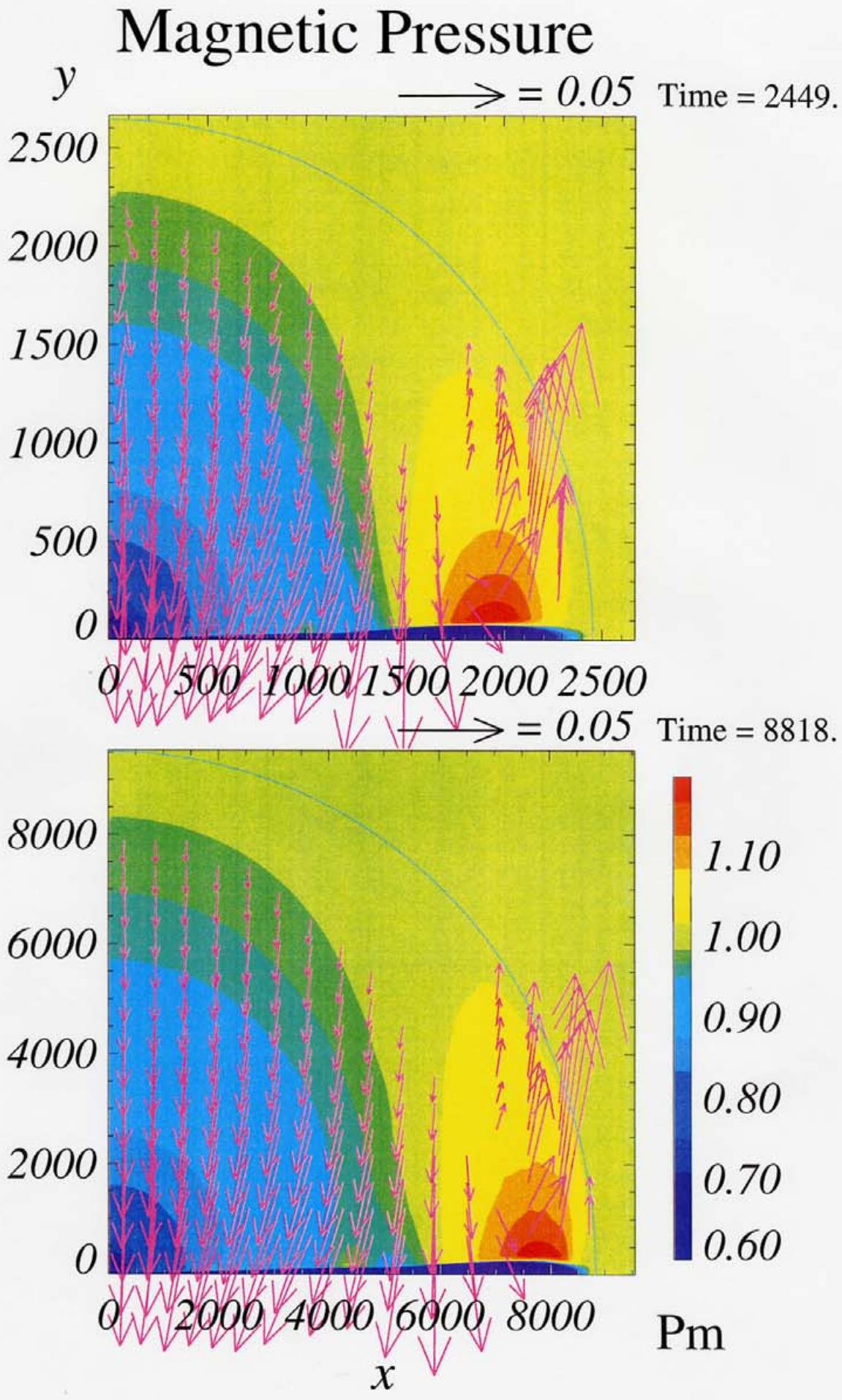
Magnetic Pressure
y
= 0.05
Time = 2449.
2500
2000
1500
1000
500
0
0 500 1000 1500 2000 2500
= 0.05
Time = 8818.
8000
6000
4000
2000
0
0 2000 4000 6000 8000
x
1.10
1.00
0.90
0.80
0.70
0.60
Pm

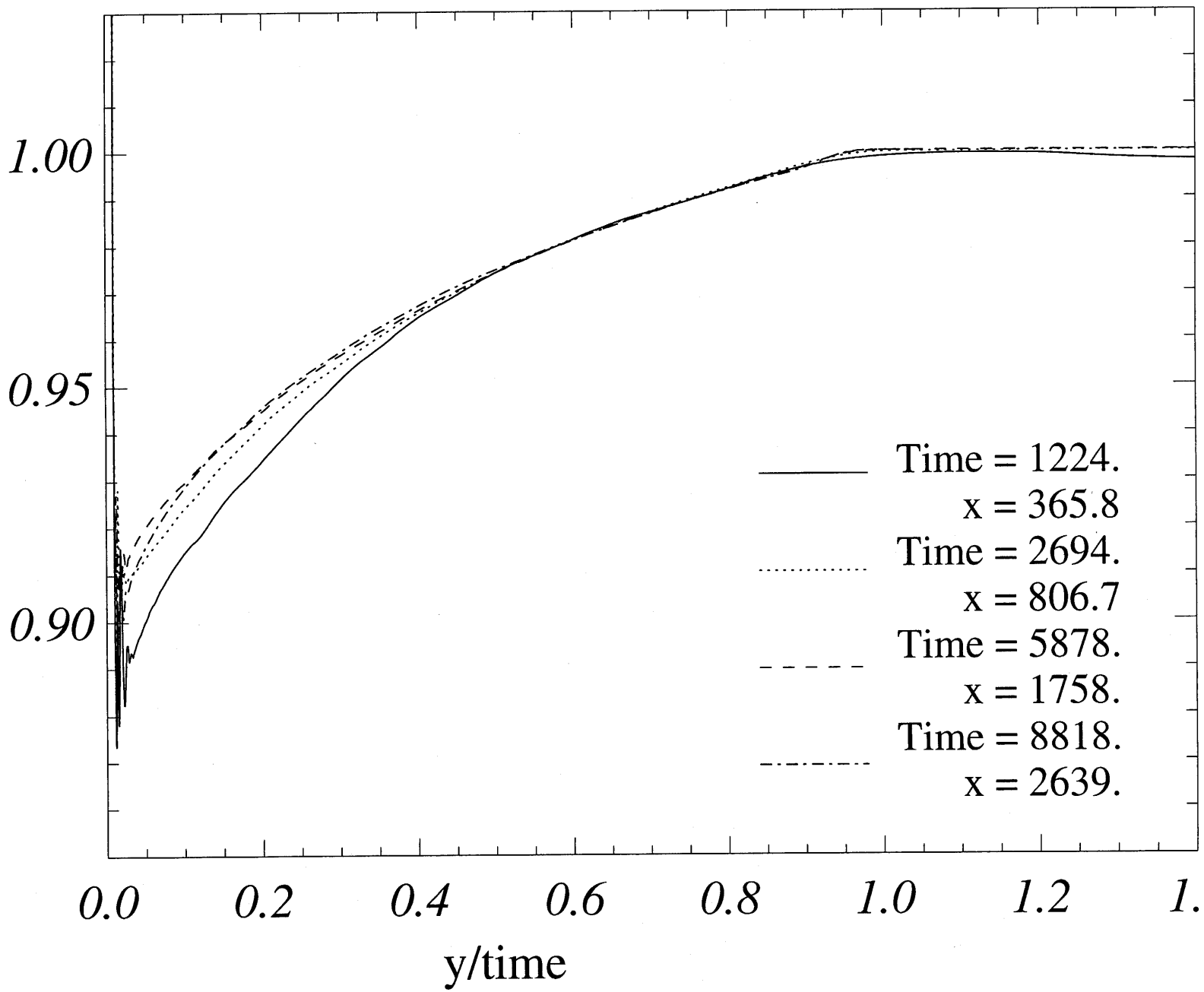
Evolution of Density Profile
1.00
0.95
0.90
0.0
0.2
0.4
0.6
0.8
1.0
1.2
1.4
y/time
Time = 1224.
x = 365.8
Time = 2694.
x = 806.7
Time = 5878.
x = 1758.
Time = 8818.
x = 2639.

Fig. 14

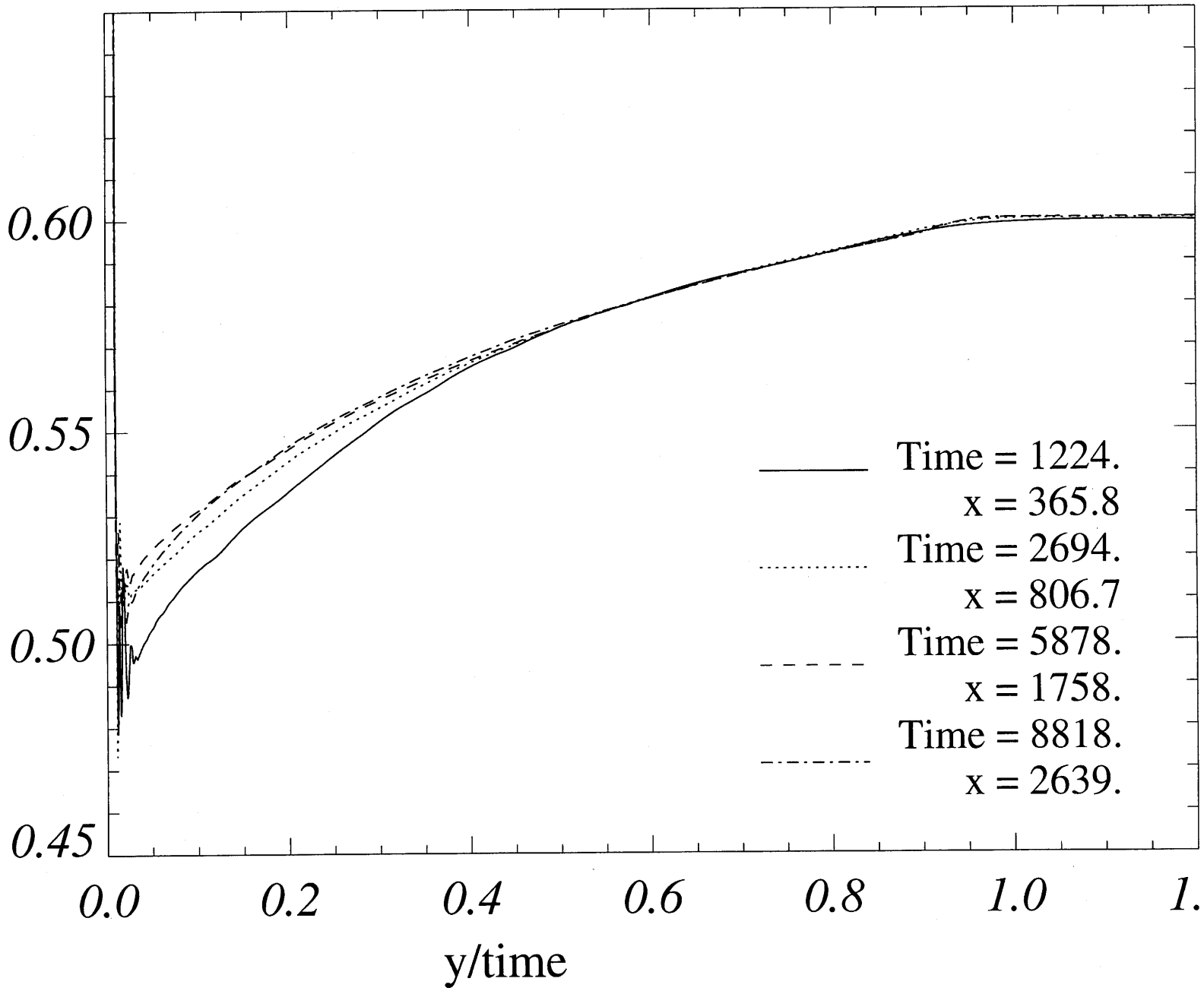
Evolution of Pg Profile
0.60
0.55
0.50
0.45
0.0
0.2
0.4
0.6
0.8
1.0
1.2
y/time
Time = 1224.
x = 365.8
Time = 2694.
x = 806.7
Time = 5878.
x = 1758.
Time = 8818.
x = 2639.

Fig. 15

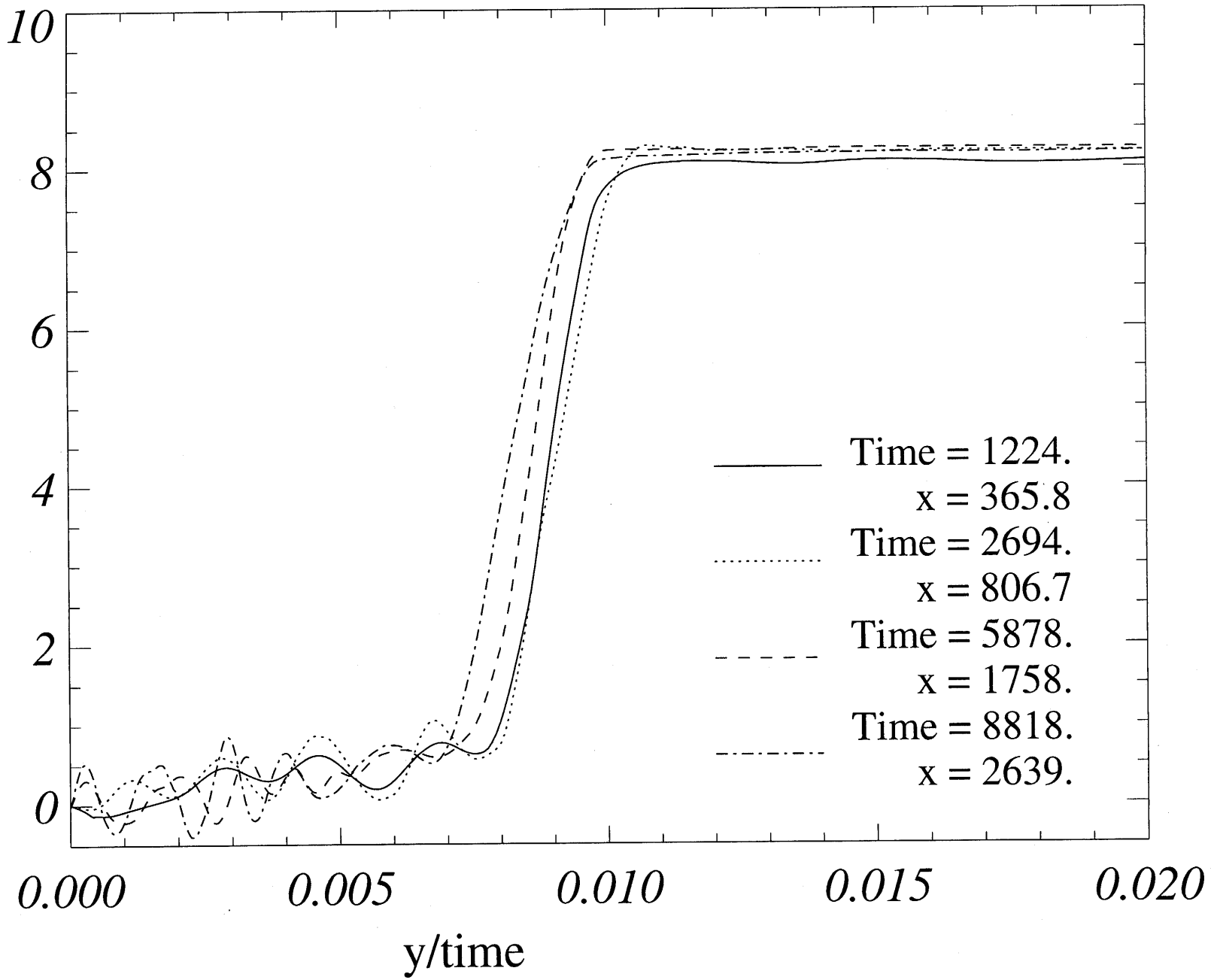
Evolution of Bx Profile
10
8
6
4
2
0
0.000
0.005
0.010
0.015
0.020
y/time
Time = 1224.
x = 365.8
Time = 2694.
x = 806.7
Time = 5878.
x = 1758.
Time = 8818.
x = 2639.

Fig. 16

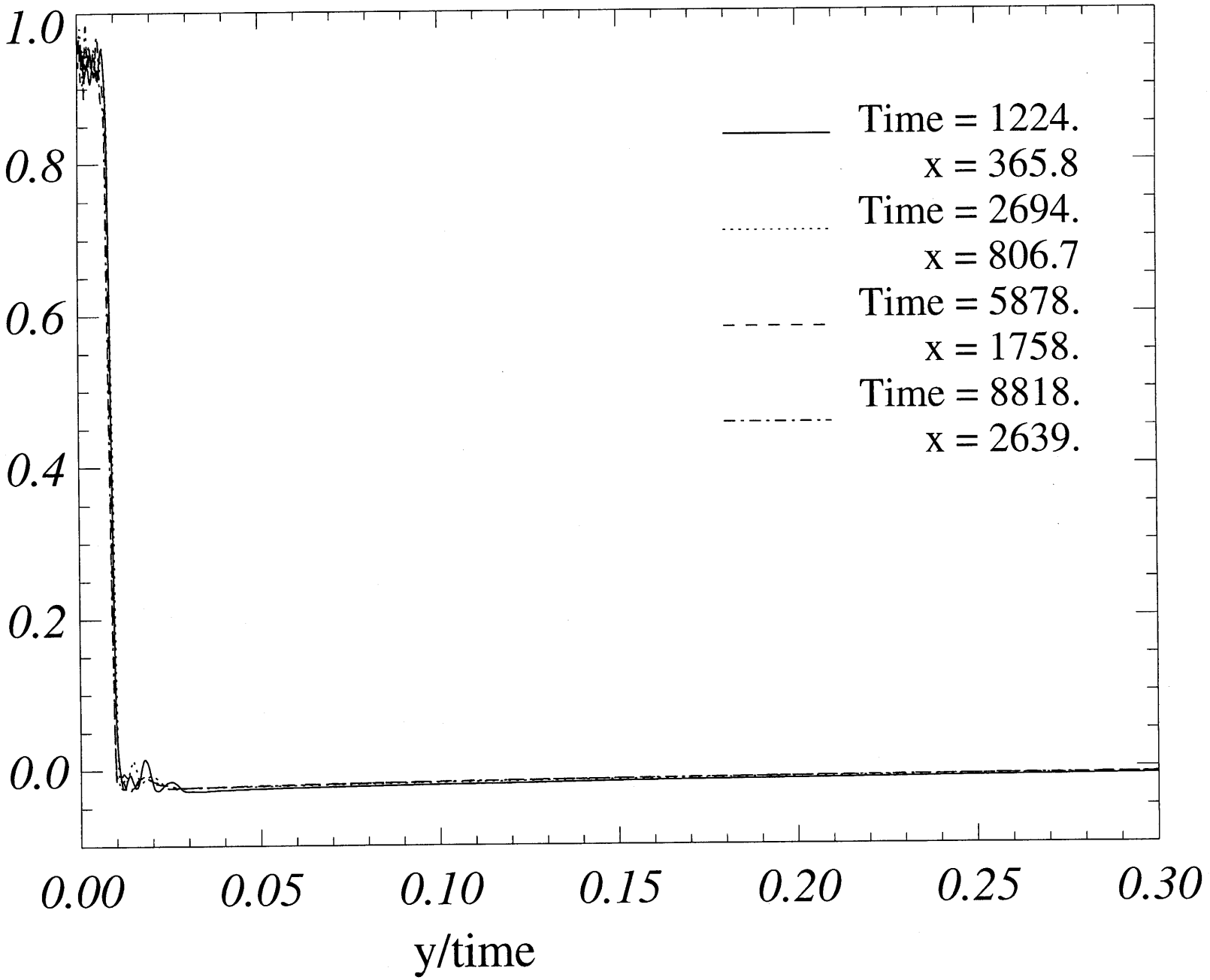
Evolution of Vx Profile
1.0
0.8
0.6
0.4
0.2
0.0
0.00
0.05
0.10
0.15
0.20
0.25
0.30
y/time
Time = 1224.
x = 365.8
Time = 2694.
x = 806.7
Time = 5878.
x = 1758.
Time = 8818.
x = 2639.

Fig. 17

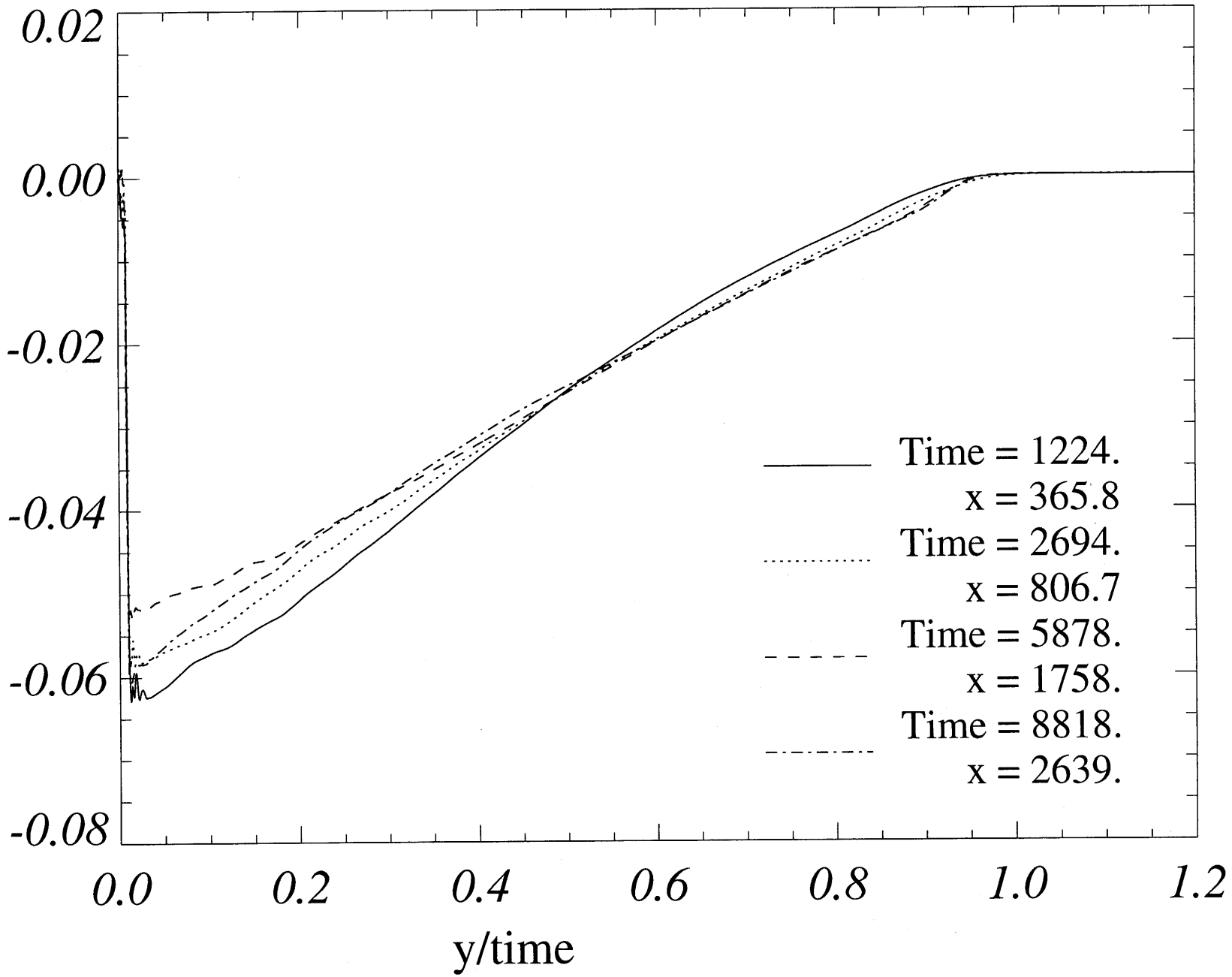
Evolution of Vy Profile
0.02
0.00
-0.02
-0.04
-0.06
-0.08
0.0
0.2
0.4
0.6
0.8
1.0
1.2
y/time
Time = 1224.
x = 365.8
Time = 2694.
x = 806.7
Time = 5878.
x = 1758.
Time = 8818.
x = 2639.

Fig. 18

Detailed Structure (Total Pressure)

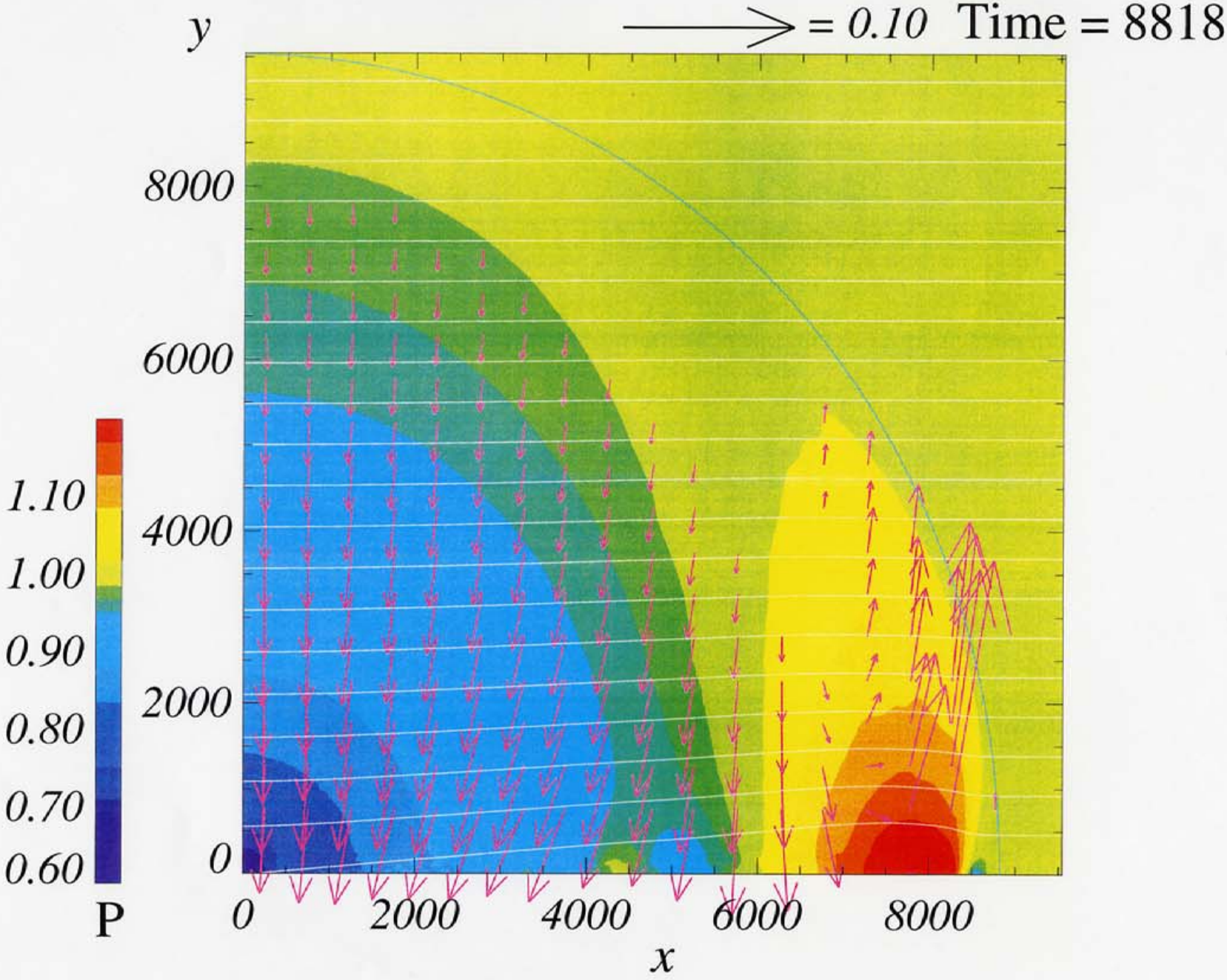

Fig. 19

Detailed Structure (Magnetic Pressure)

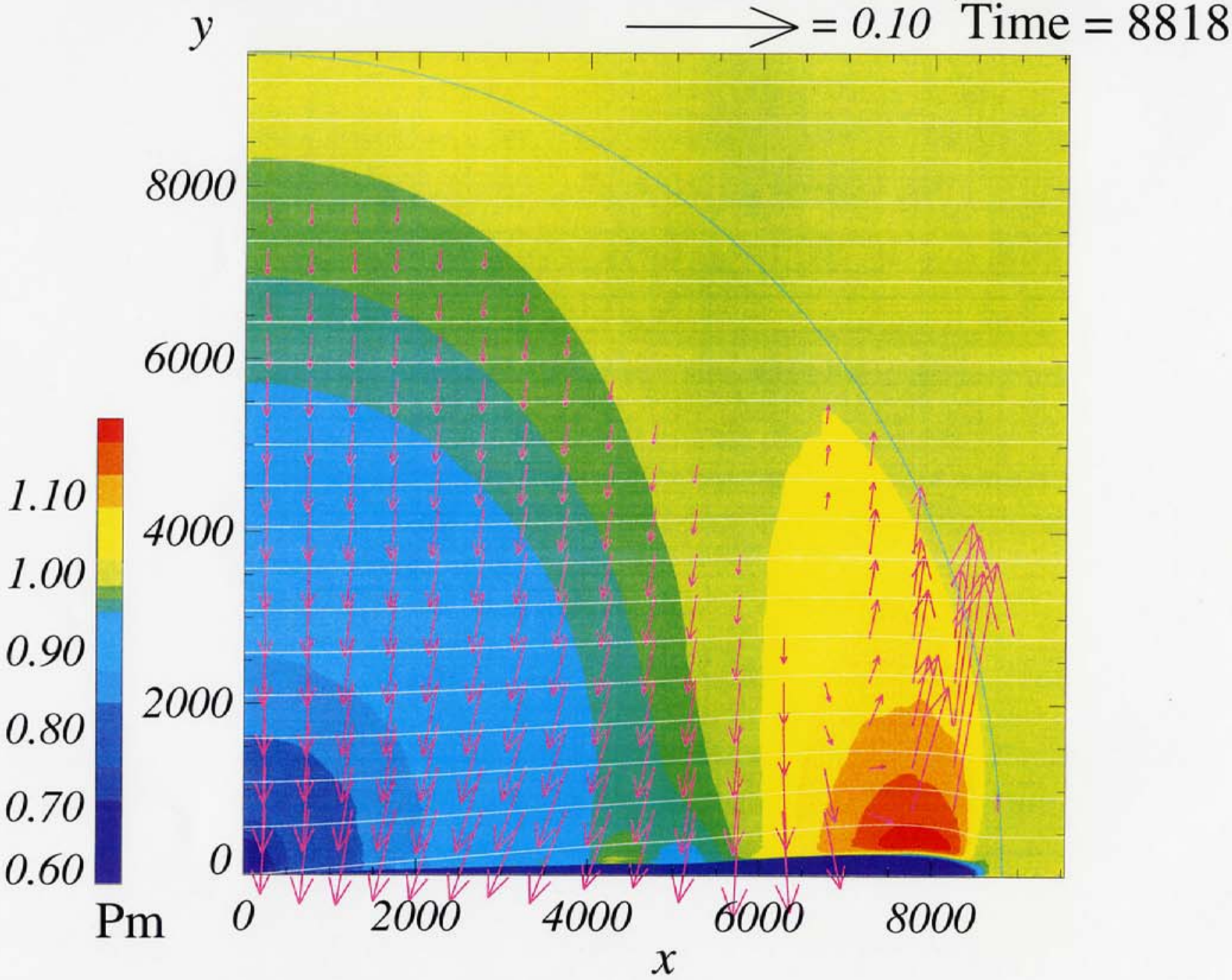

Fig. 20

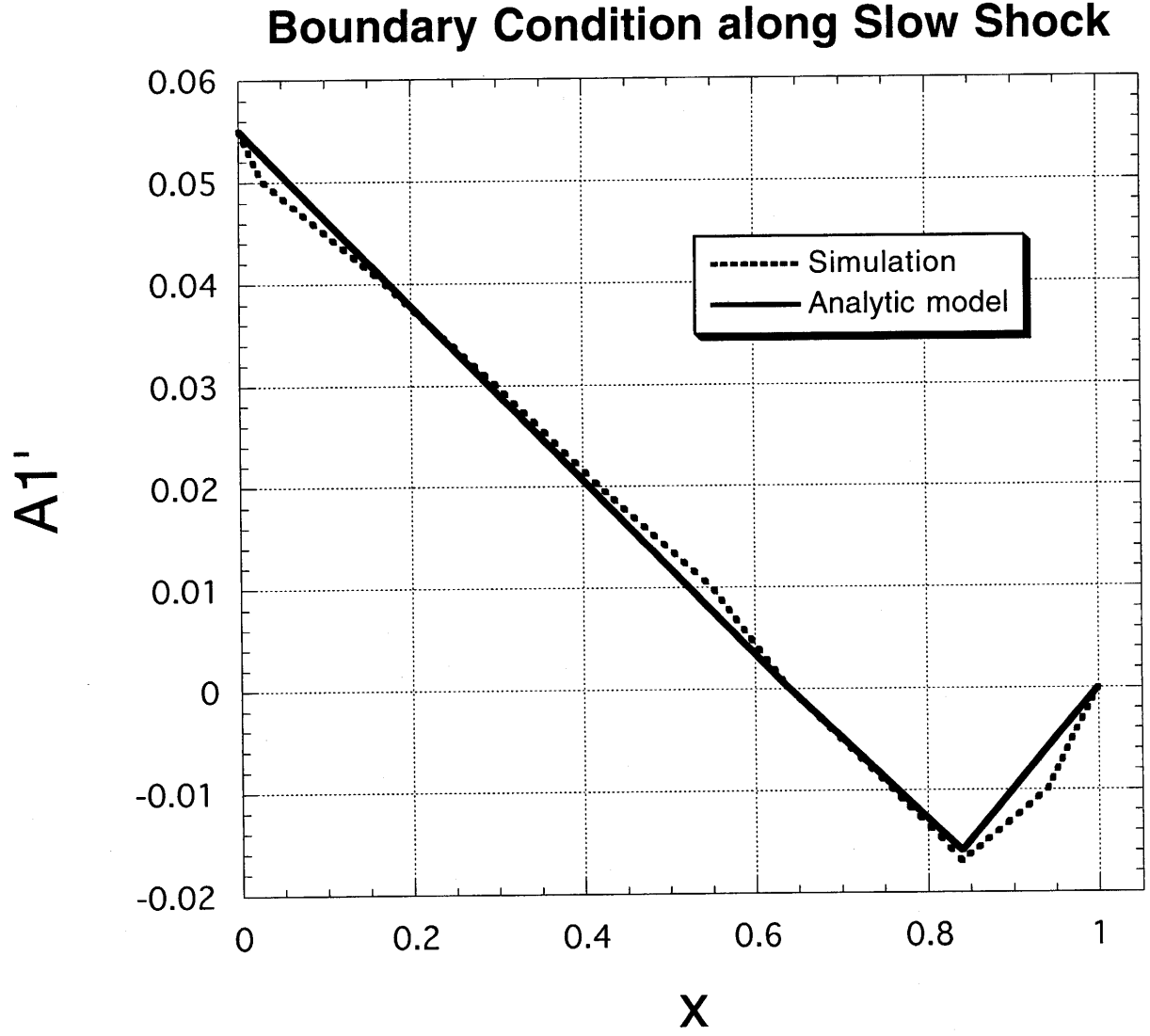
Boundary Condition along Slow Shock
0.06
0.05
0.04
0.03
0.02
0.01
0
-0.01
-0.02
A1'
0
0.2
0.4
0.6
0.8
1
X
Simulation
Analytic model

Fig. 21

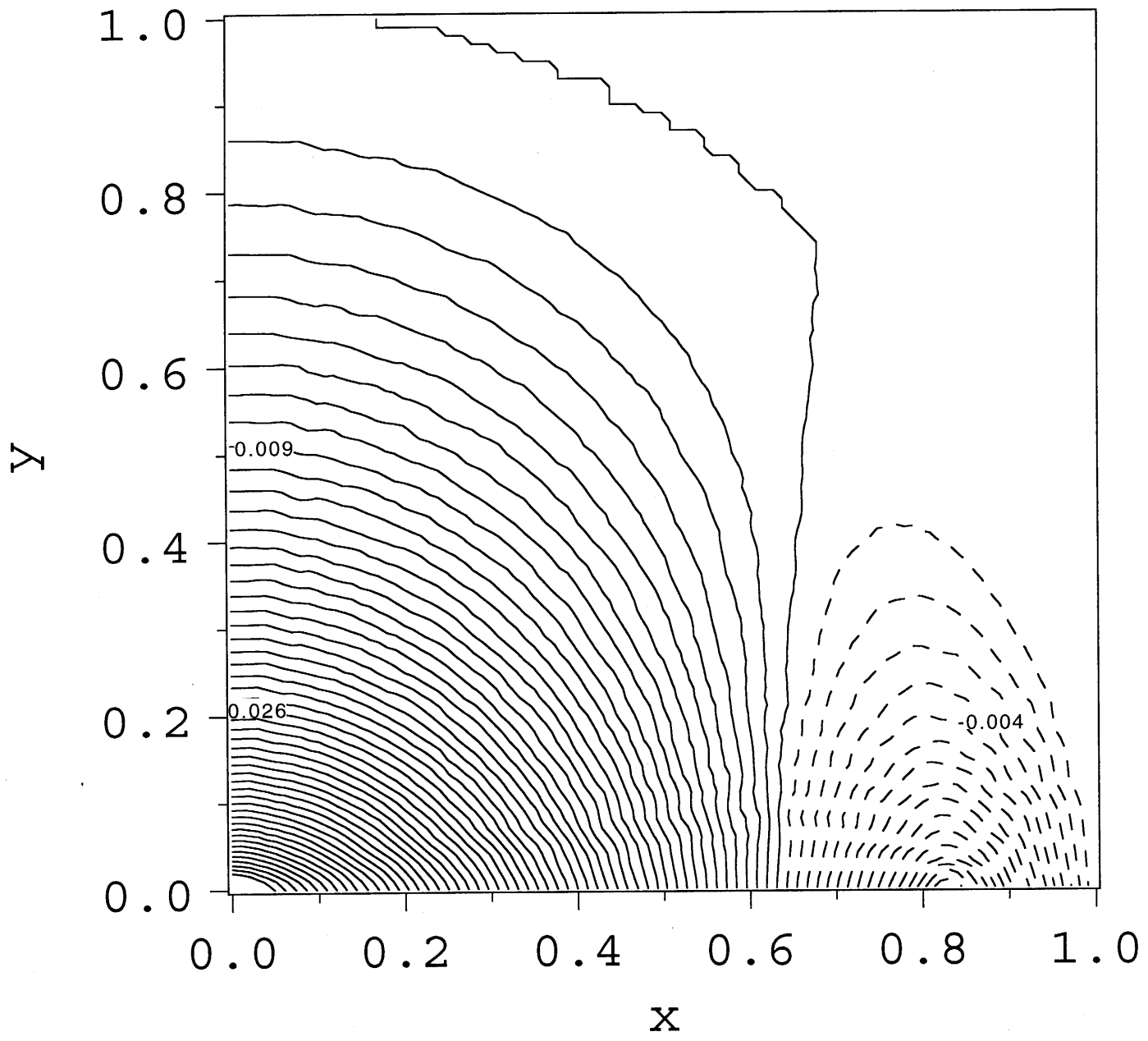
Flux Function (1st order)
1.0
0.8
0.6
0.4
0.2
0.0
y
0.009
0.026
-0.004
0.0
0.2
0.4
0.6
0.8
1.0
x

Fig. 22

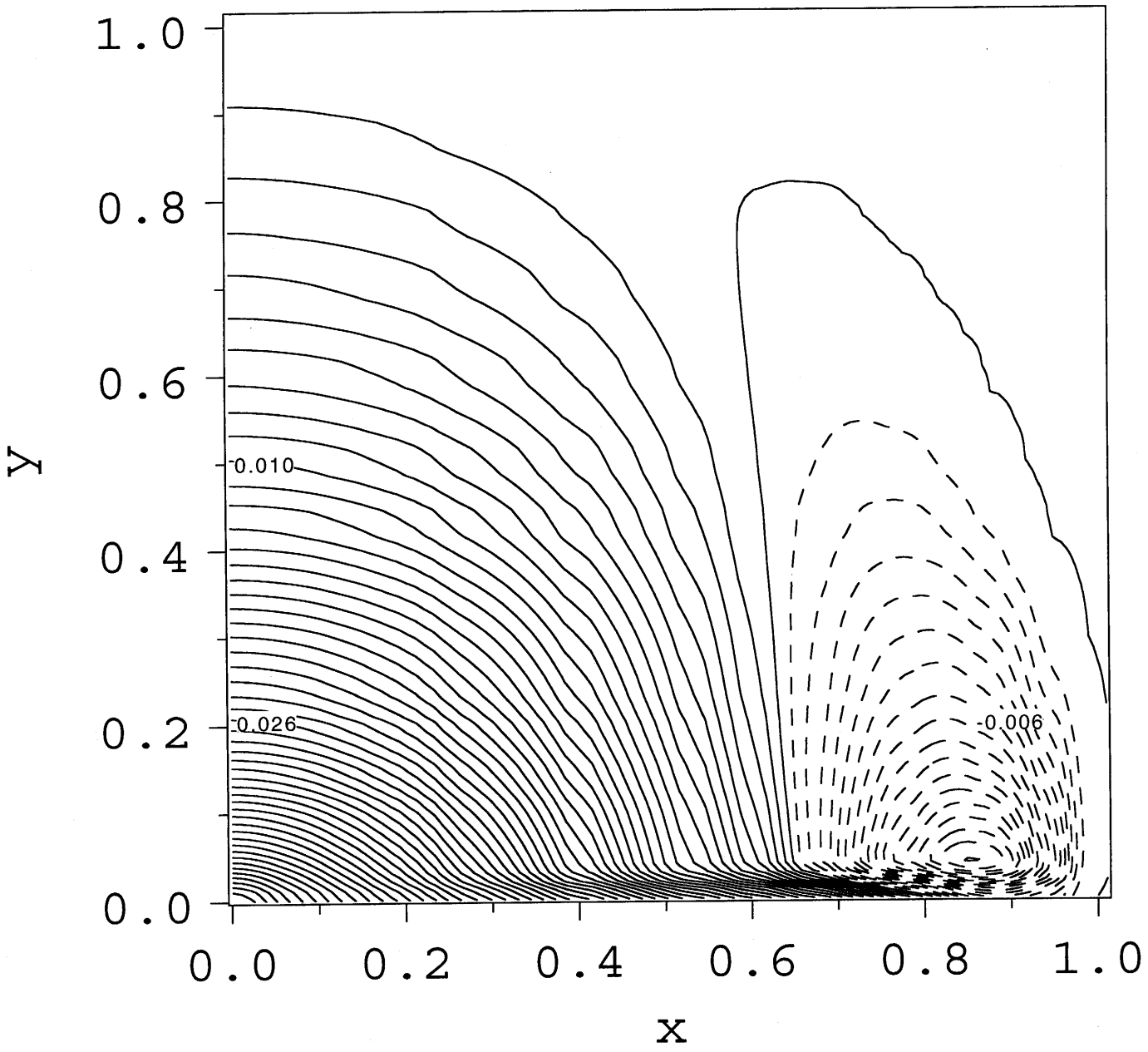
Difference in Flux Function (Sim.)
1.0
0.8
0.6
0.4
0.2
0.0
y
0.010
0.026
-0.006
0.0
0.2
0.4
0.6
0.8
1.0
x

Fig. 23

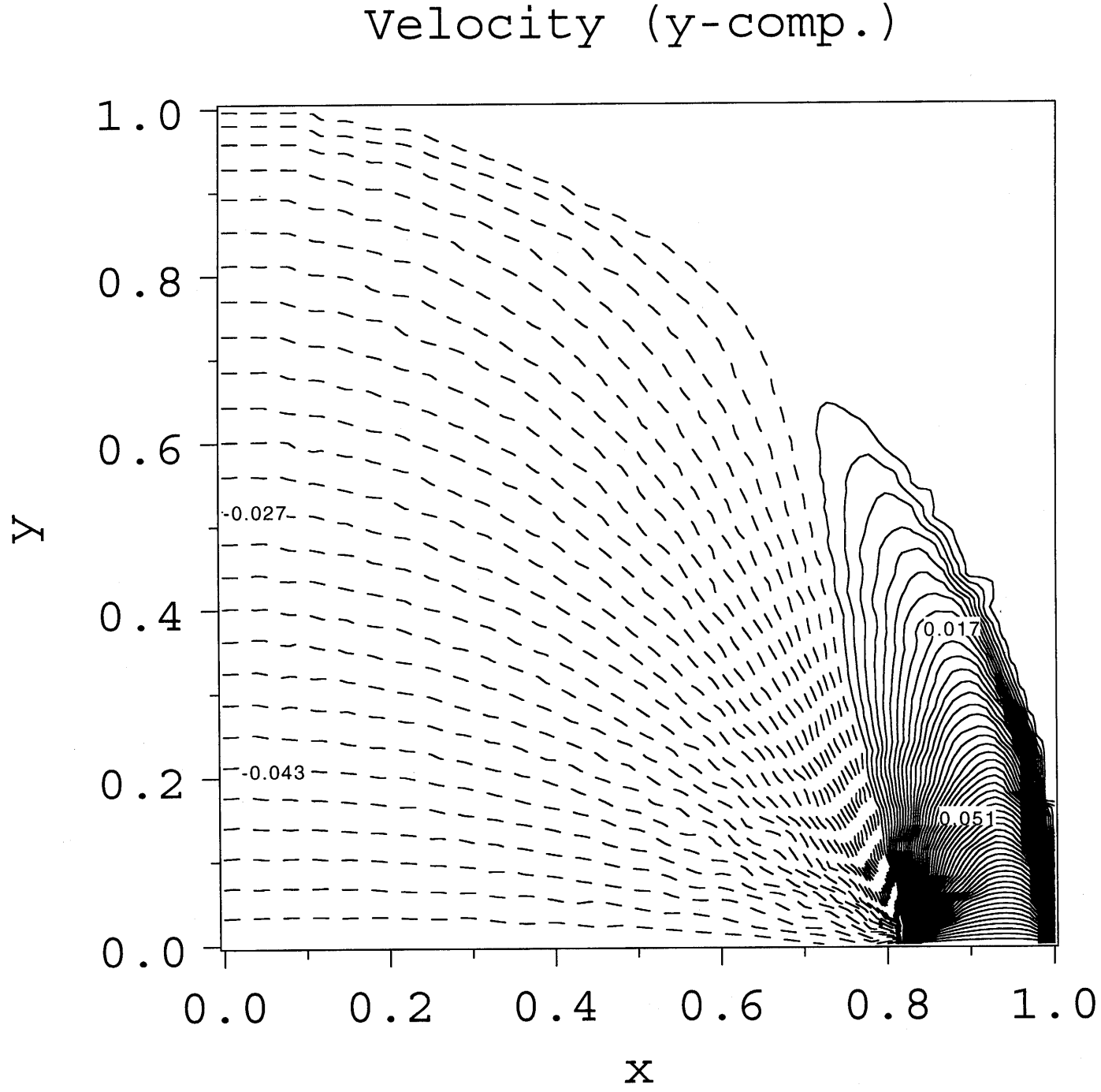
Velocity (y-comp.)
1.0
0.8
0.6
0.4
0.2
0.0
y
-0.027
-0.043
0.017
0.051
0.0
0.2
0.4
0.6
0.8
1.0
x

Fig. 24

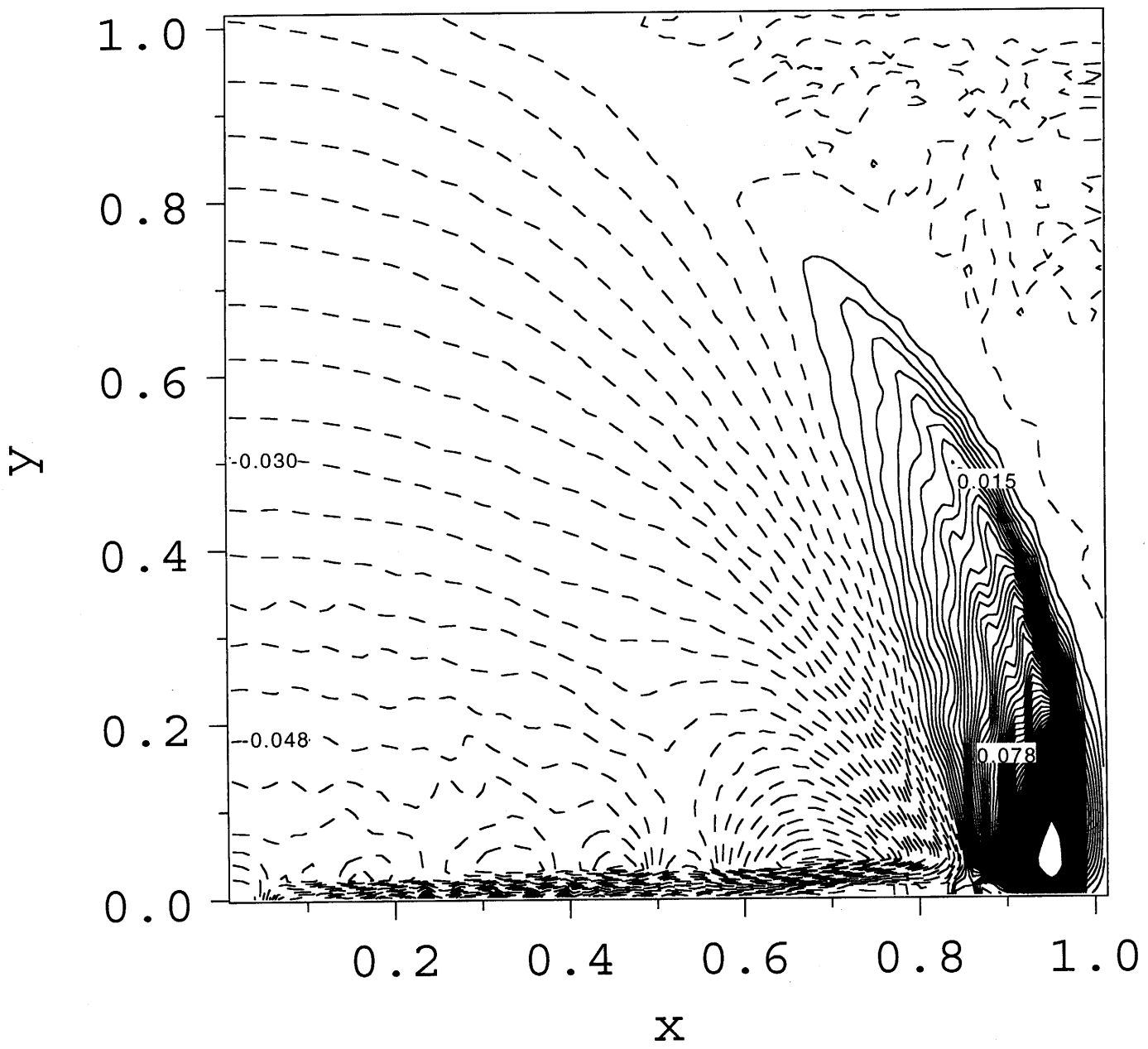
Velocity y-comp. (Sim.)
1.0
0.8
0.6
0.4
0.2
0.0
y
-0.030
-0.048
0.015
0.078
0.2
0.4
0.6
0.8
1.0
x

Fig. 25

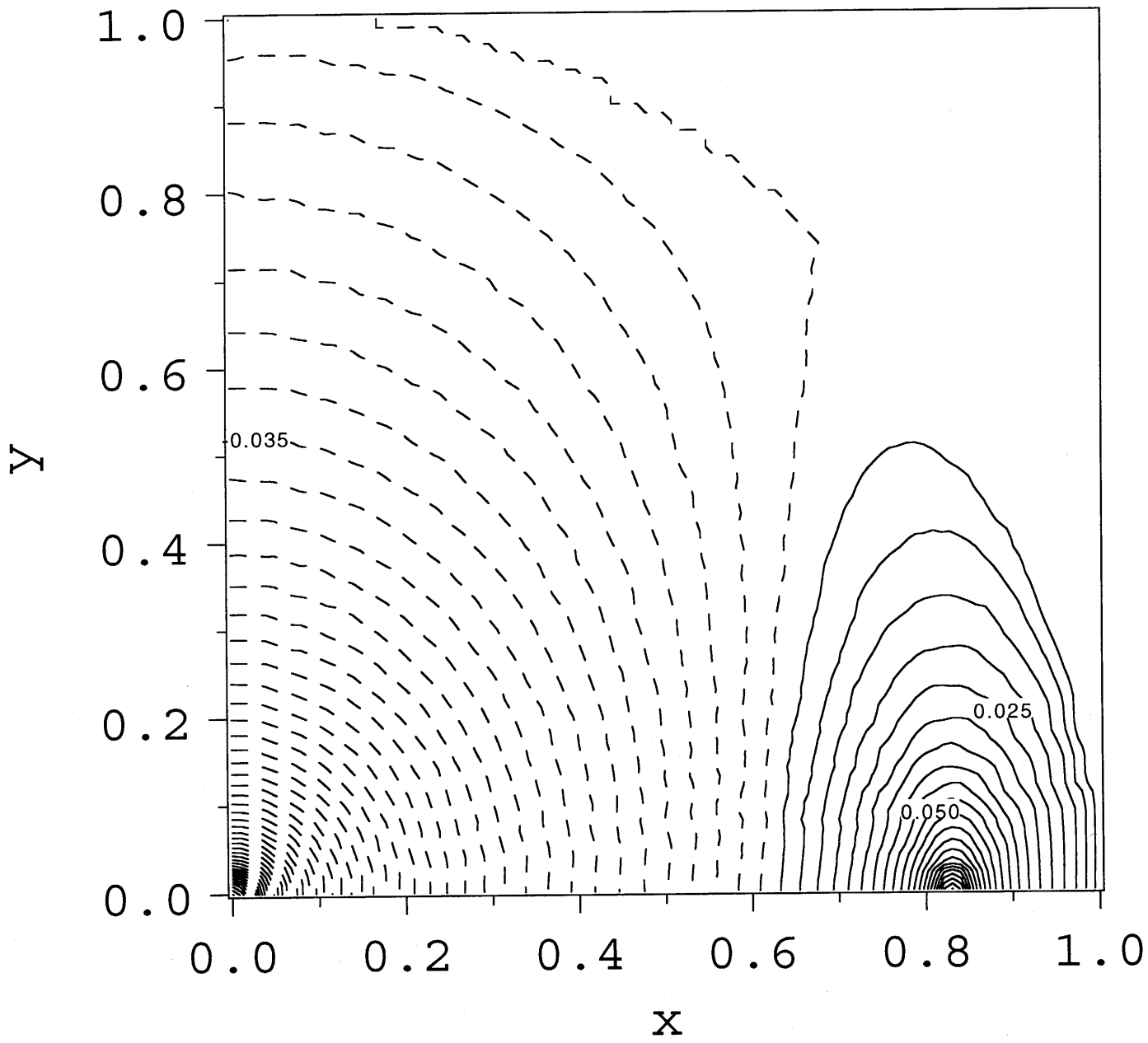
Density (=Pressure/gamma) (1st order)
1.0
0.8
0.6
0.4
0.2
0.0
y
0.035
0.025
0.050
0.0
0.2
0.4
0.6
0.8
1.0
x

Fig. 26

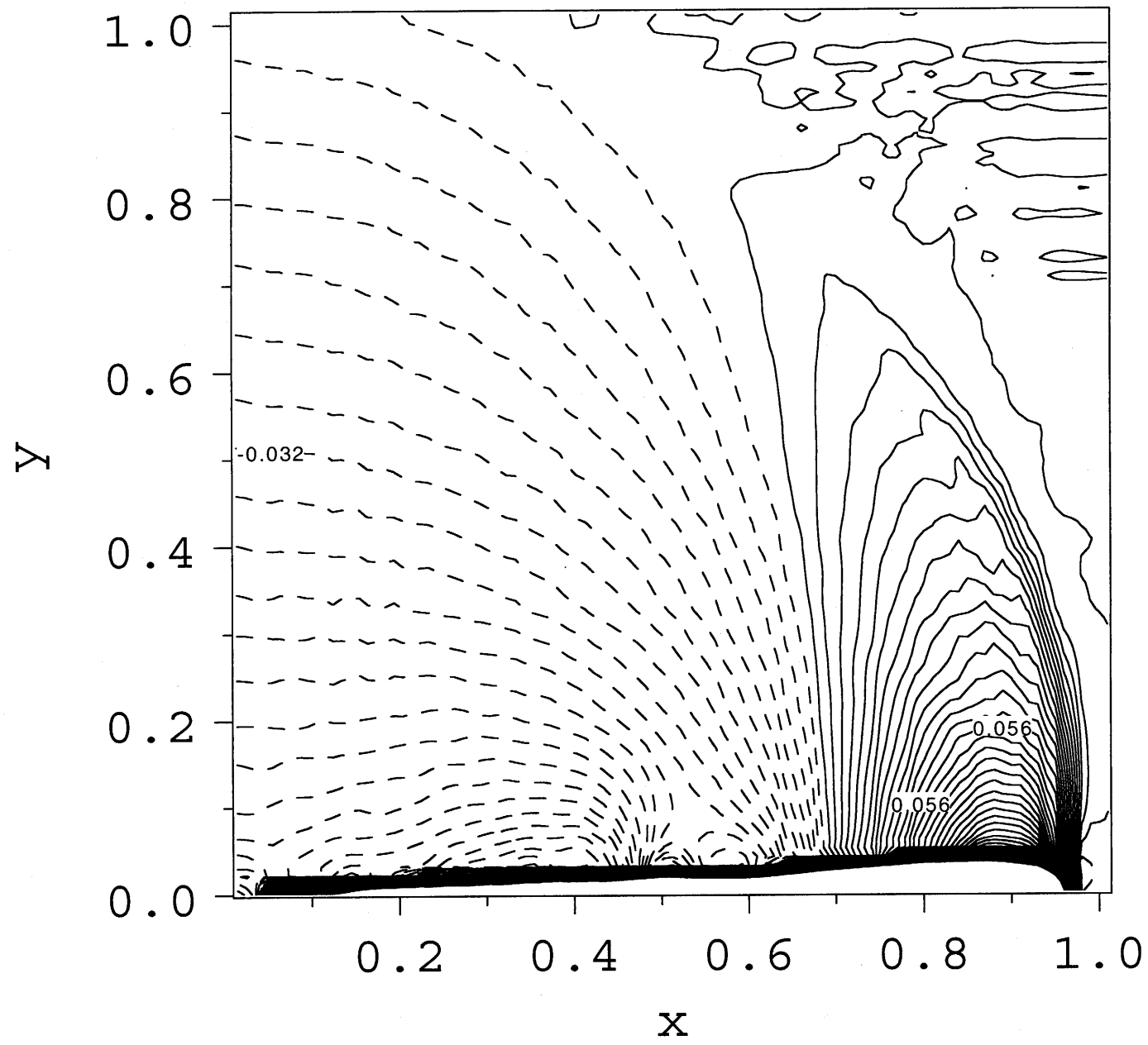
Difference in Density (Sim.)
1.0
0.8
0.6
0.4
0.2
0.0
y
-0.032
0.056
0.056
0.2
0.4
0.6
0.8
1.0
x

Fig. 27

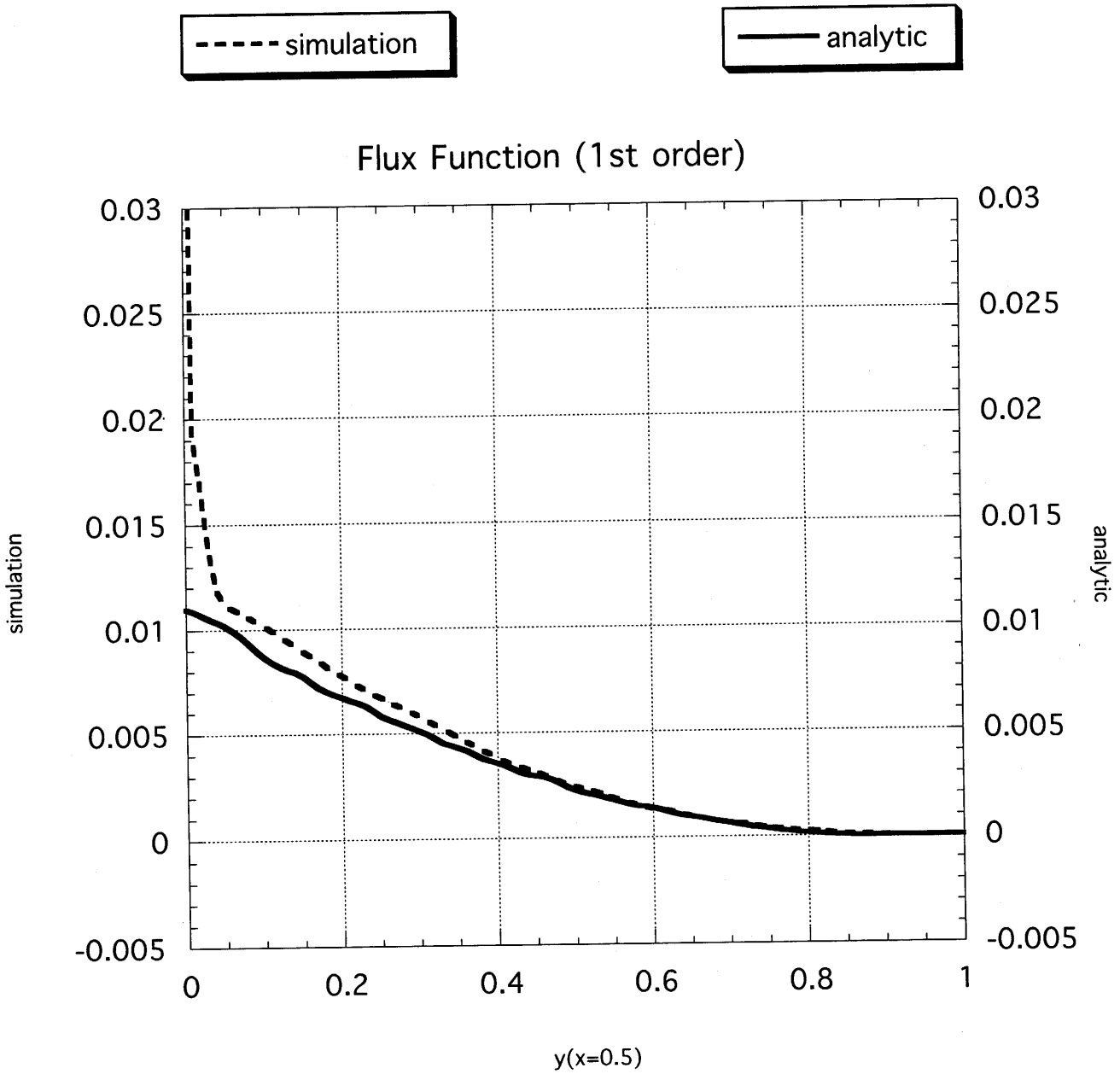
simulation
analytic
Flux Function (1st order)
0.03
0.025
0.02
0.015
0.01
0.005
0
-0.005
0
0.2
0.4
0.6
0.8
1
simulation
analytic
y(x=0.5)

Fig. 28

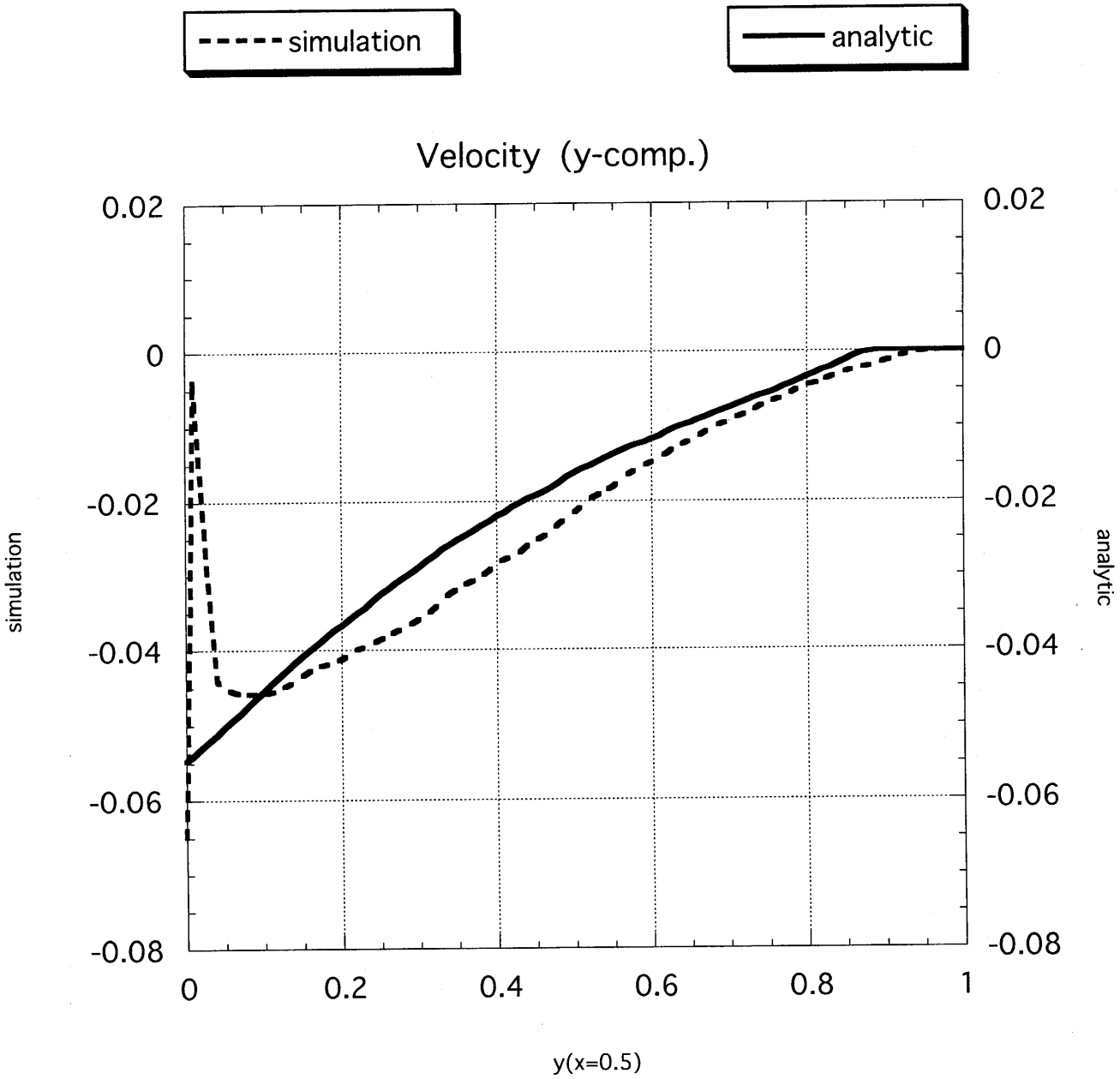
simulation
analytic
Velocity (y-comp.)
0.02
0
-0.02
-0.04
-0.06
-0.08
0
0.2
0.4
0.6
0.8
1
simulation
analytic
y(x=0.5)

Fig. 29

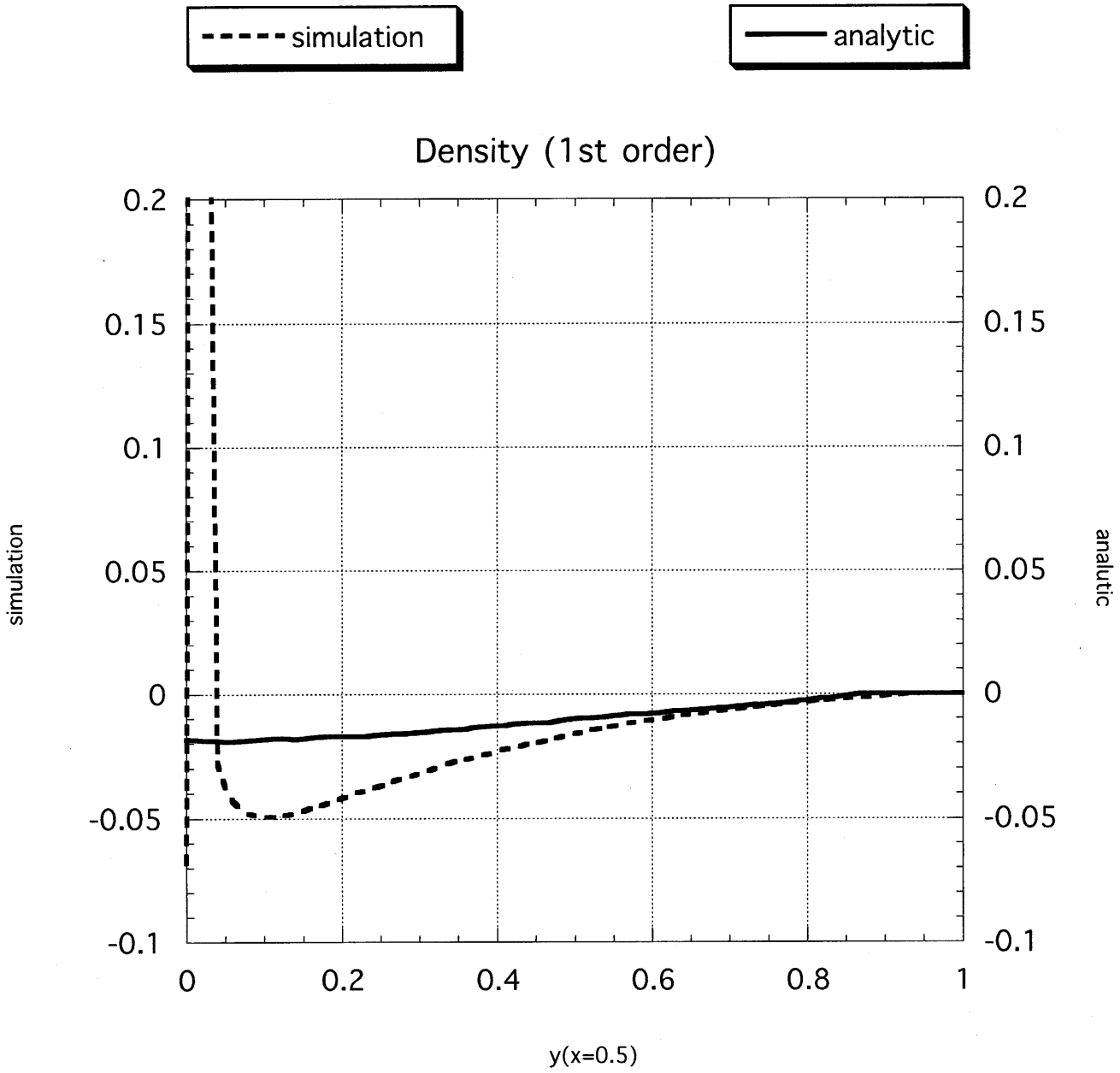
simulation
analytic
Density (1st order)
0.2
0.15
0.1
0.05
0
-0.05
-0.1
0
0.2
0.4
0.6
0.8
1
simulation
analutic
y(x=0.5)

Fig. 30

Self-Similar Evolution 2 (Magnetic Pressure)

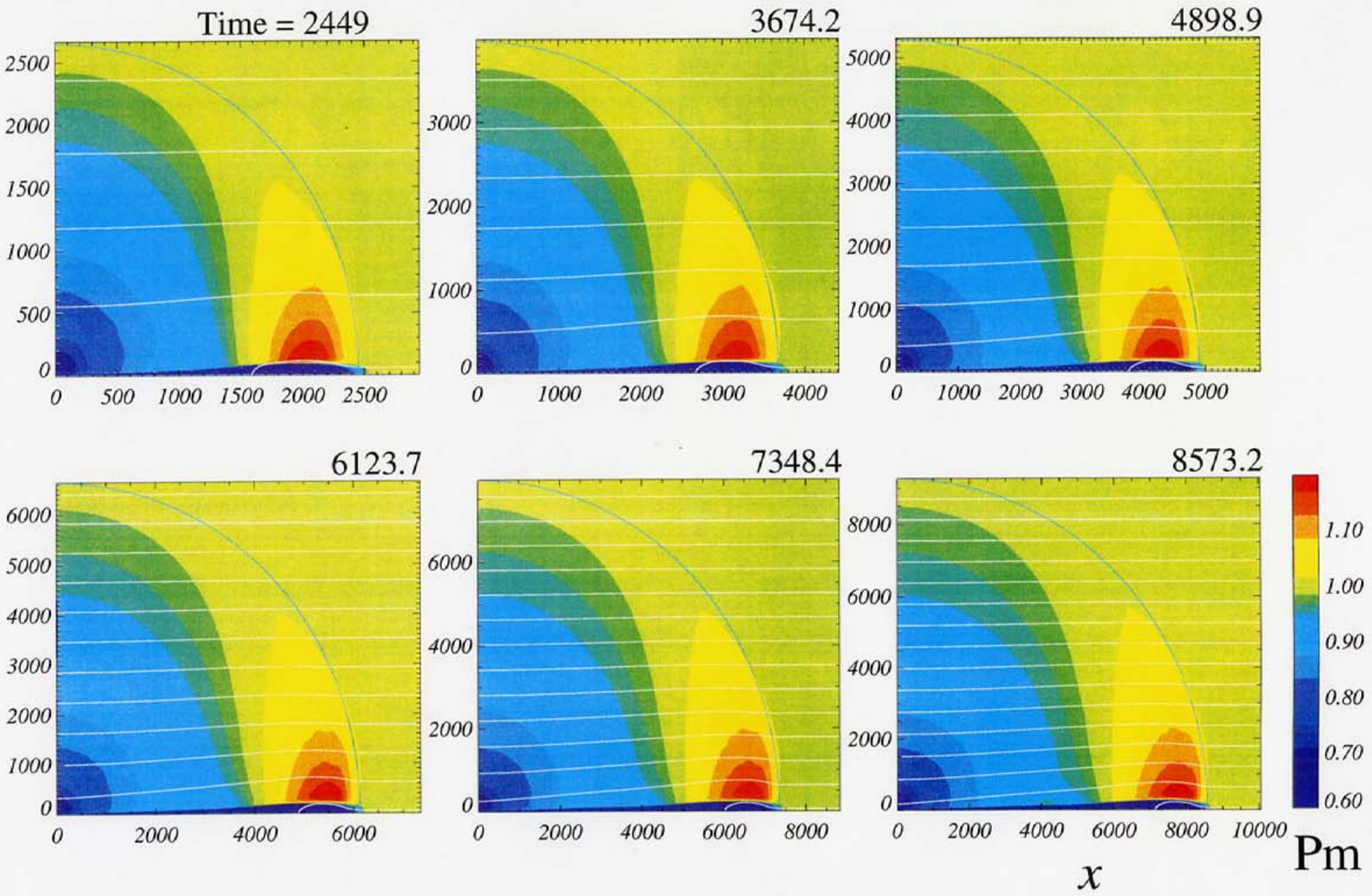

Fig. 31

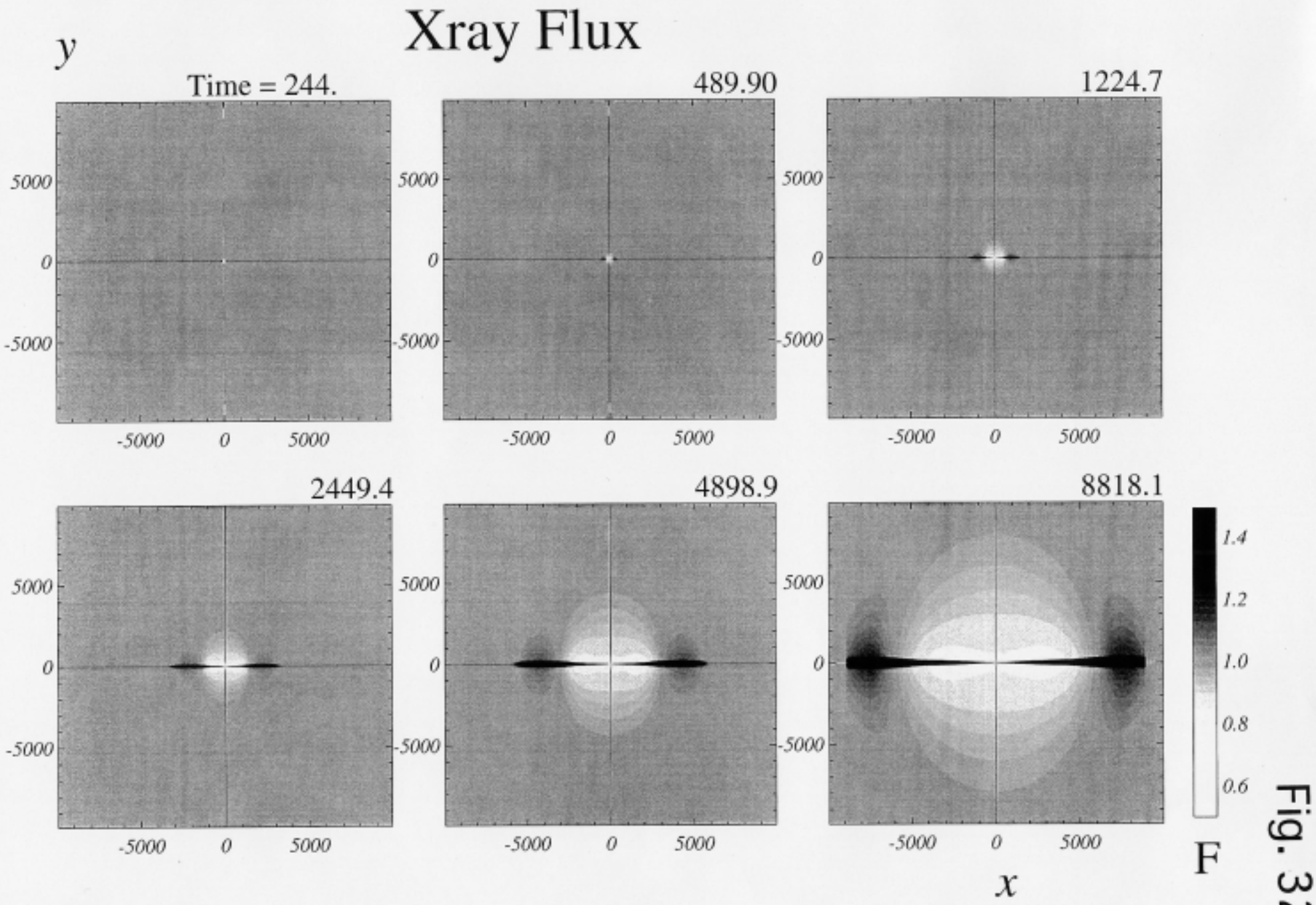
Xray Flux
y
Time = 244.
489.90
1224.7
2449.4
4898.9
8818.1
5000
0
-5000
x
F
1.4
1.2
1.0
0.8
0.6

Fig. 32

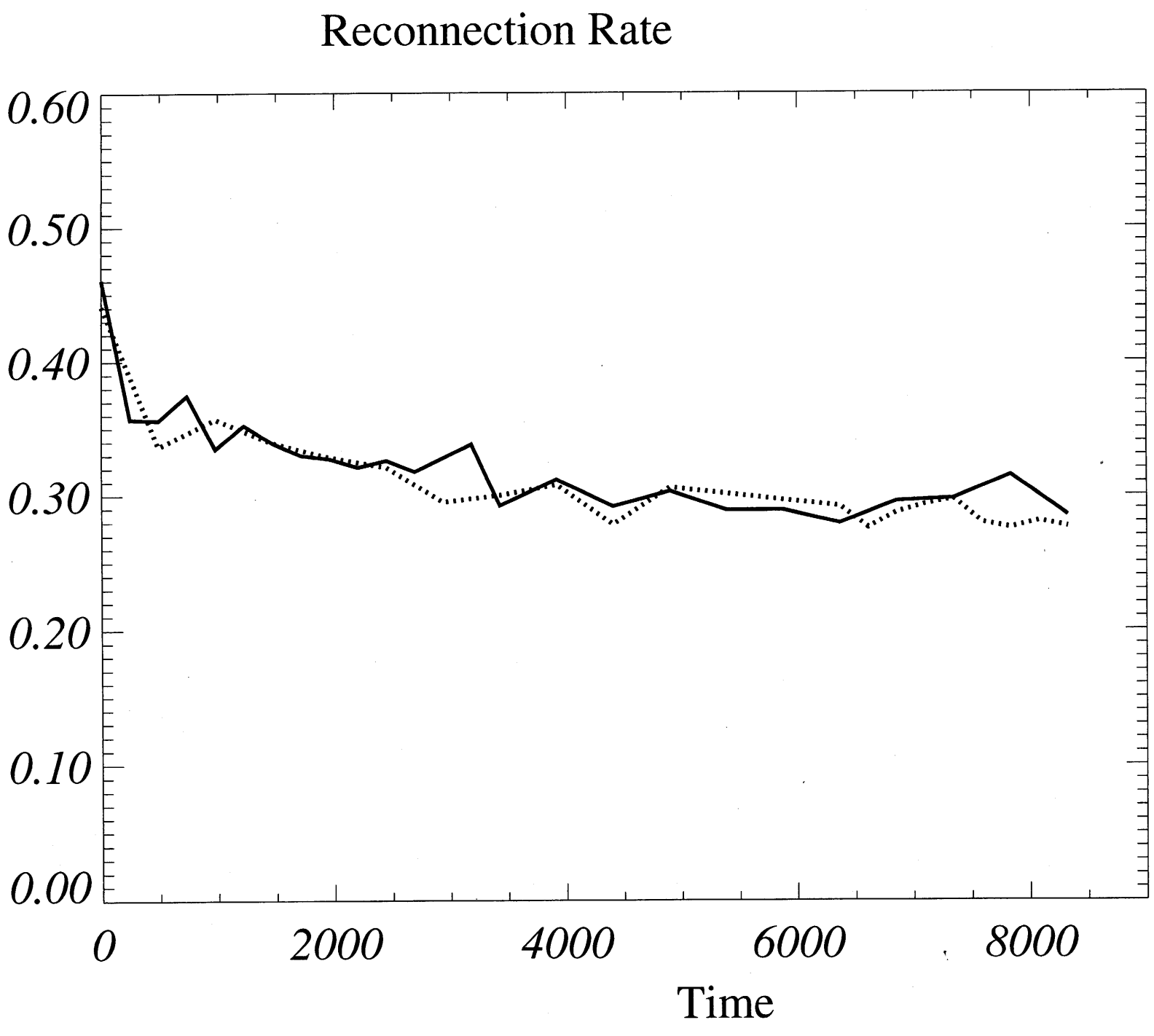
Reconnection Rate
0.60
0.50
0.40
0.30
0.20
0.10
0.00
0
2000
4000
6000
8000
Time

Fig. 33